

Arab American University
Faculty of Graduate Studies
**Department of Natural, Engineering and
Technology Sciences**
Ph.D. Program in Physics



**Magnetic, Electronic and Thermal Properties of Graphene
Monolayer**

Arwa Nazez Tawfeeq Abu Ghannam
201920345

Dissertation Committee:

Assoc. Prof. Dr. Muayad Abu Saa

Assoc. Prof. Dr. Adli Saleh

Prof. Dr. Mohammad El-Said

Prof. Dr. Hazem Khanfar

Prof. Dr. Hussin Shanak

Prof. Dr. Mohammed Abu-Jafar

**This Dissertation Was Submitted in Partial Fulfillment of the
Requirements for the Doctor of Philosophy (Ph.D.) Degree in
Physics.**

Palestine, 10/2024

© Arab American University. All rights reserved.

Arab American University
Faculty of Graduate Studies
**Department of Natural, Engineering and
Technology Sciences**
Ph.D. Program in Physics



Dissertation Approval

Magnetic, Electronic and Thermal Properties of Graphene Monolayer

Arwa Nazeh Tawfeeq Abu Ghannam

201920345

This dissertation was defended successfully on 3/10/2024 and approved by:

Dissertation Committee Members:

Name	Title	Signature
1. Assoc. Prof. Dr. Muayad Abu Saa	Main Supervisor	
2. Assoc. Prof. Dr. Adli Saleh	Members of Dissertation Committee	
3. Prof. Dr. Mohammad Elsaid	Members of Dissertation Committee	
4. Prof. Dr. Hazem Khanfar	Members of Dissertation Committee	
5. Prof. Dr. Hussein Shannak	Members of Dissertation Committee	
6. Prof. Dr. Mohammed Abu-Jafar	Members of Dissertation Committee	

Palestine, 10/2024

Declaration

I declare that, except where explicit reference is made to the contribution of others, this dissertation is substantially my own work and has not been submitted for any other degree at the Arab American University or any other institution.

Student Name: Arwa Nazeh Tawfeeq Abu Ghannam

Student ID: 201920345

Signature: *Arwa Ghannam*

Date of Submitting the Final Version of the Dissertation: 14/11/2024

Dedication

To My Family

Arwa Nazeh Tawfeeq Abu Ghannam

Acknowledgments

Thanks to Allah Almighty who enable me to do this thesis. I also place on record, my sense of gratitude to one and all who, directly or indirectly, have lent their helping hands in this thesis.

I would like to express my deepest gratitude to my advisors, Dr. Adli Saleh, Dr. Muayed Abu Saa and Prof. Dr. Mohammad El-Said for their continuous guidance throughout my PhD journey.

I am deeply indebted to my lovely family for their unconditional love, patience, and encouragement. My Mother, my husband and my siblings have always been my source of strength. To my little children, Laya, Karmel and Mohammad, your endless energy and love motivates me to continue. Your smiles and hugs kept me going during the toughest times, and I hope this achievement inspires you to pursue your dreams in future.

Magnetic, Electronic and Thermal Properties of Graphene Monolayer

Arwa Nazez Tawfq Abu Ghannam

Assoc. Prof. Dr. Muayad Abu Saa

Assoc. Prof. Dr. Adli Saleh

Prof. Dr. Mohammad El-Said

Prof. Dr. Hazem Khanfar

Prof. Dr. Hussin Shanak

Prof. Dr. Mohammd Abu-Jafar

Abstract

In this thesis, MATLAB program was used to analyze the electronic, thermal and magnetic properties of gapless and gapped graphene under an external perpendicular magnetic field. The Landau levels associated with the presence of external magnetic field of non-gapped and gapped graphene were plotted. In addition, band gap effects on the density of states of graphene was studied. The symmetry of Landau levels and density of states between conduction and valance bands are valid for both gapped and gapless graphene monolayer. At $T= 0.3\text{K}$ the oscillations in Fermi energy with magnetic field strength are more pronounced compared to that result at higher temperature ($T= 4\text{K}$). The number of oscillation at specific temperature depends only on the electron concentration and not on the energy band gap value. Several thermodynamic and magnetic quantities were studied as a function of both magnetic field strength and temperature. The introduction of band gap shifts the Schottky anomaly peak toward lower temperatures and higher specific heat values. At constant temperature, the entropy of gapped graphene versus magnetic field increases with increasing the band gap. Moreover, the Magneto Caloric Effect in both gapless and gapped graphene was plotted and analyzed in terms of the change in the entropy ($-\Delta S$). The coexistence of different types of magnetic states is verified by the observed maxima in the magnetization of graphene. Making it potentially useful in magnetic memory storage and magnetic switching applications.

Keywords: Gapless graphene, Gapped graphene, Electronic properties, Thermal properties, Magnetic properties.

Table of Contents

#	Title	Page
	Declaration	I
	Dedication	II
	Acknowledgements	III
	Abstract	IV
	List of Tables	VII
	List of Figures	VIII
	List of Definitions of Abbreviations	XII
	Chapter One: Introduction	1
1.1	Introduction	1
1.2	Problem Statement	11
1.3	Structure of the Thesis	11
	Chapter Two: Literature Review	13
	Chapter Three: Methodology	18
3.1	Dirac Hamiltonian	18
3.2	Graphene Dirac Hamiltonian	19
3.3	Density of States Calculations	22
3.4	Thermal Properties Calculations	22
3.5	Magnetic Properties Calculations	24
3.6	Fermi Energy Calculations	25
3.7	Simulation Approach	26
	Chapter Four: Results	29

4.1	Electronic Properties	29
4.1.1	Energy Spectra	29
4.1.2	Density of States	37
4.1.3	Fermi Energy Oscillations	44
4.2	Thermal Properties of Graphene Monolayer	51
4.2.1	Statistical Average Energy	51
4.2.2	Specific Heat Capacity	57
4.2.3	Entropy Calculations	63
4.3	Magnetic Properties of Graphene Monolayer	73
4.3.1	Magnetization	73
4.3.2	Magnetic Susceptibility	78
	Chapter Five: Discussion	84
	References	85
	ملخص	93

List of Tables

Table #	Title of Table	Page
4.1	Energy separation between different Landau levels of gapped graphene, $\Delta = 0 \text{ meV}$, at different magnetic field strengths.	33
4.2	Energy separation between different Landau levels of gapped graphene, $\Delta = 53 \text{ meV}$, at different magnetic field strengths.	33
4.3	Energy separation between different Landau levels of gapped graphene, $\Delta = 106 \text{ meV}$, at different magnetic field strengths.	34
4.4	Energy differences between $B = 4T$ and $B = 2T$ of gapped graphene, $\Delta = 0 \text{ meV}$ for different Landau levels.	35
4.5	Energy differences between $B = 4T$ and $B = 2T$ of gapped graphene, $\Delta = 53 \text{ meV}$ for different Landau levels.	35
4.6	Energy differences between $B = 4T$ and $B = 2T$ of gapped graphene, $\Delta = 106 \text{ meV}$ for different Landau levels.	36

List of Figures

Figure #	Title of Figure	Page
1.1	Dimensionality classification of nanostructures. Source: Garcia and Diaz-Garcia 2012). Copyright 2012, Elsevier	2
1.2	The synthesis of nanomaterials via top-down and bottom-up approaches. Copyright: 2019, Elsevier B.V. All rights reserved.	3
1.3	The structures of natural carbon allotropes including graphite, diamond and amorphous carbon (Kharisov and Kharissova 2019)	5
1.4	Carbon allotropes nanostructures with their dimensionality and hybridization (Kharisov and Kharissova 2019)	5
1.5	(a) Geometry of the graphene honeycomb-like lattice. (b) First Brillouin zone with marked corners K , \bar{K} (Ho, Lai et al. 2008).	6
1.6	(a) Band structure of graphene (b) Dirac cones at the K and \bar{K} points residing on a hexagonal plane (Bhattacharjee 2012).	8
1.7	Triangular sublattices of graphene (Cooper, D'Anjou et al. 2012).	9
1.8	The valence and conduction bands in (a) single-layer graphene, (b) double-layer graphene and (c) double-layer graphene in the presence of perpendicular electric field (Savage 2009).	9
1.9	Graphene, h-BN and graphene/h-BN lattices and schematic band structures (Chen 2022).	10
3.1	MATLAB image showing the parameters used in this thesis.	27
3.2	Flow chart of the problem.	28
4.1	Energy levels of gapless graphene as a function of magnetic field for different Landau levels.	30
4.2	Energy levels of gapped graphene, $\Delta = 53 \text{ meV}$, as a function of magnetic field for different Landau levels.	31

4.3	Energy levels of gapped graphene, $\Delta = 106 \text{ meV}$, as a function of magnetic field for different Landau levels.	32
4.4	Schematic of LLs of gapped graphene. The arrows represent the observed transition (Chen, Shi et al. 2014)	37
4.5	The density of states of gapless graphene at a uniform magnetic fields of (a) $B = 0.5 \text{ T}$ and (b) $B = 3 \text{ T}$ as a function of energy at $n=20$.	38
4.6	The density of states of gapped graphene, $\Delta = 53 \text{ meV}$, at a uniform magnetic fields of (a) $B = 0.5 \text{ T}$ and (b) $B = 3 \text{ T}$ as a function of energy at $n=20$.	39
4.7	The density of states of gapped graphene, $\Delta = 106 \text{ meV}$, at a uniform magnetic fields of (a) $B = 0.5 \text{ T}$ and (b) $B = 3 \text{ T}$ as a function of energy at $n=20$.	40
4.8	The density of states of graphene in a uniform magnetic field of 0.5 T as a function of energy for different values of the band gap, (a) $\Delta = 0 \text{ meV}$, (b) $\Delta = 53 \text{ meV}$ and (c) $\Delta = 106 \text{ meV}$ and $n=20$.	41
4.9	The density of states of gapless graphene, $\Delta = 0 \text{ meV}$, at a uniform magnetic fields of $B = 0.5 \text{ T}$ (a) $n = 5$ and (b) $n = 20$ as a function of energy.	42
4.10	The density of states of gapped graphene, $\Delta = 53 \text{ meV}$, at a uniform magnetic fields of $B = 0.5 \text{ T}$ (a) $n = 5$ and (b) $n = 20$ as a function of energy.	43
4.11	The density of states of gapped graphene, $\Delta = 106 \text{ meV}$, at a uniform magnetic fields of $B = 0.5 \text{ T}$ (a) $n = 5$ and (b) $n = 20$ as a function of energy.	44
4.12	Fermi energy as a function of magnetic field strength for different concentrations of gapless graphene, $\Delta = 0 \text{ meV}$, at constant temperature $T = 0.3 \text{ K}$.	45
4.13	Fermi energy as a function of magnetic field strength for different electron concentrations of gapped graphene, $\Delta = 53 \text{ meV}$, at constant temperature $T = 0.3 \text{ K}$.	46
4.14	Fermi energy as a function of magnetic field strength for different electron concentrations of gapped graphene, $\Delta = 106 \text{ meV}$ at constant temperature $T = 0.3 \text{ K}$.	47

4.15	Fermi energy as a function of magnetic field strength for different electron concentrations of gapless graphene, $\Delta = 0 \text{ meV}$, at constant temperature $T = 4\text{K}$.	48
4.16	Fermi energy as a function of magnetic field strength for different electron concentrations of gapped graphene, $\Delta = 53 \text{ meV}$, at constant temperature $T = 4\text{K}$.	49
4.17	Fermi energy as a function of magnetic field strength for different electron concentrations of gapped graphene, $\Delta = 106 \text{ meV}$, at constant temperature $T = 4\text{K}$.	50
4.18	Statistical average energy of gapless and gapped graphene versus temperature at constant magnetic field of 0.02 T .	52
4.19	Statistical average energy of gapless and gapped graphene versus temperature at constant magnetic field of 0.2 T .	53
4.20	Statistical average energy of gapless and gapped graphene versus temperature at constant magnetic field of 1.5 T .	54
4.21	The statistical average energy versus magnetic field strength at constant temperature of 40 K for the three values of the band gap	56
4.22	Specific heat capacity versus temperature of gapped and non-gapped graphene at a constant value of magnetic field, $B = 0.02\text{T}$.	58
4.23	Specific heat capacity versus temperature of gapped and non-gapped graphene at a constant value of magnetic field, $B = 0.3\text{T}$.	59
4.24	Specific heat capacity versus temperature of gapped and non-gapped graphene at a constant value of magnetic field, $B = 1.5 \text{ T}$.	60
4.25	Specific heat capacity versus magnetic field strength of gapped and non-gapped graphene at a constant value of Temperature, $T = 3 \text{ K}$.	61
4.26	Specific heat capacity versus magnetic field strength of gapped and non-gapped graphene at a constant value of Temperature, $T = 5 \text{ K}$.	62
4.27	Specific heat capacity versus magnetic field strength of gapped and non-gapped graphene at a constant value of Temperature, $T = 10 \text{ K}$.	63

4.28	Entropy versus temperature of gapless and gapped graphene at constant magnetic field strength of $B=0.02T$.	64
4.29	Entropy versus temperature of gapless and gapped graphene at constant magnetic field strength of $B=0.2T$.	65
4.30	Entropy versus temperature of gapless and gapped graphene at constant magnetic field strength of $B = 1.5 T$.	65
4.31	Entropy versus magnetic field of gapless and gapped graphene at different temperatures: (a) $T = 3 K$, (b) $T = 5 K$ and (c) $T = 10 K$.	68
4.32	Change in entropy of graphene versus temperature at three values of the band gap at (a) $B = 0.02T$, (b) $B = 0.2T$ and (c) $B = 1.5 T$.	70
4.33	Change in entropy as a function of magnetic field strength at a constant value of temperature: (a) $T = 3K$, (b) $T = 5 K$ and (c) $T = 10 K$.	72
4.34	Magnetization versus temperature for three values of the band gap, $\Delta = 0 meV$, $\Delta = 53 meV$ and $\Delta = 106 meV$ at four magnetic field strengths of, (a) $B = 0.02T$ (b) $B = 0.3T$, (c) $B = 1.5T$ (d) $B = 10 T$.	75
4.35	Magnetization versus magnetic field strength for three values of the band gap, (a) $\Delta = 0 meV$, (b) $\Delta = 53 meV$ and (c) $\Delta = 106 meV$ at $T = 40 K$	76
4.36	Magnetization versus magnetic field strength for three values of the band gap, (a) $\Delta = 0 meV$, (b) $\Delta = 53 meV$ and (c) $\Delta = 106 meV$ at $T = 80 K$.	77
4.37	Magnetic susceptibility versus temperature for three values of the band gap, $\Delta = 0 meV$, $\Delta = 53 meV$ and $\Delta = 106 meV$ at four magnetic field strengths of, (a) $B = 0.02T$ (b) $B = 0.2T$, (c) $B = 1.5T$ (d) $B = 10 T$	80
4.38	Magnetic susceptibility versus magnetic field strength for three values of the band gap, (a) $\Delta = 0 meV$, (b) $\Delta = 53 meV$ and (c) $\Delta = 106 meV$ at $T = 40 K$.	81
4.39	Magnetic susceptibility versus magnetic field strength for three values of the band gap, (a) $\Delta = 0 meV$, (b) $\Delta = 53 meV$ and (c) $\Delta = 106 meV$ at $T = 80 K$.	82

List of Definitions of Abbreviations

Abbreviations	Title
\hat{H}	Dirac Hamiltonian operator
c	Speed of light
\hat{p}	Momentum operator
α	Dirac matrices
β	Dirac matrices
m	Rest mass of the particle
σ	Pauli matrices
\mathbf{I}	Identity matrix
v_F	Fermi velocity
ψ	spinor wave function
E	Eigenvalues of the energy
B	Magnetic field strength
π	Canonical momentum
e	Charge of electron
Δ	Energy gap
C_v	Specific heat capacity
S	Entropy
ω_c	The cyclotron frequency
α_c	The magnetic length

n	Principle quantum number
DOS	Density of states
g_s	spin degeneracy
Γ	The broadening parameter
\bar{E}	Average energy
T	Temperature
k_B	Boltzmann constant
A	Vector potential
M	Magnetization
χ	Magnetic susceptibility
ΔS	Entropy change
E_f	Fermi energy
Z	partition function
μ	Chemical potential

Chapter One: Introduction

1.1: Introduction

Nanomaterials are an exciting class of materials because of their unique properties and diverse applications. Materials are classified as nanomaterials when their size or at least one of their dimensions falls within the range of 1 to 100 *nm* (Baig, Kammakakam et al. 2021). It is difficult to determine the exact history of the use of nanoscale items. However, these materials have been used by humans unknowingly for a variety of purposes since ancient times. For instant, approximately 4500 years ago involves the use of asbestos nanofibers to strengthen ceramic mixtures. Additionally, ancient Egyptians utilized PbS nanoparticles in hair-dyeing formulas (Baig, Kammakakam et al. 2021).

Nanomaterials exhibit dynamic optical properties such as absorption, transmission, reflection, and light emission, which often differ significantly from those of their bulk counterparts. A vast array of optical effects appropriate for a variety of applications can be produced to modifying the size, shape and surface properties of nanomaterials. This manipulation can be accomplished using a range of techniques, depending on the size, composition, and orientation of the nanomaterials. Its optical characteristics are essential in a variety of domains. They have the ability to limit their electrical properties, which can result in quantum effects, as slight modifications to their size, shape, or type can affect the colors they display. To fully utilize nanomaterials in photonics, electronics, and sensing, among other domains, it is essential to comprehend and manipulate these optical properties (Adewuyi and Lau 2021).

Dimensionality is a key feature used to categorize different structures of nanomaterials. While nanomaterials can be classified based on various criteria such as morphology, dimensionality, and composition, categorizing them according to the dimensions of confinement can be particularly useful. This definition states that all three dimensions (*x*, *y*, and *z*) of zero-dimensional (0D) nanomaterials are confined within the nanoscale. On the

other hand, two-dimensional (2D) and one-dimensional (1D) nanomaterials have one and two dimensions, respectively, in the nanoscale.

The building blocks of three-dimensional (3D) nanostructures are made up of 0D, 1D, and 2D nanomaterials. These structures are called quantum dots (0D), quantum wires (1D), and quantum wells (2D), respectively, in solid-state physics and optoelectronics. A schematic depiction of this classification is shown in Figure 1.1 (Vaseghi and Nematollahzadeh 2020).

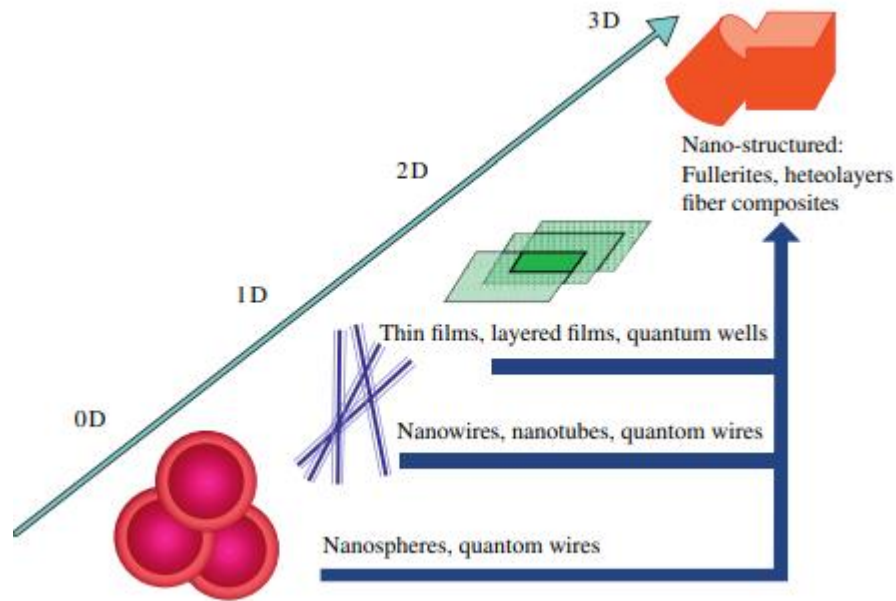


Figure 1.1 Dimensionality classification of nanostructures. Source: Garcia and Diaz-Garcia 2012). Copyright 2012, Elsevier

The synthesis of nanomaterials can be broadly categorized into two main approaches: top-down approaches and bottom-up approaches. These approaches are shown in Figure 1.2. Top-down approaches involve breaking down bulk materials to produce nanostructured materials. These methods include laser ablation, mechanical milling, electro-explosion, etching and sputtering. In contrast, Bottom-up approaches includes chemical vapor deposition, solvothermal and hydrothermal methods, the sol-gel method, soft and hard templating methods and reverse micelle methods (Baig, Kammakam et al. 2021).

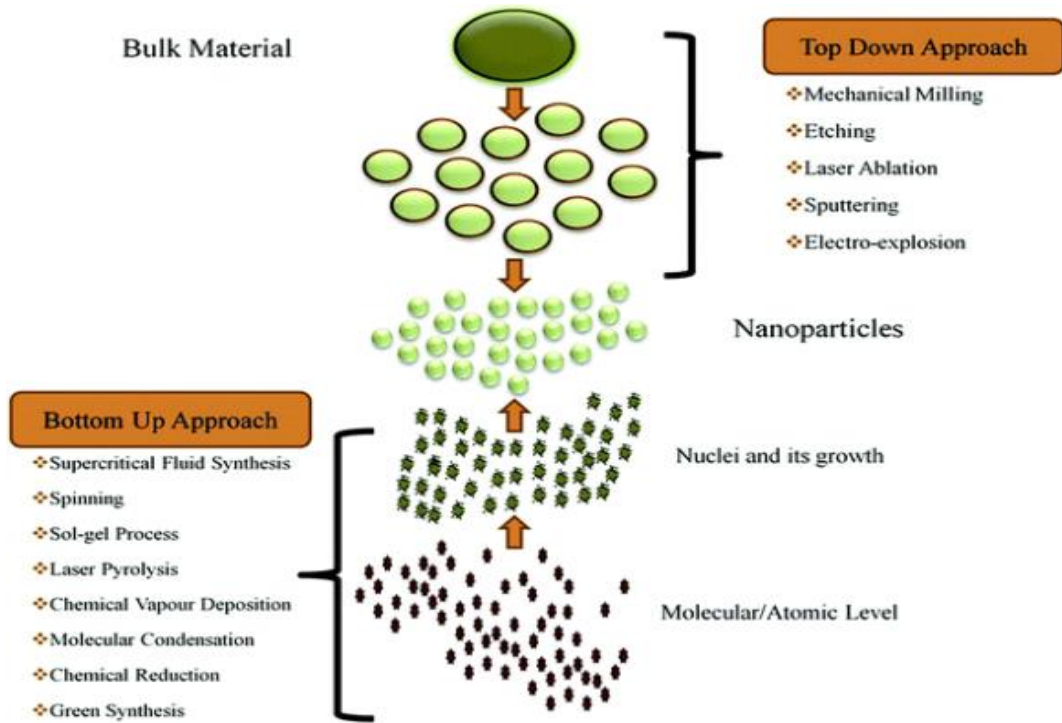


Figure 1.2 The synthesis of nanomaterials via top-down and bottom-up approaches.

Copyright: 2019, Elsevier B.V. All rights reserved.

Nanomaterials exhibit a range of unique properties that can be finely tuned by adjusting their sizes and morphologies. These materials typically possess significantly higher surface areas compared to their bulk counterparts, a property that is inherent to all nanomaterials (Tomar, Abdala et al. 2020). Additionally, the magnetic behavior of elements can change at the nanoscale, with non-magnetic elements potentially becoming magnetic (Roduner 2006). Quantum effects are more pronounced at this scale, although the specific size at which these effects appear depends on the nature of the semiconductor material (Geoffrion and Guisbiers 2020). Furthermore, nanomaterials can exhibit extraordinary thermal and electrical conductivity at the nanoscale level compared to their bulk counterparts, as demonstrated by graphene derived from graphite (Krishnan, Singh et al. 2019). They also display excellent mechanical properties absent in their macroscopic counterparts (Wu, Miao et al. 2020). The development of *2D* sheets of various nanomaterials has enabled the effective dispersion of nanoparticles of active catalysts, significantly enhancing catalyst performance (Zhu, Guo et

al. 2020). In an effort to improve performance more significantly, catalysts have recently been atomically distributed over 2D nanomaterial sheets (Liu, Xu et al. 2020).

Because of their unique features, a wide range of nanomaterials from the carbon-based nanomaterial group have been thoroughly investigated for a variety of applications. These materials customizable characteristics caused a lot of interest because of their potential applications in emerging technologies and obstacles (Mauter and Elimelech 2008) and (Chen, Zhao et al. 2020). Carbon nanotubes (CNTs), graphene, fullerenes, carbon-based quantum dots, carbon nanohorns, and other special nanomaterials are members of this group (Baig, Kammakakam et al. 2021).

Carbon can form sp -, sp^2 -, and sp^3 -hybridized chemical bonds. As a result, it may attach itself strongly to other elements to produce an endless number of organic molecules with a wide variety of chemical and biological properties. It has three known allotropes in nature including diamond, graphite and amorphous carbon (Sheng, Yan et al. 2011). Figure 1.3 shows the structure of the natural carbon allotropes. However, the synthesis of new elemental carbon allotropes is an interesting field. Graphene (Novoselov, Geim et al. 2004), carbon nanotubes (Iijima, Ajayan and Ichihashi 1992), and fullerenes (Kroto 1987) are some of the most efficient examples.

Carbon nanostructures of 0D carbon is known as carbon fullerene, and its molecular structures can vary with different number of carbons (Ye, Qi et al. 2023). In addition, carbon nanotubes are unique 1D systems. The chemical bonding of carbon nanotubes involves entirely sp^2 -hybrid carbon atoms (Kharisov and Kharissova 2019). The 2D carbon materials are known as graphene. It is formed by sp^2 -hybridization (Kharisov and Kharissova 2019).

Moreover, the most common 3D carbon allotropes are graphite and diamond (Ye, Qi et al. 2023). Diamond-like carbon (DLC) is a class of 3D carbon nanostructures (Kharisov and Kharissova 2019). DLC is an amorphous carbon material with a mixture of sp^2 and sp^3 bonds that gives it some of the characteristics of a diamond (Ryan, Böttger et al. 2022). Figure 1.4 presents the carbon allotropes with different dimensions and hybridization.

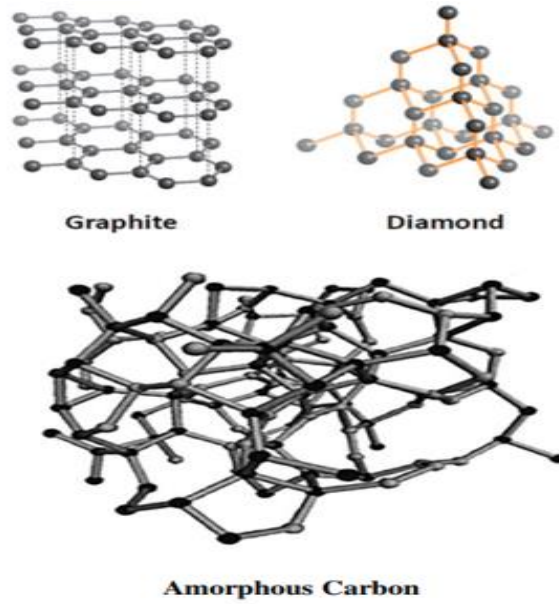


Figure 1.3 The structures of natural carbon allotropes including graphite, diamond and amorphous carbon (Kharisov and Kharissova 2019)

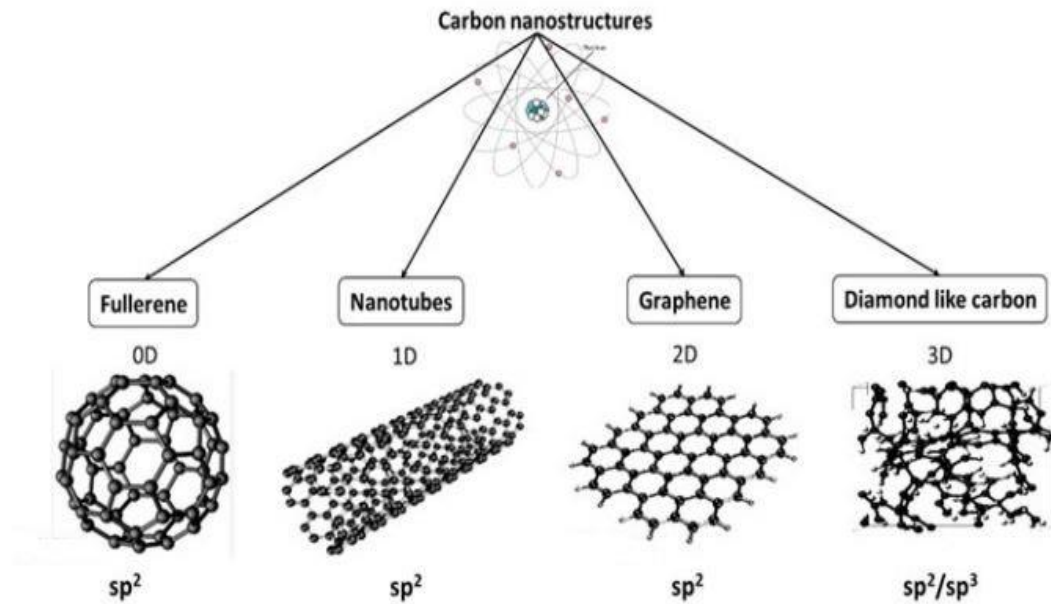


Figure 1.4 Carbon allotropes nanostructures with their dimensionality and hybridization (Kharisov and Kharissova 2019)

Graphene, a member of the carbon nanomaterial family, has quickly gained remarkable prominence since its isolation from graphite in 2004 (Sanchez, Jachak et al. 2012). It consists of one single atomic plane of graphite (Geim 2009). Its remarkable properties have the potential to revolutionize different fields, including batteries, solar cells, catalysis, supercapacitors, sensors, field-effect transistors, and membrane technology (Baig, Kammakam et al. 2021). In addition, it consists of sp^2 -hybridized, two-dimensional sheets of carbon atoms, which forms a planar structure tightly packed into a honeycomb-like lattice (Geim and Novoselov 2007). This lattice is shown in Figure 1.5 (a) in which the primitive lattice vectors in real space, \mathbf{a}_1 and \mathbf{a}_2 , is presented. In addition, vectors connecting the nearest neighbor δ_1 , δ_2 and δ_3 is also plotted. The real space lattice vectors are $\mathbf{a}_{1,2} = \frac{\sqrt{3}a}{2}(\sqrt{3}, \pm 1)$ and the corresponding reciprocal ones are $\mathbf{b}_{1,2} = \frac{2\pi}{\sqrt{3}a}(\frac{1}{\sqrt{3}}, \pm 1)$, where the interatomic distance $a = 0.142 \text{ nm}$ (Ho, Lai et al. 2008). Figure 1.5 (b) shows the first Brillouin zone which is a hexagon where two inequivalent groups of K points are formed at the corners. These points are labelled as K and K' such that (Ho, Lai et al. 2008):

$$K = \frac{2\pi}{3a}\left(1, \frac{1}{\sqrt{3}}\right), \quad K' = \frac{2\pi}{3a}\left(1, -\frac{1}{\sqrt{3}}\right)$$

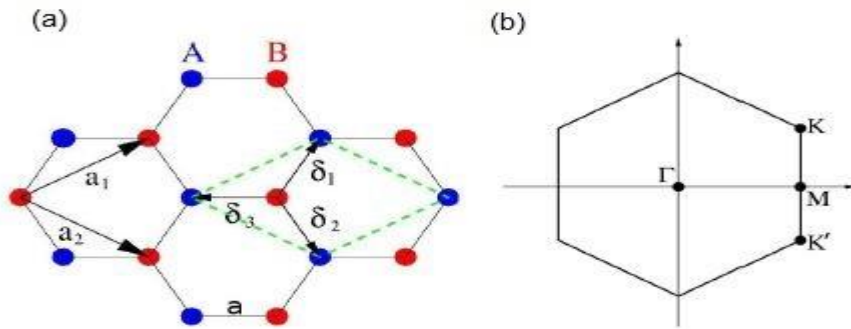


Figure 1.5 (a) Geometry of the graphene honeycomb-like lattice. (b) First Brillouin zone with marked corners K , K' (Ho, Lai et al. 2008).

Particularly, it can consider as one of the thinnest materials known and boasts exceptional mechanical strength (Geim 2009). Its transparency makes it possible for applications such as transparent light panels and touchscreens. The surface area of graphene is significantly greater than that of fullerenes, graphite, and even carbon nanotubes (Baig, Kammakakam et al. 2021). Additionally, graphene has an extraordinarily high theoretical surface area, approximately $2630 \text{ m}^2/\text{g}$ (Shubha, Praveen et al. 2023). The thermal conductivity of graphene flakes ranges from approximately 3080 to $5150 \text{ W m}^{-1} \text{ K}^{-1}$ (Ghosh, Calizo et al. 2008). Similarly, thermal conductivity values between roughly $(4.84 \pm 0.44) \times 10^3$ and $(5.30 \pm 0.48) \times 10^3 \text{ W m}^{-1} \text{ K}^{-1}$ for single-layer graphene (Balandin, Ghosh et al. 2008). This exceptional thermal conductivity surpasses that of carbon nanotubes in heat conduction. Furthermore, ultrahigh electron mobility of $200,000 \text{ cm}^2 \text{ V}^{-1} \text{ s}^{-1}$ is achieved at electron densities of around $2 \times 10^{11} \text{ cm}^{-2}$ by suspending single-layer graphene (Bolotin, Sikes et al. 2008).

The magnetic responses of graphene is different from graphite and graphene multilayers, mainly because of the different crystal symmetry and interlayer interactions (Koshino, Arimura et al. 2009), (Koshino and Ando 2007) and (Simos and Maroulis 2012). Graphene has large magnetization at low temperature and its magnetization is proportional to $-\sqrt{B}$, which is different from normal materials (Li, Chen et al. 2015).

Moreover, Graphene is classified as a zero-gap semiconductor (Bhattacharjee 2012) or semi-metal (Choi, Lahiri et al. 2010) because of its unique Dirac cone band structure near the Fermi level, which leads to an exceptionally high concentration of charge carriers and ballistic transport properties (Geim 2009). The band structure of graphene and the Dirac cones are presented in Figure 1.6 (a) and (b), respectively. In non-gapped graphene, the charge carriers behave as massless Dirac Fermions (Tu, Anh et al. 2022). Furthermore, the ability of massless electrons to travel through the honeycomb lattice over sub-micrometer distances without scattering gives opportunities for the study of quantum effects in graphene, even at room temperature (Geim 2009).

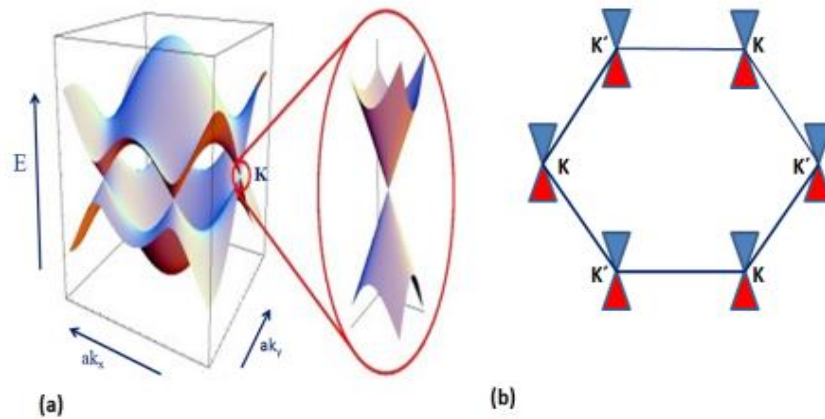


Figure 1.6 (a) Band structure of graphene (b) Dirac cones at the K and K' points residing on a hexagonal plane (Bhattacharjee 2012).

Graphene can be produced through exfoliation of graphite by Scotch tape or micromechanical cleavage. The produced graphene has excellent quality while this process is time consuming (Urade, Lahiri and Suresh 2023). A traditional technique for producing graphene with large amounts is the chemical reduction of graphene oxide through chemical oxidation and reduction methods (Urade, Lahiri and Suresh 2023). Also, thermal chemical vapor deposition is a method to produce graphene. In this method, graphene layer forms from the self-assemble of carbon radicals (Urade, Lahiri and Suresh 2023). However, the produced graphene layer must be transferred onto a substrate for the ability to use in applications. In addition, thermal decomposition of silicon carbide, un-zipping carbon nanotubes and other methods are used to produce graphene (Urade, Lahiri and Suresh 2023).

Currently, modifying graphene to introduce a gap in its energy spectrum is a significant challenge (Novoselov 2007). Electrons in small gapped graphene obey Dirac equation with mass and can be used in applications where the gap is important. The spectrum will gap if the symmetry that interchanges the two triangular sublattices of the hexagonal graphene lattice is broken (Semenoff, Semenoff et al. 2008). This may be achieved, for instance, by introducing a staggered chemical potential, which would give the electrons on the A sites a different energy than the electrons on the B sites (Semenoff, Semenoff et al. 2008). The A

and B sites are presented in Figure 1.7 in which blue and black circles represent the A and B sites, respectively.

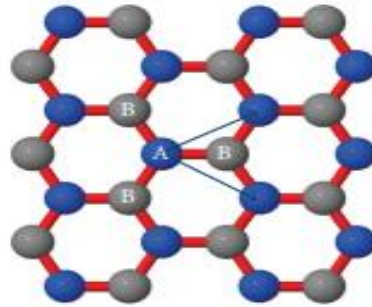


Figure 1.7 Triangular sublattices of graphene (Cooper, D’Anjou et al. 2012).

It may also result from bond deformations on the graphene lattice (Hou, Chamon et al. 2007), which are comparable to those observed in the research on carbon nanotubes (Chamon 2000). Using multi-layer graphene, in which the layers can be layered so that their interaction breaks the sublattice symmetry, is a third option (Hou, Chamon et al. 2007). In addition, the introduction of perpendicular electric field to double layer graphene generates a tunable band gap by creating asymmetry (Savage 2009). Figure 1.8 (a) and (b) shows the conduction and valence bands in single and double-layer graphene with no band gap. However, (c) subplot shows the separation between the conduction and valence bands which introduces a band gap due to the perpendicular electric field in the case of double-layer graphene.

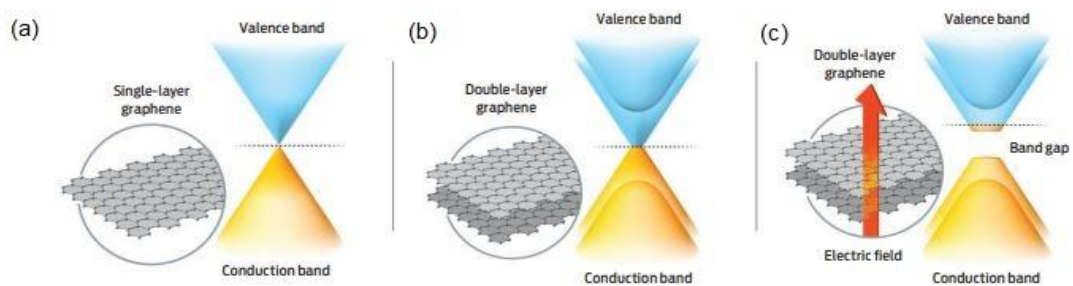


Figure 1.8 The valence and conduction bands in (a) single-layer graphene, (b) double-layer graphene and (c) double-layer graphene in the presence of perpendicular electric field (Savage 2009).

Placing graphene on a substrate makes the two sublattices in graphene unbalanced which in turn introduces a band gap (Tu, Anh et al. 2022). As an example, a small band gap at graphene's Dirac points is opened up due to lattice mismatch interface model on graphene and h-BN interface. The interlayer interaction between graphene and h-BN breaks the equivalence of the two sublattices in graphene (Zhao, Li and Zhao 2014). At the charge neutral point, a 100-300 K band gap was observed in zero twisted angle graphene/h-BN (Chen 2022). The lattices and schematic band structures of graphene, h-BN and graphene/h-BN are presented in Figure 1.9.

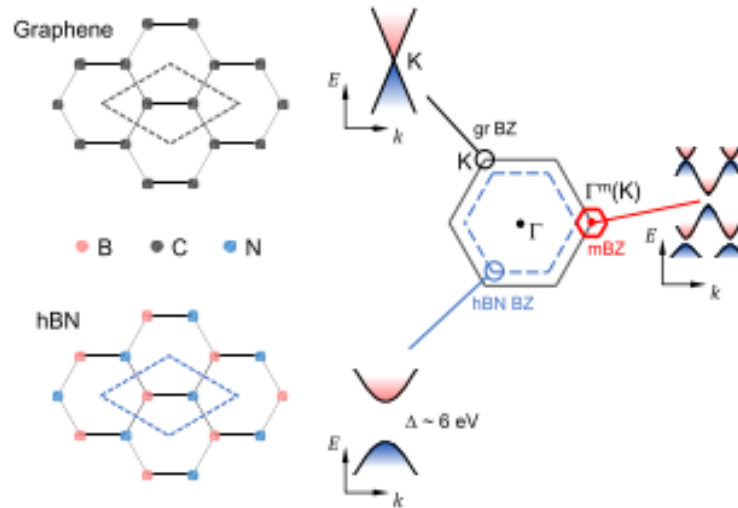


Figure 1.9 Graphene, h-BN and graphene/h-BN lattices and schematic band structures (Chen 2022).

When graphene is grown on SiC substrate, an approximately 0.26 eV energy band gap is produced (Choi, Lahiri et al. 2010). In all cases, the gap must be significantly smaller than the nearest neighbor hopping amplitude, $t \sim 2.7$ eV, in order to preserve the Dirac equation's characteristics (Hou, Chamon et al. 2007).

1.2: Problem Statement:

The enhancement of the gapped graphene is a challenge problem which have been under the focus of researchers. Recent developing trails focused on the effect of magnetic field to solve this difficulty. In this thesis we are to use a two dimensional graphene subjected to magnetic field and introduce a band gap. The presence of these two factors, external magnetic field and band gap, lead to two terms in the potential, one for each factor. The Hamiltonian of the system is well defined.

After fixing the Hamiltonian, analytical and simulation solution were used to solve the eigenvalue problem. In other words, to find the eigenenergy spectra of this system. One important step is to analyze the system statistically through the calculation of the partition function.

The electronic, thermal and magnetic properties of the system such as energy spectra, density of states, Fermi energy calculation, heat capacity, entropy, magnetization, magnetic susceptibility and Magneto Caloric Effect were considered under the influence of changing temperature, magnetic field and band gap. This was carried out using computational and analytical method. MATLAB program was used for this purpose. The findings were analyzed to determine the field of applications.

1.3: Structure of the Thesis:

This thesis is structured into four chapters, each addressing part of the study. Chapter one, Introduction provides a brief introduction about nanomaterials and graphene, physical properties of graphene, problem of statement. Chapter Two, Literature Review, review of relevant literature. Chapter Three, Methodology, states the theories of this study including Dirac Hamiltonian, Graphene Dirac Hamiltonian, Density of States Calculations, Thermal Properties Calculations, Magnetic Properties Calculations, Fermi Energy Calculations and

Simulation Approach. Chapter Four, Results, presents the simulation approach and the main computational findings about the electronic, thermal and magnetic properties of gapped graphene. Finally, Chapter Five, Discussion, summarizes the main findings, and suggests potential directions for future work.

Chapter Two: Literature Review

One work on graphene monolayer is the investigation of Landau levels associated with a uniform magnetic field and affected by the presence of another spatially modulated magnetic field. Peierl's tight-binding model was used to investigate the effects of modulation on the Landau levels. A spatially modulated magnetic field's period, strength, and direction determine graphene's magneto-electronic characteristics. The density of states exhibits a delta-function-like structure due to a robust Landau level at the Fermi level and one dimension parabolic subbands around the original Landau levels. In addition, the strength has a significant impact on the density of states and band-edge state energies. However, the period and direction have no effects (Ho, Lai et al. 2007).

Another work is the direct measurement of graphene's fermi energy using a double-layer heterostructure. In this work, the fermi energy as a function of the carrier density in mono layer graphene was probed using graphene double layer, at zero and large magnetic fields. The Fermi velocity, Landau level spacing and broadening were determined by this technique (Kim, Jo et al. 2012).

Theoretical studies on the thermodynamic properties graphene monolayer in the presence of a perpendicular magnetic field. The degeneracy of the Landau levels is lifted due to the electric modulation and converted to bands. The width of these bands oscillates with the magnetic field. Also, an analytical asymptotic expression was derived to determine the critical temperature and magnetic field for the damping of magnetic oscillations in the considered thermodynamic quantities (Nasir, Khan et al. 2009).

As a result of using Wirtinger calculus to study the characteristics of zero-energy states in monolayer graphene in the existence of circular magnetic field in Aharonov–Bohm geometry, the proof of Aharonov–Casher theorem is required (Rumyantsev, Kunavin et al. 2021).

Density functional theory was used to study the magnetic and electronic properties of armchair-hexagonal (AHEX) and zigzag-triangular (ZTRI) graphene quantum dots in the presence of alkali metals as dopants. The undoped systems were found to be stable as

confirmed by the binding energy. Despite doping lower single layer structures stability, in bilayer systems the binding energy increases. On the magnetic side, doped AHEX dots exhibit transition from diamagnetic to ferromagnetic state. Doping also affects the optical properties significantly, the gap in hexagonal flakes decreases from about 3.7 eV to 1.5 eV in the case of Na dopants in the upper position (Osman, Abdelsalam et al. 2021).

The Graphene quantum dots were found to have potential applications in energy storage systems, biomedicine and sensors. Particularly, photoluminescence (PL) and electrochemiluminescence (ECL) sensors (Kumar, Deshmukh et al. 2020).

The electronic study of a modified magnetic quantum dot, consists of magnetic fields distributed in space in an inhomogeneous way, revealed that the electron magnetic confinement arises in the plane where the value of the magnetic field inside the dot differ from outside it. Also, varying the direction of the magnetic field inside and outside the dot quietly changes the energy spectrum. For instance, taking fields of opposite directions is more interesting than the same one. In addition, introducing an electrostatic potential to the system will change the total energy spectrum and increases it. However, the magnetic quantum dots confinement disappear in case of parabolic potential (Kim, Ihm et al. 2001).

Magnetic quantum dots in graphene can be obtained either by strain-induced pseudo-magnetic field or by inhomogeneous magnetic field. Particularly, calculations for the circularly symmetric dot were done in details. The missing flux is used to determine the number of bound state that a dot has (De Martino and Egger 2010).

The dual resonance property was reported in the ballistic conductance via a quantum Hall graphene nanoribbon with magnetic quantum dot. In such magnetic quantum dot, Dirac Fermions is localized and display anisotropic eigenenergy spectra and broken time-reversal symmetry. Localized and quantum Hall edge states exhibit twofold resonances: Breit-Wigner and Fano resonances. An understanding to the twofold is completed after fitting the Fano-Breit-Wigner line shape from the double quantum dot model with the numerical results. One reason for the twofold resonance is the valley mixing that arises from the coupled system. Whereas Fano resonance has weak coupling, the Breit-Wigner resonance has strong one (Myoung, Ryu et al. 2019).

A system of many electron quantum dot was confined using a parabolic potential in the existence of a perpendicular magnetic field and single magnetic ion. From the electron-electron correlations, the energy spectrum was obtained. Also, the addition energy was calculated which displays cups as a function of the magnetic field. For large magnetic fields, composite Fermions are related to the vortex properties of the many-particle ground state wave function. In addition, the spin-pair-correlation is strongly influenced by the impurity position. However, for a small magnetic fields, a ferromagnetic-antiferromagnetic transition results from the spin-exchange energy and the Zeeman terms. Shifting a magnetic ion away from the quantum dot center leads to re-entrant antiferromagnetic-ferromagnetic-antiferromagnetic transition as a function of the Coulomb interaction strength. As a result of the thermodynamic analysis, the susceptibility and heat capacity show peaks (Nguyen and Peeters 2008).

The eigenspinors for K and K' points were determined for a magnetic quantum dot in grapheme covered by an infinite sheet of grapheme with an energy gap. Under certain conditions, the energy levels show the symmetric and anti-symmetric behaviors. The presence of an energy gap lowers the density of electrons in the quantum dot, this is an indication of electron trapping (Farsi, Belouad et al. 2020).

A semiconductor quantum dot combined with a single-layer graphene can be used to build optoelectronic devices with improved sensitivity and also can be applies in photodetector and photovoltaics. Mutual energy transfer between the quantum dots dominates the emission properties at large separation (Dutta, Kakkar et al. 2021).

It is worth mentioning that the few recent interesting theoretical studies have concentrated on the magnetic behaviors of the graphene-like quantum dots based on Monte Carlo (MC) and Effective Field Theory (EFT) simulation. It is revealed that the graphene-like quantum dots exhibit the compensation behavior, reentrant phenomena and rich hysteresis behaviors as a result of different parameters such as the exchange couplings, the crystal field, sizes and dilutions (Sun, Wang et al. 2021).

Based on the Monte Carlo simulation, the magnetic and thermodynamic behaviors of the graphene-like quantum dots described by a ferrimagnetic mixed-spin ($3/2$, $5/2$) Ising

model was investigated. The magnetization, magnetic susceptibility, internal energy and the specific heat as a function of temperature have been studied under various physical parameters. It is found that the value of the blocking temperature increases while decreasing the crystal field or increasing the exchange coupling and external magnetic field. Also, it is found that the triple-loop hysteresis behavior for certain parameters is impossible. Increasing the exchange coupling and decreasing the absolute values of the crystal field and temperature can be used to improve the area of the hysteresis loops (Dutta, Kakkar et al. 2021).

The Monte Carlo simulation was used to investigate the magnetic properties of diamond shaped graphene quantum dots by varying their sizes. The magnetizations and magnetic susceptibilities was studied with dilutions x (magnetic atom), several sizes L (carbon atom) and exchange interaction J between the magnetic atoms. The all magnetic susceptibilities have been situated at the transitions temperatures of each parameters. It is found that, the values of susceptibilities increase as the values of x , L and J increase. In addition, the effect of exchanges interactions and crystal field on the magnetization was studied. Moreover, the superparamagnetism behavior was found for a weak values of exchange interactions (Sun, Wang et al. 2021).

Works on bilayer and trilayer graphene found a band gap is induced in to the bilayer graphene's band structure by applying an electric field. In addition, an intrinsic insulated state with $2 - 3 \text{ meV}$ gap is observed in high mobility bilayer devices. However, the transition temperature of these devices is found to be $\sim 5 \text{ K}$ (Masrour and Jabar 2018). Researches on armchair graphene nanoribbons investigated that applying a perpendicular magnetic field modified its electronic properties from semiconducting to metallic states. Also, the band gap was modulated by theoretical studies (Lee, Myhro et al. 2013).

The entropy, specific heat capacity and susceptibility of quantum rings in monolayer graphene was analytically calculated using Shannon and Tsallia formalisms. Shannon entropy calculations stated the periodic behavior in the thermodynamic quantities with magnetic field. However, Tsallia calculations reveled the peak structure (Kumar, Jalil et al. 2010). Pakdel and Maleki employed the transfer matrix method and Dirac-Weyl Hamiltonian

to study the electronic transport properties of gapped graphene with a scalar potential barriers and perpendicular magnetic field (Khordad, Sedehi et al. 2022).

One thesis used the non-equilibrium Green's function formalism to study the transport properties of graphene with magnetic impurities. Also, the magneto transport properties of graphene antidote lattice under perpendicular magnetic field was investigated (Pakdel and Maleki 2024).

Theoretical and experimental studies on the intrinsic diamagnetism of graphene in order to understand the magnetic response of chiral massless fermions were developed. In this studies, comprehensive formulas to predict the variation of graphene magnetization with temperature and magnetic field were developed (Li, Chen et al. 2015).

Effective mass model and the self-consistent Born approximation were used by Koshino and Ando to study the magnetization of graphene monolayer in the presence of the disorder (Koshino and Ando 2007). Even in the disorder, the susceptibility has a long tail proportional to the inverse of the Fermi energy and a prominent diamagnetic peak at zero energy (Koshino and Ando 2007).

Fukuyama and Kubo obtained a chemical potential diamagnetism in graphene taking the interband effect into consideration (Fukuyama and Kubo 1969). The Landau levels of graphene in a magnetic field was figured out by McClure. In addition, he derived the susceptibility of graphene at high temperature limit (McClure 1956). Raoux et al. derived the zero- temperature susceptibility of graphene and showed that the electron Berry phase has critical role in the orbital magnetism of graphene (Raoux, Morigi et al. 2014)

The Monte Carlo simulation was employed to probe into the magnetic behaviors and magnetocaloric effect of the nano-graphene bilayer (Sun, Wang et al. 2021). In addition, the oscillating magnetocaloric effect of a multilayer graphene in Bernal and rhombohedral stacking was investigated to expand the understanding of the effect on a single layer graphene (Alisultanov, Paixao et al. 2014).

Chapter Three: Methodology

3.1: Dirac Hamiltonian

In relativistic quantum theory, the energy of a particle is described by quantum mechanical operator called Dirac Hamiltonian. This energy is derived from Dirac equation, which was constructed by Pauli Dirac to treat quantum mechanical problems and special relativity.

The expression for Dirac Hamiltonian operator (\hat{H}) (Schwabl 2008):

$$\hat{H} = c\boldsymbol{\alpha} \cdot \hat{\mathbf{p}} + \beta mc^2 \quad (3.1.1)$$

Where:

c : is the speed of light

$\hat{\mathbf{p}}$: is the momentum operator ($\hat{\mathbf{p}} = -i\hbar\nabla$)

$\boldsymbol{\alpha}$ and β : are 4×4 Dirac matrices

m : is the rest mass of the particle

The Dirac matrices are defined in terms of Pauli matrices ($\boldsymbol{\sigma}$) and the 2×2 identity matrix (\mathbf{I}) as follows (Sakurai and Napolitano 2020):

$$\boldsymbol{\alpha} = \begin{pmatrix} 0 & \boldsymbol{\sigma} \\ \boldsymbol{\sigma} & 0 \end{pmatrix} \quad (3.1.2)$$

$$\beta = \begin{pmatrix} \mathbf{I} & 0 \\ 0 & -\mathbf{I} \end{pmatrix} \quad (3.1.3)$$

In case of massless particles, where the second term (βmc^2) in the Hamiltonian expressed in equation 3.1.1 goes to zero, the Dirac Hamiltonian reduced from quadratic to linear expression. In other words, the particle momentum is dominant in the energy determination rather than its rest mass.

3.2: Graphene Dirac Hamiltonian

In graphene Brillouin zone, the dispersion relation near the Dirac points is linear. As a result, its electronic properties are characterized by massless Dirac Fermions. The Dirac Hamiltonian for graphene can be written as below (Gu 2011):

$$\hat{H} = v_F(\boldsymbol{\sigma} \cdot \mathbf{p}) \quad (3.2.1)$$

Where v_F is the Fermi velocity in graphene

Substituting this Hamiltonian in Dirac equation (Thaller 2013):

$$\hat{H}\psi = E\psi \quad (3.2.2)$$

ψ is the spinor wave function composed of two components (ψ_A, ψ_B), each represents the amplitude of the electron on one sublattice (A or B) in graphene lattice, respectively.

$$\psi = \begin{pmatrix} \psi_A \\ \psi_B \end{pmatrix} \quad (3.2.3)$$

E is the energy or the eigenvalues corresponds to the eigenvector ψ .

As an extension to the Hamiltonian in equation 2.2.1, the electronic single particle Hamiltonian of gapped graphene in the presence of perpendicular magnetic field, $\mathbf{B} = (0, 0, B)$ can be represented by (Tu, Anh et al. 2022):

$$\hat{H} = v_F(\sigma_x \pi_x + \tau \sigma_y \pi_y) + \Delta \sigma_z \quad (3.2.4)$$

The Pauli matrices are defined as follows (Adewuyi and Lau 2021):

$$\sigma_x = \begin{pmatrix} 0 & 1 \\ 1 & 0 \end{pmatrix} \quad (3.2.5)$$

$$\sigma_y = \begin{pmatrix} 0 & -i \\ i & 0 \end{pmatrix} \quad (3.2.6)$$

$$\sigma_z = \begin{pmatrix} 1 & 0 \\ 0 & -1 \end{pmatrix} \quad (3.2.7)$$

Whereas the canonical momentum $\pi = (p + eA)$, $\tau = \pm 1$ for K, K' valleys, respectively. Δ is the energy gap.

The eigenvalues and the eigenvectors corresponding to the previous Hamiltonian are obtained by solving the associated eigenvalue problem. Specifically, the eigenenergies for n greater than zero are (Tu, Anh et al. 2022):

$$E_\eta \equiv E_{n,p} = p[n(\hbar\omega_c)^2 + (\Delta/2)^2]^{1/2} = pE_n \quad (3.2.8)$$

Where p takes the values ± 1 for conduction and valance bands, respectively. Besides, n stands for the landau levels and takes the values $0, 1, 2, 3, \dots$. The cyclotron frequency is $\omega_c = v_F \sqrt{2}/\alpha_c$ with $v_F = 1.06 \times 10^6 \text{m/s}$ and $\alpha_c = (\hbar/eB)^{1/2}$.

The obtained discrete energy levels are due to the occurrence of Landau quantization in the presence of a magnetic field. It's worth noting that the landau levels associated with the K and K' valleys are degenerate. Also, the different spin states at a particular landau level have the same energy. In conclusion, graphene energy spectrum result from Eq. 3.2.8 is valley and spin degenerates.

The eigenfunctions $|\eta\rangle$ corresponding to E_η can be expressed as (Tu, Anh et al. 2022):

$$|\eta\rangle = \frac{1}{\sqrt{L_y}} \psi_{n,p}(x) e^{ik_y y} \quad (3.2.9)$$

Where

$$\psi_{n,p}^K(x) = \begin{pmatrix} A_{n,p} \phi_{n-1}(x - x_0) \\ ipB_{n,p} \phi_n(x - x_0) \end{pmatrix} \quad (3.2.10)$$

$$\psi_{n,p}^{K'}(x) = \begin{pmatrix} pB_{n,p} \phi_n(x - x_0) \\ iA_{n,p} \phi_{n-1}(x - x_0) \end{pmatrix} \quad (3.2.11)$$

Here, $\phi_{n,p}(x - x_0)$ represent the one dimensional oscillator functions with the center $x_0 = \alpha_c^2 k_y$, and $A_{n,p}$, $B_{n,p}$ are normalization coefficients such that:

$$A_{n,p} = \sqrt{\frac{pE_n + \Delta/2}{2pE_n}} \quad (3.2.12)$$

and

$$B_{n,p} = \sqrt{\frac{pE_n - \Delta/2}{2pE_n}} \quad (3.2.13)$$

For the zeroth Landau level, the eigenvalue for the energy $E_{0,p} = -\tau(\Delta/2)$ can be obtained by substituting $n = 0$ in Eq. 3.2.8. For the K point, this energy locates in the valance band. However, it locates in the conduction band for the K' point. The eigenfunctions associated with this level are $\phi_{0,p}(x) = (0 \quad \phi_0)^T$.

3.3: Density of States calculations

Density of states (*DOS*) refers to the number of available electronic states at each energy level within a material. Also, it can be used to analyze its electronic structure. The density of states is given by (Tu, Anh et al. 2022):

$$DOS(E) = \frac{g_s}{2\pi\alpha_c^2} \sum_{n,p,\tau} \delta(E - E_n) \quad (3.3.1)$$

Where:

g_s : is the spin degeneracy and represents the number of states that corresponds to E_n ($g_s = 2$).

$\delta(E - E_n)$: is the Dirac delta function centered at the energy E_n .

In numerical calculation, the density of states is expressed in terms of Gaussian distribution (Gammag and Villagonzalo 2012):

$$DOS(E) = \frac{1}{\sqrt{2\pi}\Gamma^2} \sum_{n,p,\tau} \exp\left(-\frac{(E - E_n)^2}{2\Gamma^2}\right) \quad (3.3.2)$$

Such that Γ indicates the broadening of the energy levels.

3.4: Thermal Properties calculations

In the domain of statistical mechanics, the average energy (\overline{E}) for a physical system, such as graphene in a magnetic field, is typically expressed in terms of the partition function Z . The partition function encapsulates information about the system's thermodynamics, with average energy being mathematically defined as (Arora, Gupta et al. 2023):

$$Z = \sum_n e^{-\beta E_n} \quad (3.4.1)$$

Where E_n signifies the energy of the n-th state, and the summation spans all possible states. The expression for the average energy can be written as (Elsaid, Shaer et al. 2020):

$$\langle \bar{E} \rangle = -\frac{1}{Z} \frac{\partial Z}{\partial \beta} \quad (3.4.2)$$

Such that $\beta = \frac{1}{k_B T}$ is the inverse of the temperature, with k_B being the Boltzmann constant and T is the temperature in Kelvin.

This average energy can be used to calculate thermal physical quantities of the system as specific heat capacity, entropy and the change in entropy. In particular, the specific heat capacity (C_v) is a material property that reflects how it absorbs and stores thermal energy. Mathematically, it can be calculated as the derivative of (\bar{E}) with respect to temperature as follows (Arora, Gupta et al. 2023), (Sedehi and Khordad 2021) and (Khordad and Sedehi 2018):

$$C_v = \frac{\partial \langle \bar{E} \rangle}{\partial T} \quad (3.4.3)$$

Here (\bar{E}) is the total average energy of charge carriers, electrons and holes. Calculations of (C_v) provides a measurement of the thermal response of the material. In particular, higher values of (C_v) means that higher energy is required to raise the material temperature. In addition, the value of (C_v) is an indicator of thermal stability. For instance, materials with smaller (C_v) values exhibit less stability in temperature for a given amount of heat compared with materials with (C_v) higher values. In other words, materials with small value of (C_v) reveal fast temperature change.

The degree of disorder or randomness in a system is described by entropy (S). The expression used to calculate the entropy is (Arora, Gupta et al. 2023), (Sedehi and Khordad 2021) and (Khordad and Sedehi 2018):

$$S = k_B \ln(Z) - k_B \beta \frac{\partial Z}{\partial \beta} \quad (3.4.4)$$

This relation connects the entropy with the partition function and temperature. In general, entropy describes how energy is distributed among the microstates of the system at a given value of temperature. According to the 2nd law of thermodynamics, the entropy of a isolated system increases with time. In addition, entropy is a connection between the macroscopic and microscopic properties of the system.

3.5: Magnetic Properties Calculations

Magnetic properties of a material is determined by its interaction with an external magnetic field (B). Application of a magnetic field affects the energy levels of charge carriers and as a result the total average energy of the system. Magnetization (M) is a quantitative expression for the relation between this change in energy and the magnetic field. It can be obtained through the following expression (Elsaid, Shaer et al. 2020):

$$M = - \frac{\partial(\bar{E})}{\partial B} \quad (3.5.1)$$

Another quantity that can be used for magnetic classification of materials is the magnetic susceptibility (χ). It can be calculated as follows (Elsaid, Shaer et al. 2020):

$$\chi = \frac{\partial M}{\partial B} \quad (3.5.2)$$

According to the magnitude and sign of (χ), materials are classified into paramagnetic, ferromagnetic and diamagnetic. Small and positive values of (χ) indicates that the material is paramagnetic. While, large and positive values means that the material is ferromagnetic. Meanwhile, negative values are related to diamagnetic materials.

It is significant to calculate the change in entropy (ΔS) of a system as the magnetic field (B) changes from zero to a non-zero value, while the temperature (T) remains constant.

The following relation is used to calculate (ΔS) (Arora, Gupta et al. 2023), (Sedehi and Khordad 2021) and (Khordad and Sedehi 2018) :

$$\Delta S = S(B, T) - S(0, T) \quad (3.5.3)$$

The entropy change ($-\Delta S$) can be used to observe the thermal response of a magnetic material to an applied magnetic field through the Magneto Caloric Effect (MCE). In this effect, materials change heat through a temperature change (ΔT) in an adiabatic process. In summary, the MCE is characterized by two quantities, the change in entropy and change in temperature. The MCE's primary use is in magnetic refrigeration, which was first proposed in the late 1920s using adiabatic demagnetization (Alisultanov, Paixao et al. 2014). Materials with some magnetic order have stronger MCE (Li, Nishimura et al. 2008).

3.6: Fermi Energy Calculations

At absolute temperature T , the Fermi-Dirac distribution function $f(E)$ is defined as the probability of finding the electron at certain level. The mathematical expression of this distribution is given by (Roduner 2006):

$$f(E) = \left[\frac{\exp(E - \mu)}{k_B T} + 1 \right]^{-1} \quad (3.6.1)$$

Where μ is the chemical potential. At zero Kelvin the chemical potential equals the fermi energy (E_F). The probability of finding an electron at energy higher than the fermi level is zero. However, the probability of finding an electron at energy less than the fermi energy is equal to 1.

And the electron density (n_e) is given by (Roduner 2006):

$$n_e = \int_0^{\infty} dE \text{DOS}(E) f(E) + \int_{-\infty}^0 dE \text{DOS}(E) [1 - f(E)] \quad (3.6.2)$$

3.7: Simulation Approach

This section focuses on the computational method applied to the study of graphene's electronic, thermal and magnetic properties in the presence of a magnetic field. The analysis of these properties was performed using MATLAB. These properties including the energy spectra, density of states, fermi energy calculations, partition function, average energy, specific heat capacity, entropy, change in entropy, magnetization and magnetic susceptibility were all numerically determined using MATLAB scripts. Calculations involves a three values of the band gap and a range of temperatures and magnetic field strengths.

The first step in the numerical analysis was defining the input parameters. These parameters include the constants, material properties, the band gap values, temperature and magnetic field ranges. Figure 3.1 shows an image of the MATLAB script with theses parameters and their values in detail.

Creating a loop structure in MATLAB to cycle over the specified ranges of temperature and magnetic field is the next step. the partition function and related thermodynamic quantities were computed for every combination of temperature T and magnetic field B . For each of the three bandgap values, this procedure was repeated.

```

% Derived constants and conversions
nm = 1E-9 * m;           % Conversion factor for nanometers to meters
eV = 1.60218E-19 * J;    % Conversion factor for electronvolts to Joules
mass_e = 9.10938E-31 * kg; % Electron mass in kilograms
h_bar = (6.62607E-34) / (2 * pi) * (J * sec); % Reduced Planck constant
charge_e = 1.6E-19 * coulomb; % Elementary charge in Coulombs
% Material properties
p1 = 1;                  % Charge carrier type for conduction band
p2 = -1;                 % Charge carrier type for valence band
vf = 1.06 * 10^6;       % Fermi velocity in meters per second

% Physical constant
kB = 8.61733326 * 10^-5; % Boltzmann constant in eV per Kelvin

% Define range of magnetic field values (Tesla) and Landau levels (n)
B_range = [0:0.001:10];
n_max = 30;

% Define range of Bandgap range (eV)
delta_values = [0, 53e-3, 106e-3];

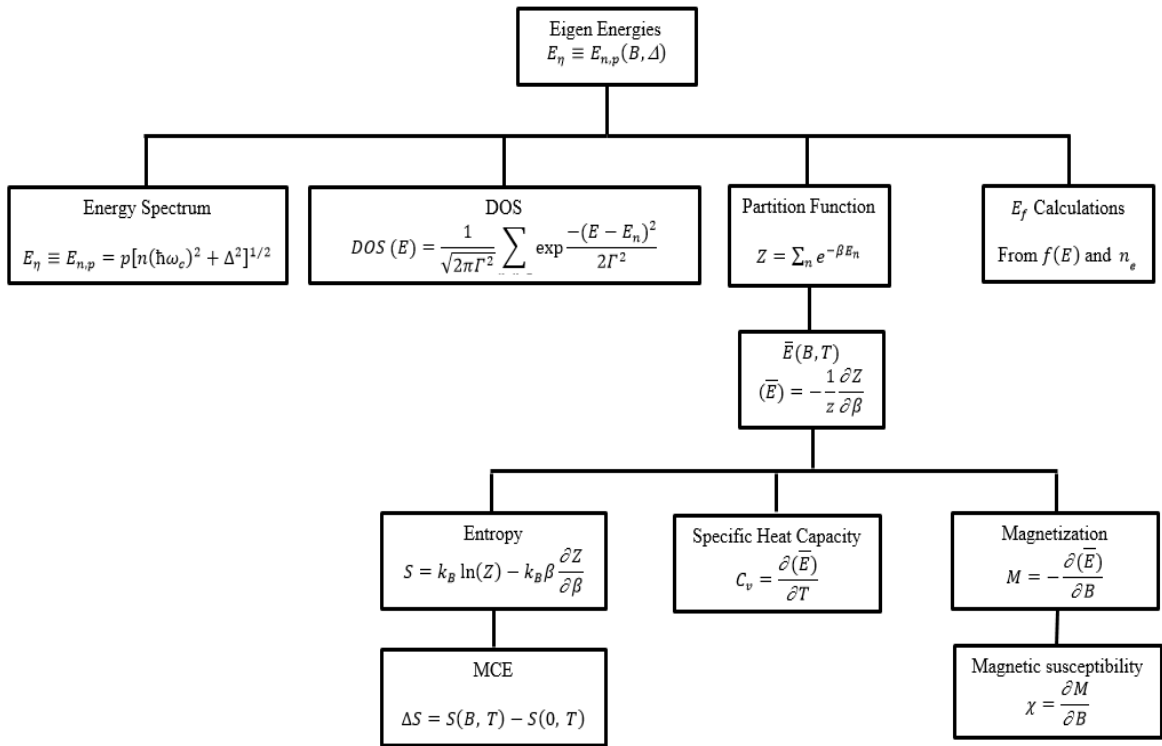
% Define temperature range
T_range = [0:1:300];

```

Figure 3.1 MATLAB image showing the parameters used in this thesis.

Figure 3.2 shows a flow chart of the problem where the eigenenergies were used to plot the energy spectrum, calculate the density of states and fermi energy for the three values of the band gap. In addition, the average energy of charge carries in graphene were determined from the partition function in order to calculate the magnetic and thermal properties of gapless and gapped graphene at different values of the magnetic field strength and temperature.

The relations used for the calculations is presented in the figure. For example, the specific heat capacity was computed by using the temperature derivative of the average energy. In addition, average energy and partition function was used to calculate the entropy. Magnetization was obtained by differentiating the average energy with respect to the magnetic field. However, magnetic susceptibility was calculated by differentiating the magnetization with respect to the magnetic field.



3.2 Flow chart of the problem.

Chapter Four: Results

In this chapter, graphene response to magnetic field, temperature and varying band gap values ($\Delta = 0, 53, \text{ and } 106 \text{ meV}$) will be investigated. The focus is on analyzing key properties including energy spectra, density of states, Fermi-energy calculation, average energy calculations, specific heat capacity, entropy, entropy changes, magnetization and susceptibility.

4.1: Electronic Properties

In this section, the electronic properties of gapless and gapped graphene will be displayed including the energy spectra, the density of states and Fermi-energy calculations.

4.1.1: Energy spectra

Figure 4.1 illustrates the energy spectra of electrons and holes in non-gapped graphene as a function of the magnetic field strength (B) in Tesla (T). The vertical axis represents the energy (E) in electron volts (eV). The five lower curves correspond to Landau levels ($n = 1$ to 5) within the valence band (VB), while the upper curves represent Landau levels ($n = 1$ to 5) within the conduction band (CB). The intermediate blue line is corresponding to ($n = 0$) Landau level, which is common for the conduction and valence bands. It is located at the Dirac point where the two bands overlap. In addition, this level is independent of the field strength. Other Landau levels are symmetric around the zero level. For every Landau level in the conduction band, there is a symmetric level in the valence band.

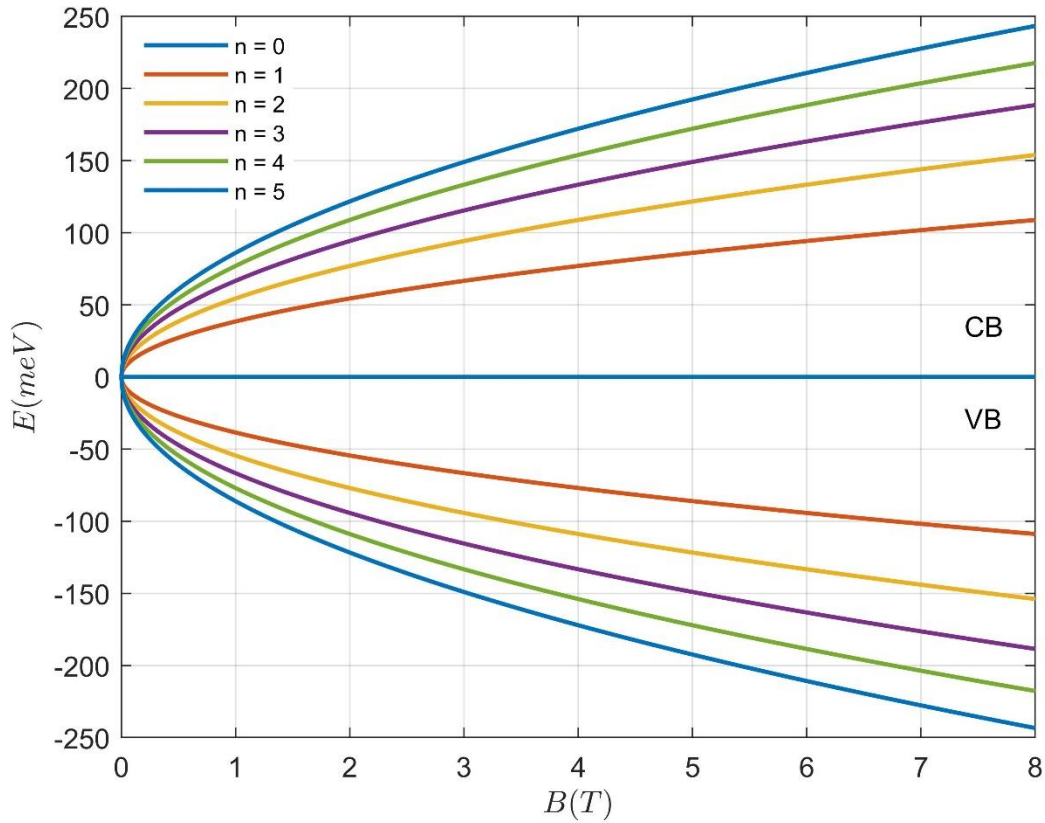


Figure 4.1 Energy levels of gapless graphene as a function of magnetic field for different Landau levels.

The introduction of a band gap: $\Delta = 53 \text{ meV}$ effect on graphene Landau levels (LL) is presented in Figure 4.2. As the figure shows, the ($n = 0$) LL is splitting in to two lines, one is shifted upward by 26.5 meV in the conduction band while the other is shifted downward by -26.5 meV in the valence band. This shift affects the entire spectrum of energy levels, encompassing both the valence and conduction bands. Similar to non-gapped graphene, LL are symmetric in the conduction and valence bands. In addition, the zeroth Landau levels exhibit no magnetic field dependency.

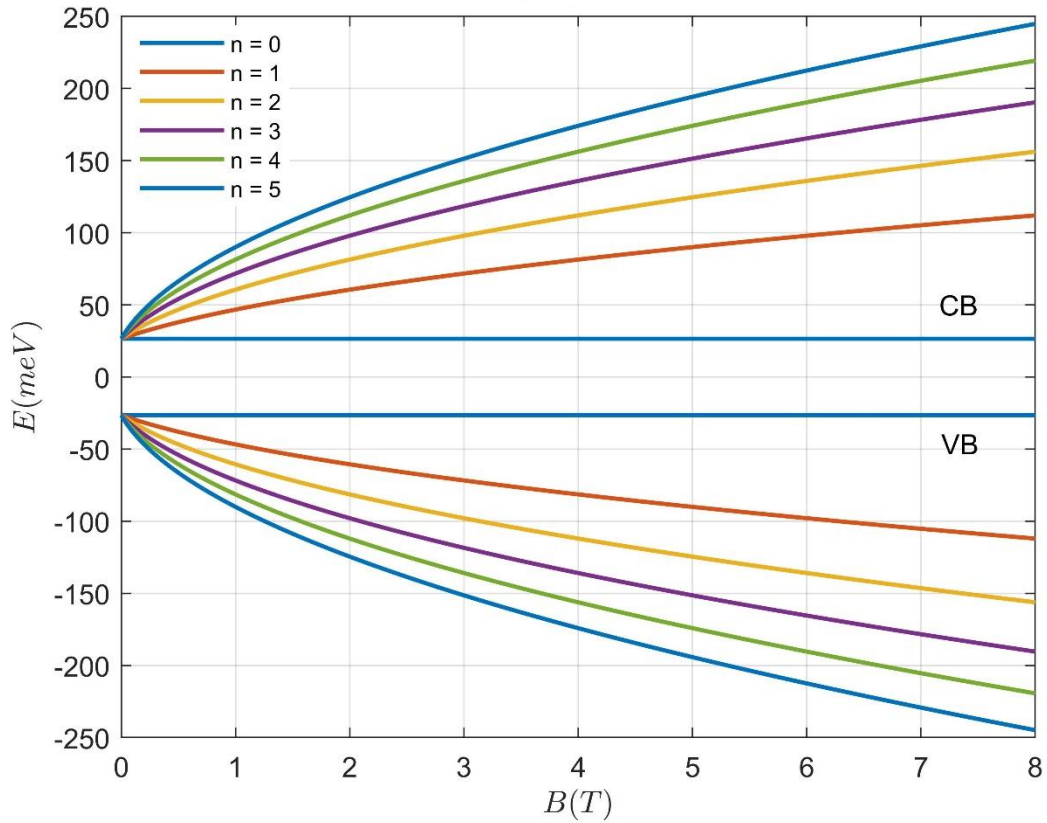


Figure 4.2 Energy levels of gapped graphene, $\Delta= 53 \text{ meV}$, as a function of magnetic field for different Landau levels.

Increase the band gap to $\Delta= 106 \text{ meV}$ has similar effects on the energy spectra. For instance, the presence of this gap maintain the symmetry in the levels. However, the zeroth LLs are vertically displaced by $\pm \frac{\Delta}{2}$ for the conduction and valence bands, respectively. The introduction of band gap: $\Delta= 106 \text{ meV}$ effect on graphene Landau levels (LL) is presented in Figure 3.5. Notably, as (Δ) increases, the energy levels in both bands displace such that they no longer intersect at zero energy.

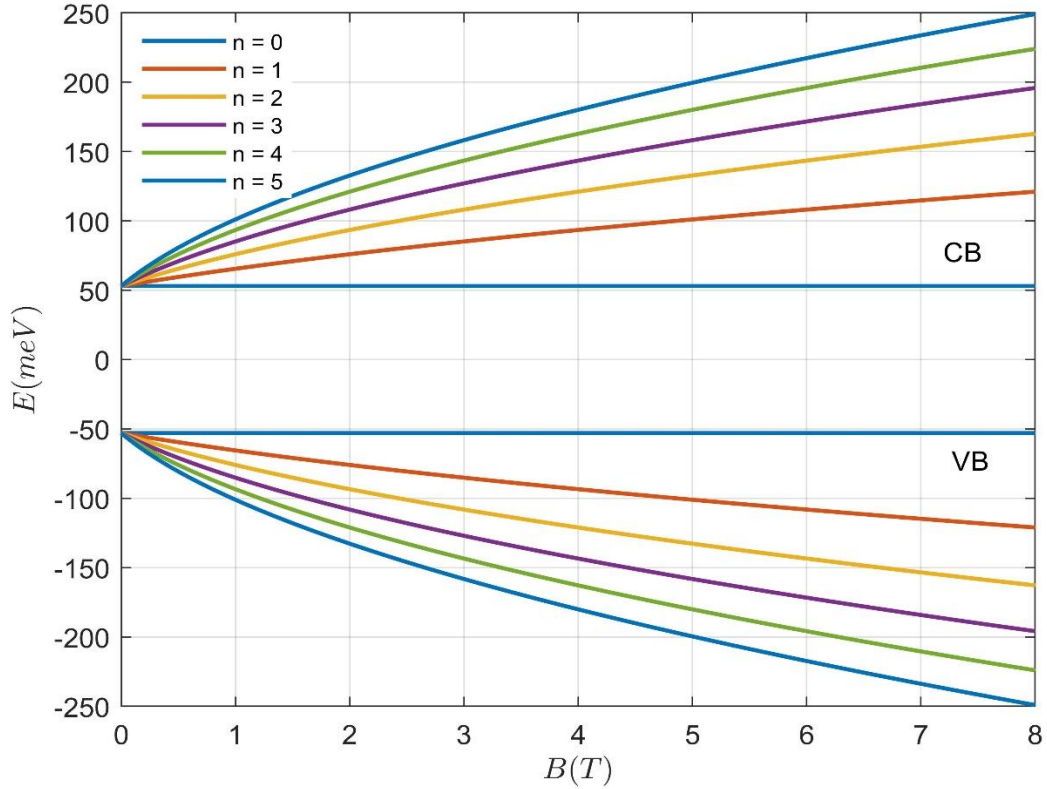


Figure 4.3 Energy levels of gapped graphene, $\Delta = 106 \text{ meV}$, as a function of magnetic field for different Landau levels.

Across all Figures, 4.1, 4.2 and 4.3, the energy levels for electrons and holes in graphene display an absolute increase with increasing magnetic field strength for all Landau levels and band gap values. This trend reflects the theoretical quantization of Landau levels in graphene under the effect of perpendicular magnetic field. According to equation 3.2.8, $E_{n,p} = p[n(\hbar\omega_c)^2 + (\Delta/2)^2]^{1/2} = pE_n$, the energy of LLs in graphene rise with increasing B , reflecting the growing energy separation ($\Delta E_{n+1,n} = E_{n+1}(B) - E_n(B)$) between the levels as the magnetic field strength increases. This energy separation is calculated at three different magnetic field strengths and presented in Table 4.1, 4.2 and 4.3 for gapless and gapped graphene. Across all tables, calculating ($\Delta E_{n+1,n}$) at $B = 6 \text{ T}$ reveals higher energy separation than $B = 4 \text{ T}$ and $B = 2 \text{ T}$ for different Landau levels.

Table 4.1 Energy separation between different Landau levels of gapless graphene at different magnetic field strengths.

$\Delta = 0 \text{ meV}$			
	$B = 2T$	$B = 4T$	$B = 6T$
$ \Delta E_{1,0} $	54.427 meV	76.971 meV	94.270 meV
$ \Delta E_{2,1} $	22.544 meV	31.883 meV	39.048 meV
$ \Delta E_{3,2} $	17.299 meV	24.464 meV	29.963 meV
$ \Delta E_{4,3} $	14.584 meV	20.624 meV	25.260 meV
$ \Delta E_{5,4} $	12.848 meV	18.170 meV	22.254 meV

Table 4.2 Energy separation between different Landau levels of gapped graphene, $\Delta = 53 \text{ meV}$, at different magnetic field strengths.

$\Delta = 53 \text{ meV}$			
	$B = 2T$	$B = 4T$	$B = 6T$
$ \Delta E_{1,0} $	34.035 meV	54.905 meV	71.424 meV
$ \Delta E_{2,1} $	20.869 meV	30.627 meV	38.002 meV
$ \Delta E_{3,2} $	16.518 meV	23.893 meV	29.490 meV
$ \Delta E_{4,3} $	14.109 meV	20.280 meV	24.976 meV
$ \Delta E_{5,4} $	12.520 meV	17.934 meV	22.060 meV

Table 4.3 Energy separation between different Landau levels of gapped graphene, $\Delta = 106 \text{ meV}$, at different magnetic field strengths.

$\Delta = 106 \text{ meV}$			
	$B = 2T$	$B = 4T$	$B = 6T$
$ \Delta E_{1,0} $	22.969 meV	40.453 meV	55.147 meV
$ \Delta E_{2,1} $	17.484 meV	27.617 meV	35.319 meV
$ \Delta E_{3,2} $	14.693 meV	22.395 meV	28.200 meV
$ \Delta E_{4,3} $	12.923 meV	19.343 meV	24.180 meV
$ \Delta E_{5,4} $	11.671 meV	17.277 meV	21.507 meV

In addition, higher Landau levels ($n = 3, 4,$ and 5) within each band (valence or conduction) exhibit a steeper slope in energy versus magnetic field strength compared to lower levels ($n = 0, 1,$ and 2) at the same band gap value. This behavior result from the theoretical prediction that $(\Delta E_n = E_n(B_2) - E_n(B_1))$ between Landau levels grows with \sqrt{nB} , leading to more significant shifts for higher index levels. In this context, a steeper slope indicates that the energy of higher Landau levels increases more rapidly with increasing magnetic field strength compared to lower Landau levels. This behavior is clear in Table 3.4- Table 3.6, where the absolute energy differences between $B_2 = 4T$ and $B_2 = 2T$, $(\Delta E_n = E_n(B_2 = 4T) - E_n(B_1 = 2T))$, is calculated for gapless and gapped graphene monolayer. As indicated in the tables, the energy difference results from increasing the magnetic field strength is larger in the case of $n=5$ compared to less n values.

Table 4.4 Energy differences between $B = 4T$ and $B = 2T$ of gapless graphene for different landau levels.

$\Delta = 0 \text{ meV}$			
n	$ E_n(B = 2T) $	$ E_n(B = 4T) $	$ E_n(B = 4T) - E_n(B = 2T) $
0	0 meV	0 meV	0 meV
1	54.427 meV	76.971 meV	22.544 meV
2	76.971 meV	108.854 meV	31.883 meV
3	94.270 meV	133.318 meV	39.048 meV
4	108.854 meV	153.943 meV	45.089 meV
5	121.702 meV	172.113 meV	50.411 meV

Table 4.5 Energy differences between $B = 4T$ and $B = 2T$ of gapped graphene, $\Delta = 53 \text{ meV}$ for different landau levels.

$\Delta = 53 \text{ meV}$			
n	$ E_n(B = 2T) $	$ E_n(B = 4T) $	$ E_n(B = 4T) - E_n(B = 2T) $
0	26.500 meV	26.500 meV	0 meV
1	60.535 meV	81.405 meV	20.870 meV
2	81.405 meV	112.033 meV	30.628 meV
3	97.924 meV	135.926 meV	38.002 meV
4	112.033 meV	156.207 meV	44.174 meV
5	124.554 meV	174.141 meV	49.587 meV

Table 4.6 Energy differences between $B = 4T$ and $B = 2T$ of gapped graphene, $\Delta = 106 \text{ meV}$ for different Landau levels.

$\Delta = 106 \text{ meV}$			
n	$ E_n(B = 2T) $	$ E_n(B = 4T) $	$ E_n(B = 4T) - E_n(B = 2T) $
0	53.000 meV	53.000 meV	0 meV
1	75.969 meV	93.454 meV	17.485 meV
2	93.454 meV	121.071 meV	27.617 meV
3	108.147 meV	143.467 meV	35.320 meV
4	121.071 meV	162.811 meV	41.740 meV
5	132.742 meV	180.089 meV	47.347 meV

The previous results are in consistent with the experimental studies on graphene/born-nitride heterostructures. Experiment have shown that the detected energies of graphene/born-nitride exhibit an approximate linear dependence on \sqrt{B} . In addition, these energies exhibit a non-zero energy at zero magnetic field. The observed transitions between Landau levels (T_i) are represented in Figure 4.4 These transitions confirm the Landau level formation in gapped graphene (Chen, Shi et al. 2014). Another experimental study of infrared spectroscopy to investigate Landau levels in graphene confirmed the linear relation between \sqrt{B} and the energy of graphene (Jiang, Henriksen et al. 2007).

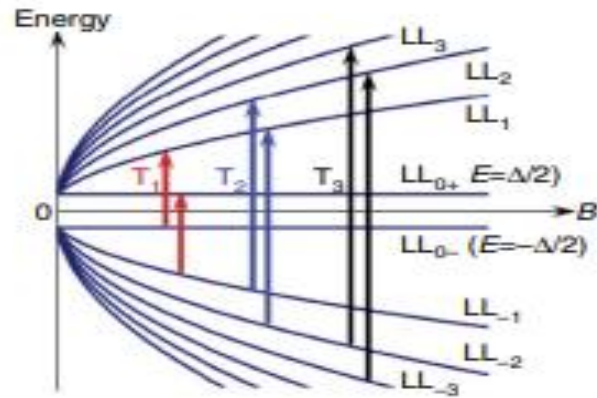


Figure 4.4 Schematic of LLs of gapped graphene. The arrows represent the observed transition (Chen, Shi et al. 2014)

4.1.2: Density of States

The density of states (DOS) of gapless graphene, $\Delta = 0 \text{ meV}$, is calculated and plotted in Figure 4.5 at two different values of the magnetic field strength: (a) $B = 0.5 \text{ T}$ and (b) $B = 3 \text{ T}$. As the figure displays, the DOS appears as a series of delta functions or Gaussian-like peaks, reflecting the discrete Landau levels results due to the presence of the magnetic field. The electron-hole symmetry observed in the energy spectrum is reflected in the density of states. In addition, the presence of the zeroth LL at zero energy leads to non-zero density of state at this energy. Notably, the space between peaks increases as the field's strength increases from 0.5 T to 3 T . As a result, the peaks are more pronounced in the case of higher fields. In a certain range of magnetic field, the number of peaks in the DOS spectrum reduces as the magnetic field increased from 0.5 T to 3 T . This reduction is due to the more spaced LLs at higher fields.

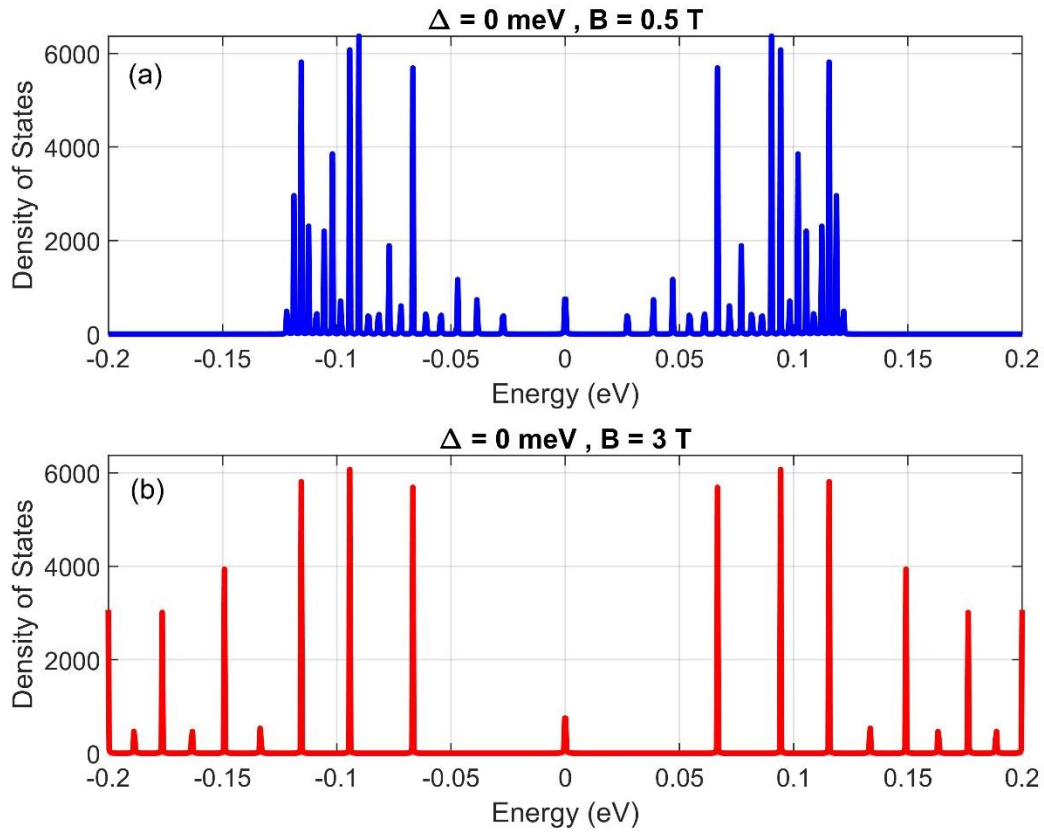


Figure 4.5 The density of states of gapless graphene at a uniform magnetic fields of (a) $B = 0.5 \text{ T}$ and (b) $B = 3 \text{ T}$ as a function of energy at $n=20$.

The density of states of gapped graphene, $\Delta = 53 \text{ meV}$, under the effect of magnetic field is plotted in Figure 4.6. It displays similar trend to that observed in the non-gapped graphene. Including, the effect of increasing magnetic field on the spacing between peaks. However, there are changes due to the band gap introduction as the absence of the zero energy peak. Moreover, comparing the DOS for gapless and 53 meV gap graphene under 0.3 T magnetic field, reveals that peaks are shifted toward higher positive and negative energy values.

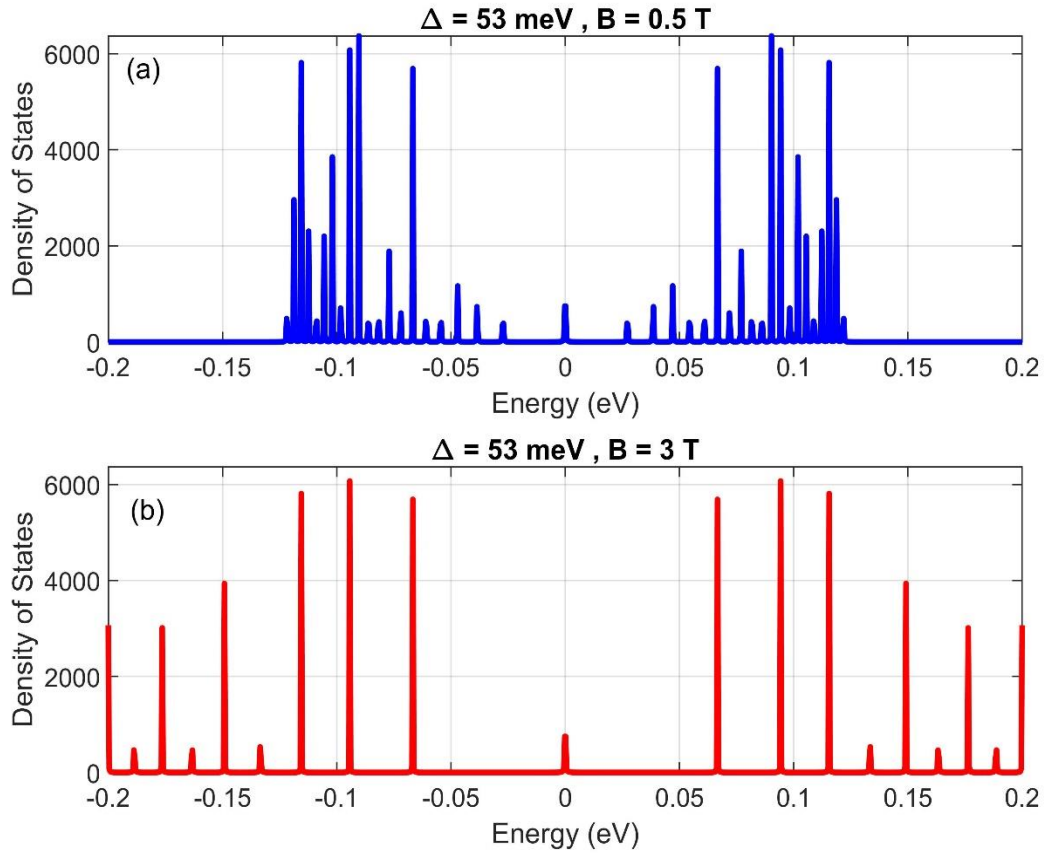


Figure 4.6 The density of states of gapped graphene, $\Delta = 53 \text{ meV}$, at a uniform magnetic fields of (a) $B = 0.5 \text{ T}$ and (b) $B = 3 \text{ T}$ as a function of energy at $n=20$.

A further increase in the band gap to $\Delta = 106 \text{ meV}$ effects on the DOS is pictured in Figure 4.7. As clear from this figure, the DOS at zero energy vanishes and remains zero up to the values of $\pm \frac{\Delta}{2}$, creating a pseudo-gap in the density of states. One can notice from Figure 4.8 that this larger gap causes a more significant shift in the peak positions compared to the 53 meV gap and gapless graphene. In general, band gaps alter the absolute positions of the DOS peaks, but they do not break the symmetry. It's worth noting that, the DOS at all magnetic field strengths and bandgap values is calculated taking into account constant number of Landau levels, up to $n=20$.

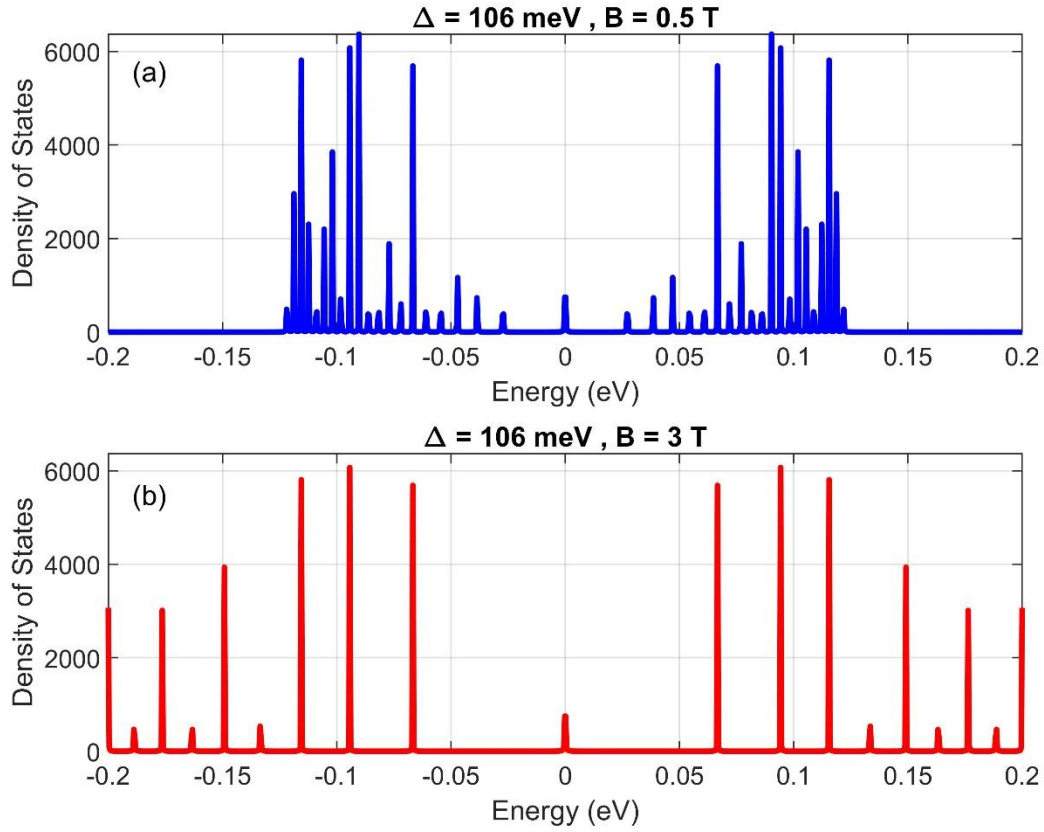


Figure 4.7 The density of states of gapped graphene, $\Delta = 106 \text{ meV}$, at a uniform magnetic fields of (a) $B = 0.5 \text{ T}$ and (b) $B = 3 \text{ T}$ as a function of energy at $n=20$.

Figure 4.8 shows the density of states versus energy for gapless and gapped graphene considering 20 LLs in the calculations at $B = 0.3 \text{ T}$. The effect of band gap introduction on the DOS is very clear especially at zero energy. As presented, $\Delta = 53 \text{ meV}$ leads to a pseudo gap in the DOS, no peaks, ranging from -26.5 meV to 26.5 meV in the energy-axis. However, this gap extends from -53 meV to 53 meV in the case of $\Delta = 106 \text{ meV}$. In general, the pseudo gap in the DOS width rang from $-\Delta/2$ to $+\Delta/2$. The number of peaks in gapped graphene is larger than that of non-gapped graphene by one peak, which is related to the splitting of the zero energy peak

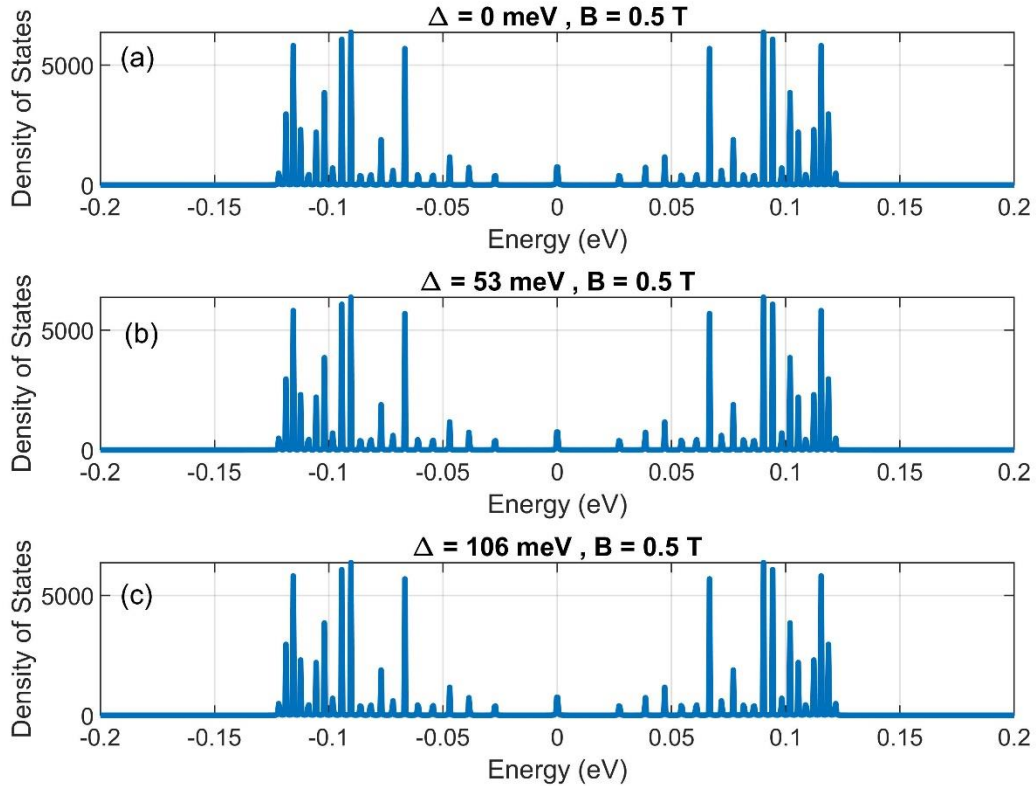


Figure 4.8 The density of states of graphene in a uniform magnetic field of 0.5 T as a function of energy for different values of the band gap, (a) $\Delta = 0 \text{ meV}$, (b) $\Delta = 53 \text{ meV}$ and (c) $\Delta = 106 \text{ meV}$ and $n=20$.

Another significant issue to study, is the effect of the number of Landau levels on the density of states. As appear from Figure 4.9, the DOS of non-gapped graphene versus energy is plotted at two different numbers of LLs: (a) $n=5$ and (b) $n=20$. Higher number of Landau levels give rise to more pronounced peaks in the same energy range. According to subplot (a), the number of peaks is five peaks in each side of the energy range plus one peak appears due to the 0 LL. At the same value of the magnetic field but with $n = 20$, the number of peaks rises to 20 in addition to the zeroth LL peak, as in (b) subplot.

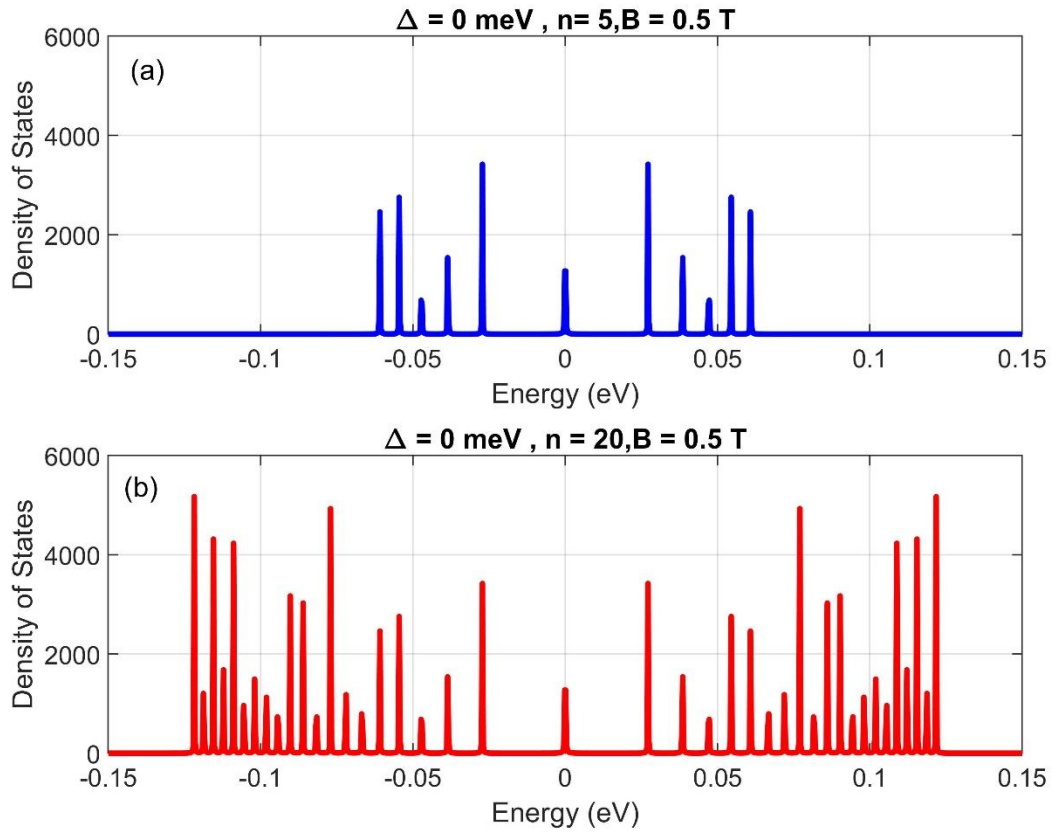


Figure 4.9 The density of states of gapless graphene, $\Delta = 0 \text{ meV}$, at a uniform magnetic fields of $B = 0.5 \text{ T}$ (a) $n = 5$ and (b) $n = 20$ as a function of energy.

The presence of $\Delta = 53 \text{ meV}$ gap in graphene effect on the density of states is represented in Figure 4.10. Two subplots are plotted at the same value of $B = 0.5 \text{ T}$, but with different n values: (a) $n = 5$ and (b) $n = 20$. As before, including higher states in to the DOS calculations leading to the appearance of more peaks. The number of peaks is related to n value. Taking into account the effect of the gap introduction on the 0 LL peak, the number of peaks in each side of the energy range is equal to $n + 1$. As presented in (a) subplot, there are six peaks at each side. However, (b) subplot displays 21 peaks at each side. In addition, the first six peaks appear at energy values similar to that in (a) subplot with the same value of DOS.

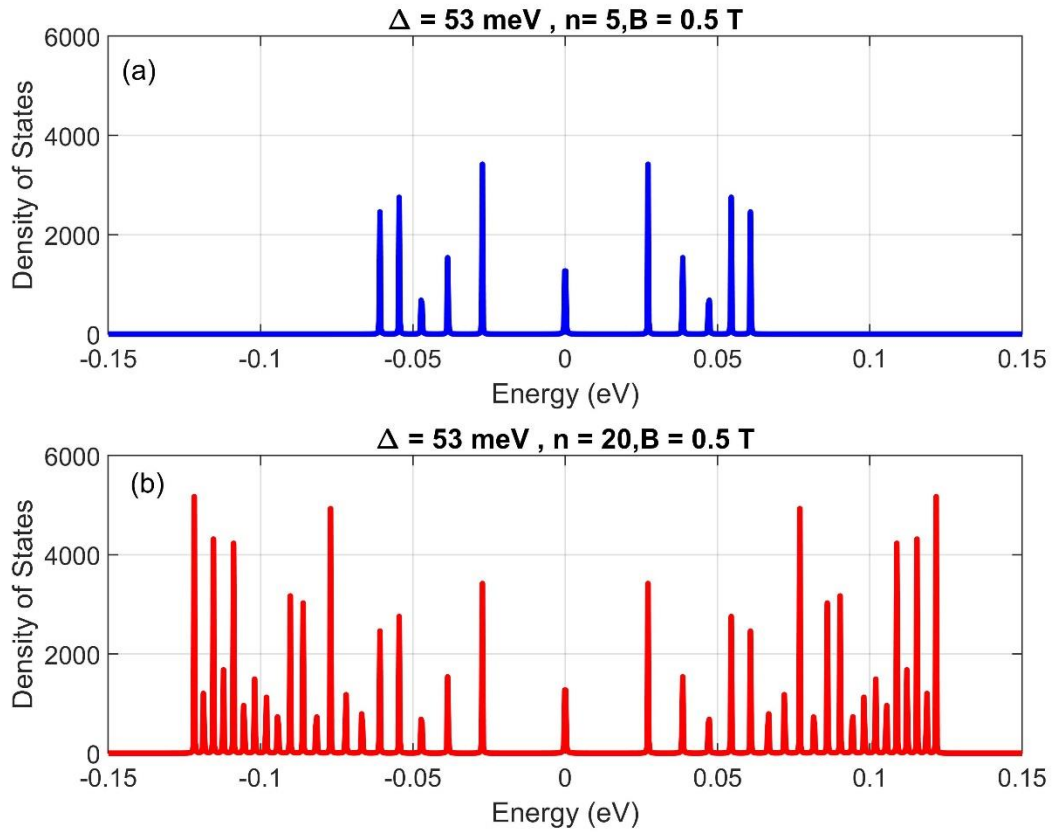


Figure 4.10 The density of states of gapped graphene, $\Delta = 53 \text{ meV}$, at a uniform magnetic fields of $B = 0.5 \text{ T}$ (a) $n = 5$ and (b) $n = 20$ as a function of energy.

As a conclusion to the previous discussion, gapped graphene exhibit one more peak in the DOS due to the splitting of the $n = 0$ Landau level. This is also clear in Figure 3.13 for gapped graphene, $\Delta = 106 \text{ eV}$, at $B = 0.5 \text{ T}$. The number of peaks in (a) subplot is 6 peaks on each side of the energy range. In addition, there are 21 peaks in each side for (b) subplot, $n=20$.

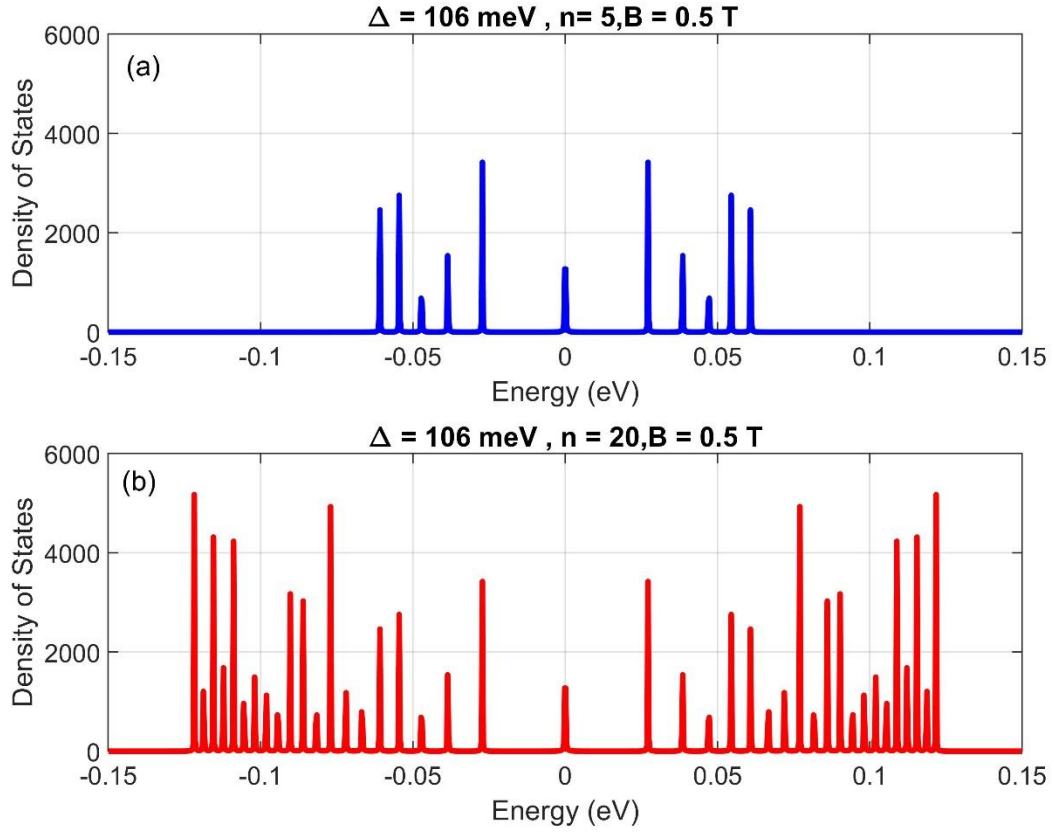


Figure 4.11 The density of states of gapped graphene, $\Delta = 106 \text{ meV}$, at a uniform magnetic fields of $B = 0.5 \text{ T}$ (a) $n = 5$ and (b) $n = 20$ as a function of energy.

4.1.3: Fermi Energy Oscillations

The Fermi level (E_F) is obtained from the electron concentration (n_c) using equations 3.6.1 and 3.6.2. The resulted numerical data for non-gapped graphene is plotted at three different concentrations: blue curve for $n_c = 3 \times 10^{16} \text{ m}^{-2}$, red curve for $n_c = 6 \times 10^{16} \text{ m}^{-2}$ and orange for $n_c = 9 \times 10^{16} \text{ m}^{-2}$ at a relatively small temperature, $T = 0.3 \text{ K}$, in Figure 4.12. The behavior of all curves, regardless of the concentration value exhibits oscillations in the Fermi energy. As observed from this figure, the amplitude of oscillations increases with magnetic field strength. In addition, orange curve exhibits higher E_F values

than red and blue curves. In conclusion, increasing the electron concentration leads to upward displacement of the Fermi oscillation. The higher the increase in the concentration, the more the displacement of the oscillations. The Fermi energy curves reaches its maxima at about 0.014 eV , 0.011 eV and 0.008 eV for $n_c = 3 \times 10^{16} \text{ m}^{-2}$, $6 \times 10^{16} \text{ m}^{-2}$ and $9 \times 10^{16} \text{ m}^{-2}$, respectively. However, they reach a minima of approximately 0.010 eV , 0.0082 eV and 0.0058 eV for $n_c = 3 \times 10^{16} \text{ m}^{-2}$, $6 \times 10^{16} \text{ m}^{-2}$ and $9 \times 10^{16} \text{ m}^{-2}$, respectively. At certain magnetic field strength oscillations disappear and the Fermi energy reaches a constant value of 0 eV . Lower concentration leads to vanishing at smaller magnetic fields. For instance, blue curve, goes to zero at nearly $B = 0.048 \text{ T}$. while, red and orange curves oscillate up to $B = 0.089 \text{ T}$ and 0.133 T , in that order. Previous studies on moving electrons in graphene under high magnetic field ensures the oscillations in the Fermi energy with magnetic field (Yang, Peeters et al. 2010).

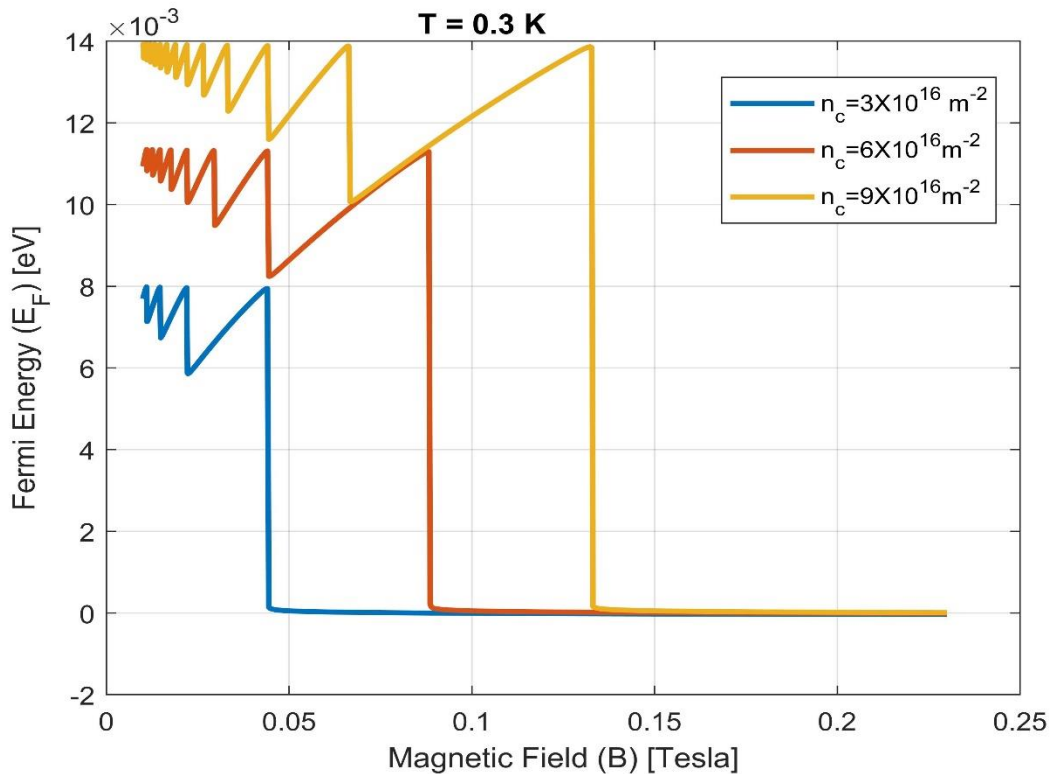


Figure 4.12 Fermi energy as a function of magnetic field strength for different concentrations of gapless graphene, $\Delta = 0 \text{ meV}$, at constant temperature $T = 0.3 \text{ K}$.

The effect of introducing a band gap on the Fermi energy versus magnetic field at constant temperature is also studied under three different electron concentrations. Figure 4.13 shows the Fermi energy versus magnetic field of gapped graphene, $\Delta = 53 \text{ meV}$, blue, red and orange curves display the oscillatory behavior of E_F at electron concentrations of $3 \times 10^{16} \text{ m}^{-2}$, $6 \times 10^{16} \text{ m}^{-2}$ and $9 \times 10^{16} \text{ m}^{-2}$, respectively. Similar to oscillations in the case of non-gapped graphene, increasing the magnetic field leads to an increase in the oscillation's amplitude. For the blue, red and orange curves, the amplitude of the Fermi energy approximately reaches maximum value of 27.5 eV , 28.7 meV and 29.8 meV , respectively. After reaching this maxima, they go to 26.5 meV at different B values. The range of oscillatory behavior increases as the electron concentration increases.

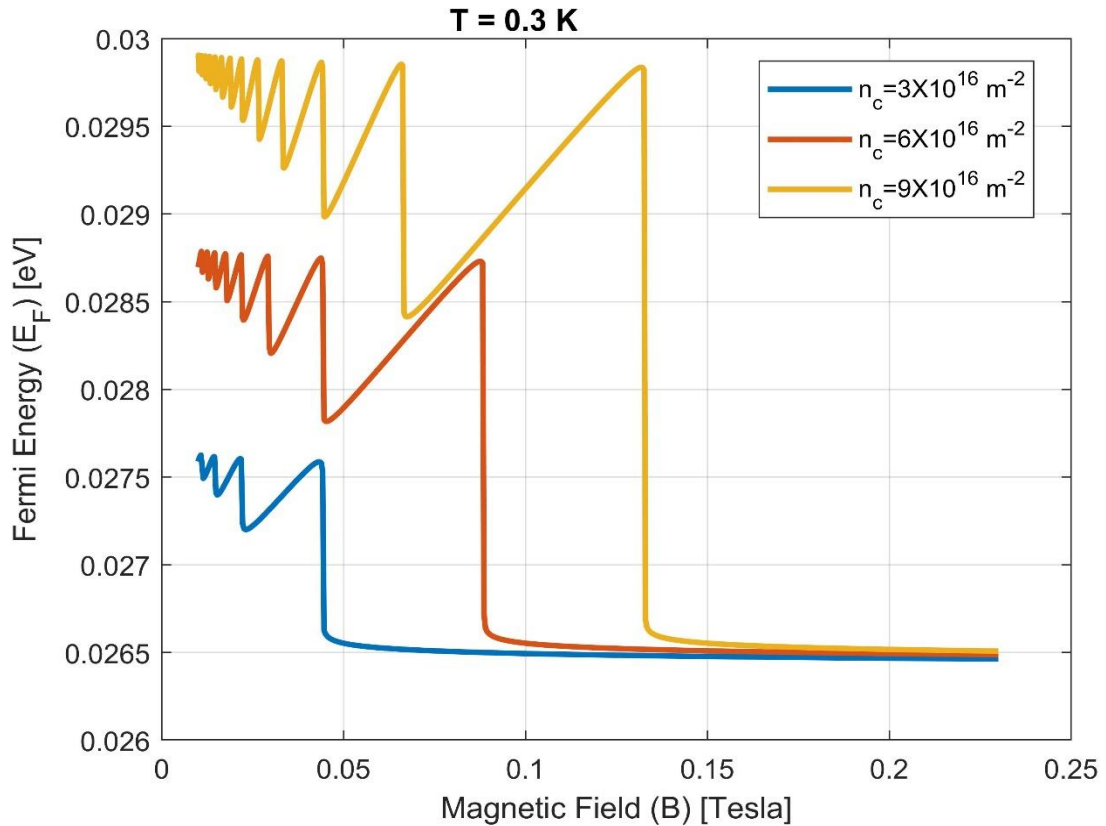


Figure 4.13 Fermi energy as a function of magnetic field strength for different electron concentrations of gapped graphene, $\Delta = 53 \text{ meV}$, at constant temperature $T = 0.3 \text{ K}$.

In Figure 4.14, the Fermi energy of $\Delta = 106 \text{ meV}$ gap graphene is plotted against the magnetic field at $T = 0.3 \text{ K}$. Again the oscillatory behavior in the small magnetic field range is presented for the three electron concentrations presented in the legend. Also, the vertical shift in the oscillations of Fermi energy resulting from increasing the concentration of electrons is pronounced. The oscillations peak at 53.5 meV , 45.1 meV and 54.7 meV for $3 \times 10^{16} \text{ m}^{-2}$, $6 \times 10^{16} \text{ m}^{-2}$ and $9 \times 10^{16} \text{ m}^{-2}$, in the stated order. After that, they converge to 0.053 eV at different strengths of the magnetic field. For instance, the blue curve converges nearly at $B = 0.06 \text{ T}$. However, the other two curves reach energy equals to half of the band gap (Δ) at higher magnetic field values.

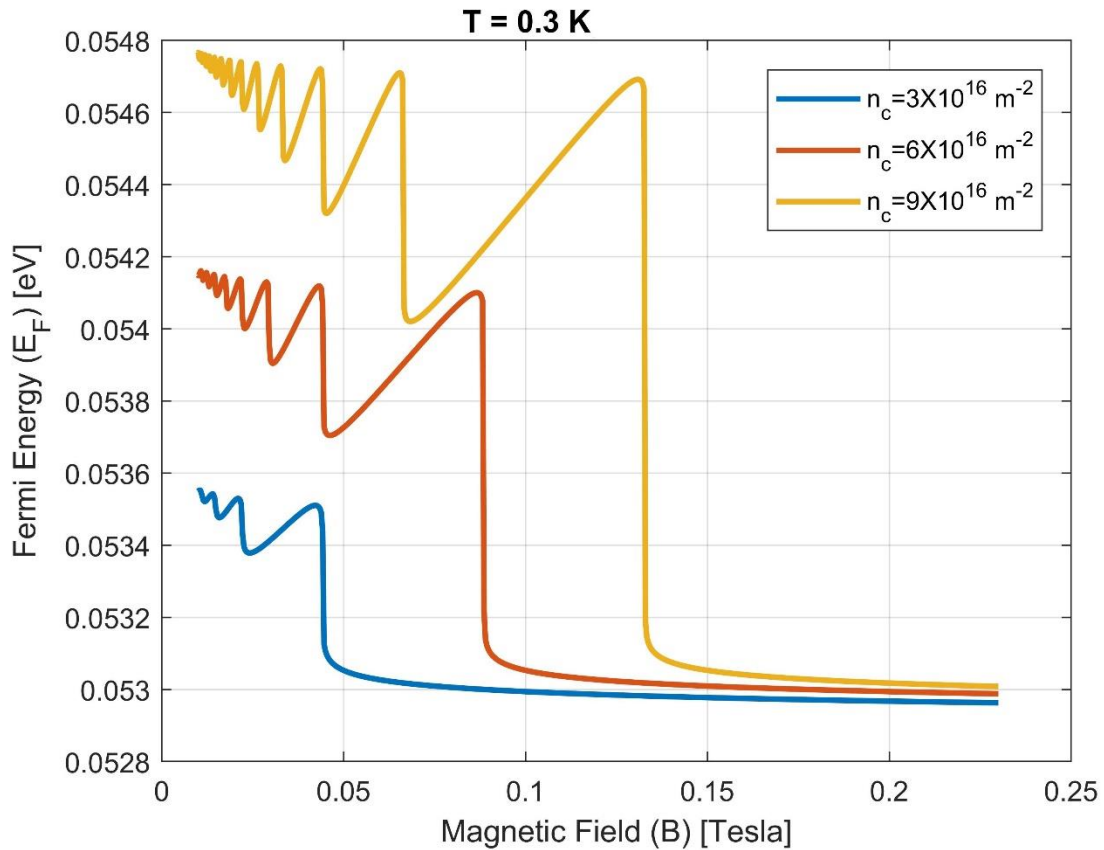


Figure 4.14 Fermi energy as a function of magnetic field strength for different electron concentrations of gapped graphene, $\Delta = 106 \text{ meV}$ at constant temperature $T = 0.3 \text{ K}$.

The behavior of the Fermi energy of non-gapped is also studied at a relatively high temperature, $T = 4 K$, for the previous three values of (n_c) . The obtained data is plotted in Figure 4.15. The oscillatory behavior in the F_F versus B curves is still evident but less pronounced compared to that in Figure 4.12. In addition, this figure reflects the effect of increasing the concentration on the (F_F) curve which was observed at lower temperature. For instance, Fermi energy goes to greater values with higher electron concentration.

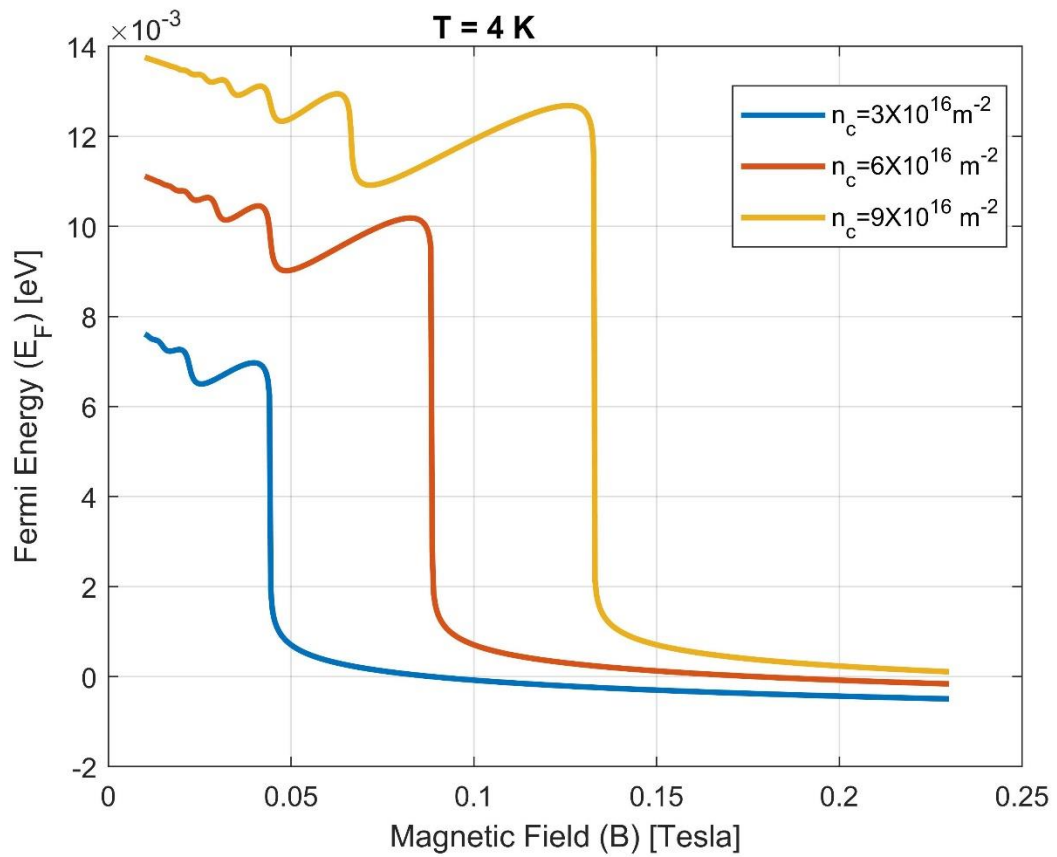


Figure 4.15 Fermi energy as a function of magnetic field strength for different electron concentrations of gapless graphene, $\Delta = 0 \text{ meV}$, at constant temperature $T = 4 K$.

Moreover, the study of higher temperature effects on (E_F) behavior for gapped graphene, $\Delta = 53 \text{ meV}$, is pictured in Figure 4.16. From the figure, the oscillations are not

clear in the blue curve at $n_c = 3 \times 10^{16} \text{ m}^{-2}$. However, they weakly appear at higher concentrations, as seen in the red and orange curves, with relatively significant oscillations at $n_c = 9 \times 10^{16} \text{ m}^{-2}$. For the non-oscillatory curve, (E_F) decreases as magnetic field increases. In the plotted range of B , the three curves do not converge to certain value as for small T .

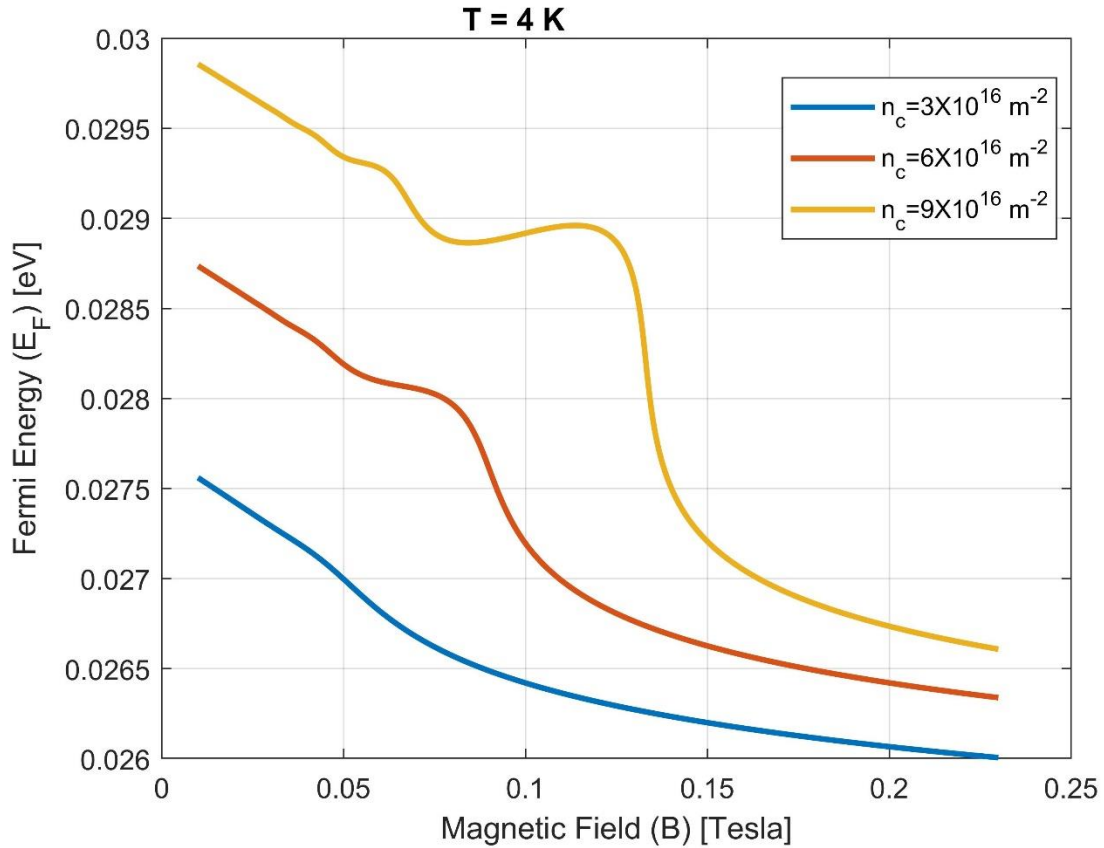


Figure 4.16 Fermi energy as a function of magnetic field strength for different electron concentrations of gapped graphene, $\Delta = 53 \text{ meV}$, at constant temperature $T = 4 \text{ K}$.

The oscillatory behavior in (E_F) versus (B) curves tends to disappear as the gap increased to $\Delta = 106 \text{ meV}$, as displayed in Figure 4.17. Across all concentrations values, the Fermi energy tends to decrease as the field strength increases. In addition, higher concentrations exhibit larger Fermi energy at each value of the magnetic field. Comparing

this figure to Figure 4.14, one can see that for all concentrations, the Fermi energy is reduced for higher temperature.

At higher temperature, thermal energy ($k_B T$) can smear the Fermi energy, which means the electrons are not sharply confined to the Fermi surface. For the oscillations to remain observable, the thermal energy must be small enough compared to the spacing between Landau levels (Peeters and Vasilopoulos 1992).

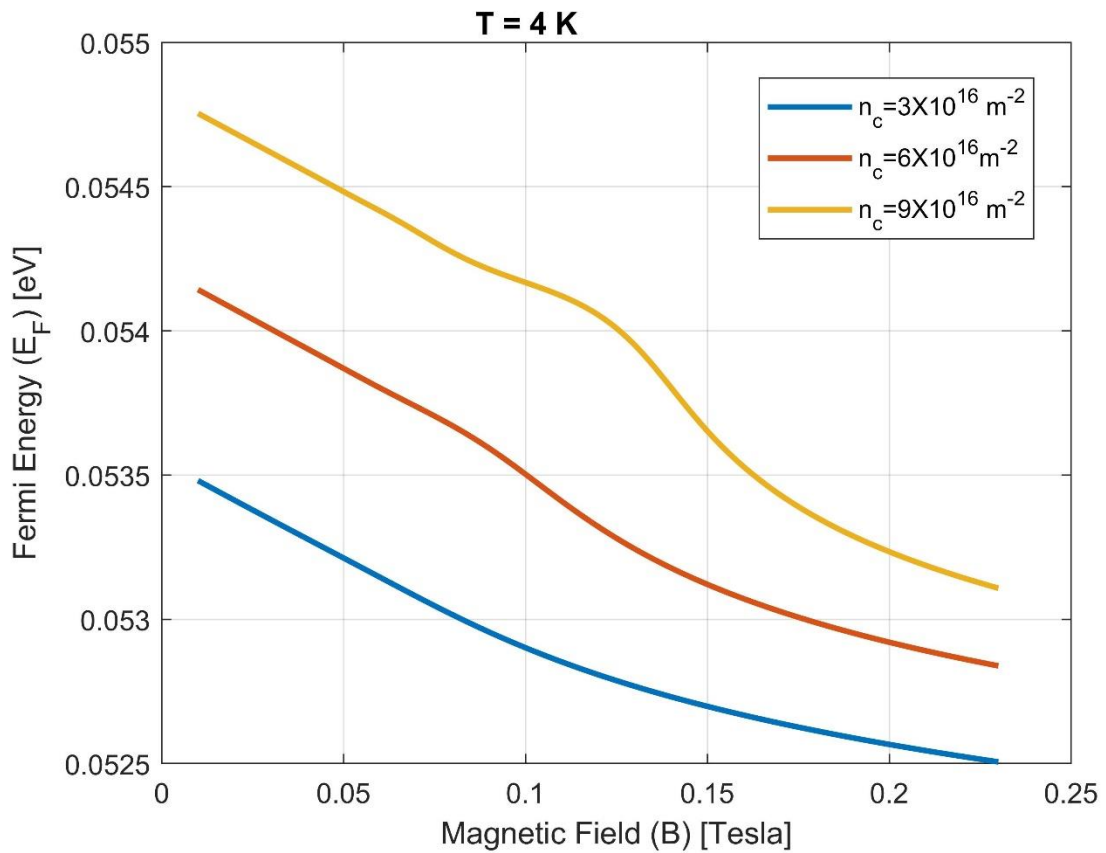


Figure 4.17 Fermi energy as a function of magnetic field strength for different electron concentrations of gapped graphene, $\Delta = 106 \text{ meV}$, at constant temperature $T = 4 \text{ K}$.

The Landau level's locations shift and periodically pass through the Fermi energy as the magnetic field changes. Consequently, oscillations in the population of electrons near the Fermi surface also occur (Yampol'Skii, Savel'ev et al. 2008).

Commenting on the above discussion of (E_F) oscillations at different temperatures. At low temperature, quantum oscillation is clearly observed in low magnetic field range. However, higher temperature makes the distinguishing between the oscillation at very low magnetic fields harder. In addition, the small amplitude of oscillations at low magnetic field is due to the narrower Landau levels. For higher electron density, the number of electrons in each Landau level is increased. These levels become less spaced causing more levels to intersect with the fermi energy at a given B range. This explain why more oscillations are appearing at higher electron concentration (Peeters and Vasilopoulos 1992)

4.2: Thermal Properties of Graphene Monolayer

4.2.1: Statistical Average Energy

Introducing a band gap (Δ) in graphene alters the energy spectrum and density of states, which consequently impacts the average energy (\bar{E}) of electrons and holes. Figure 4.18 illustrates this phenomenon with a series of curves showing the calculated average energy of charge carrier, electrons and holes in graphene, measured in electron volts (eV), as a function of temperature (T) in Kelvin (K). This presentation provides insight into how different band gap values influence the behavior of the average energy of electrons and holes in graphene at a relatively small magnetic field of $0.02 T$. Each curve corresponds to average energy calculated at specific value of the band gap (Δ). As indicated in the legend: blue, red and orange curves are corresponding to $\Delta= 0, 53$ and $106 meV$, respectively. Here, the blue curve, which corresponds to non-gapped graphene, displays a continuous increase in the

average energy as the temperature increase. However, red and orange lines, corresponds to gapped graphene, show a non-consistent increase in the average energy with temperature. The differences between the curves in the \bar{E} -axis are not constant at all temperatures and vary from one point to another.

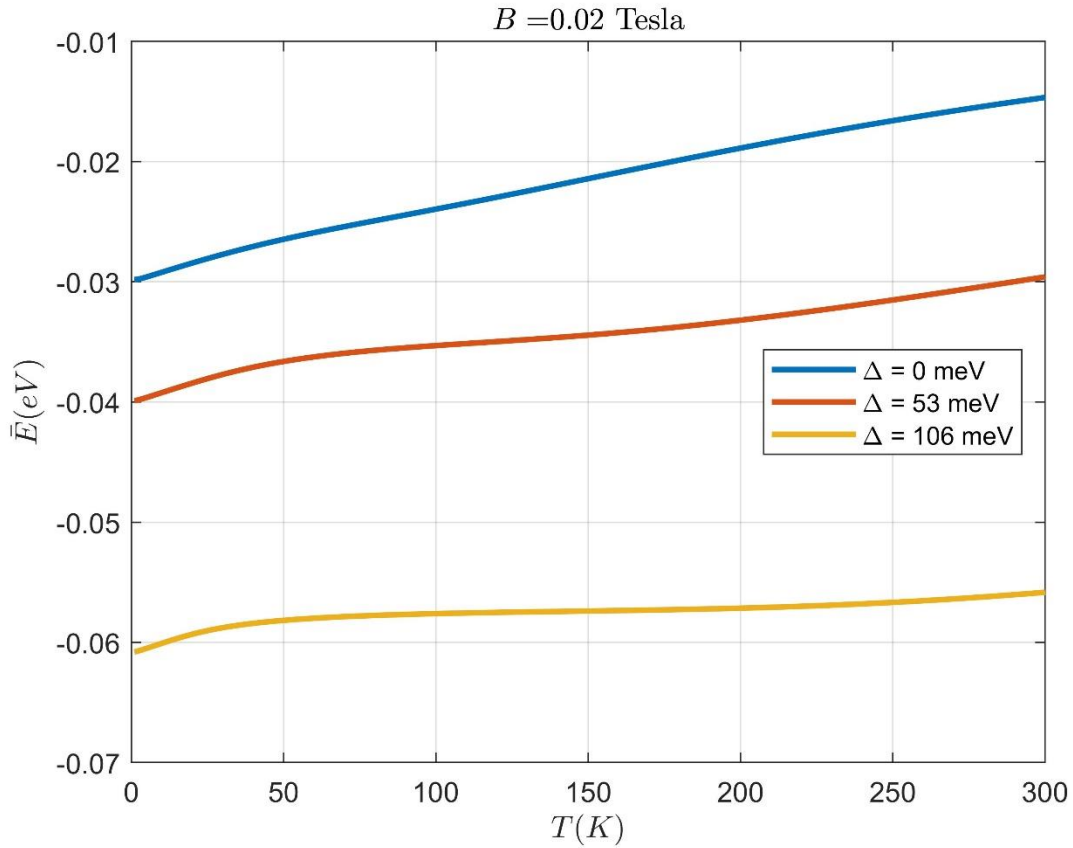


Figure 4.18 Statistical average energy of gapless and gapped graphene versus temperature at constant magnetic field of 0.02 T.

When the field strength elevated to $B = 0.2$ T, as displayed in Figur 4.19, \bar{E} increses with temperature. Additionally, this increase occurs in such a way that the differences between the blue and the red or orange curves remain nearly constant at any temperature.

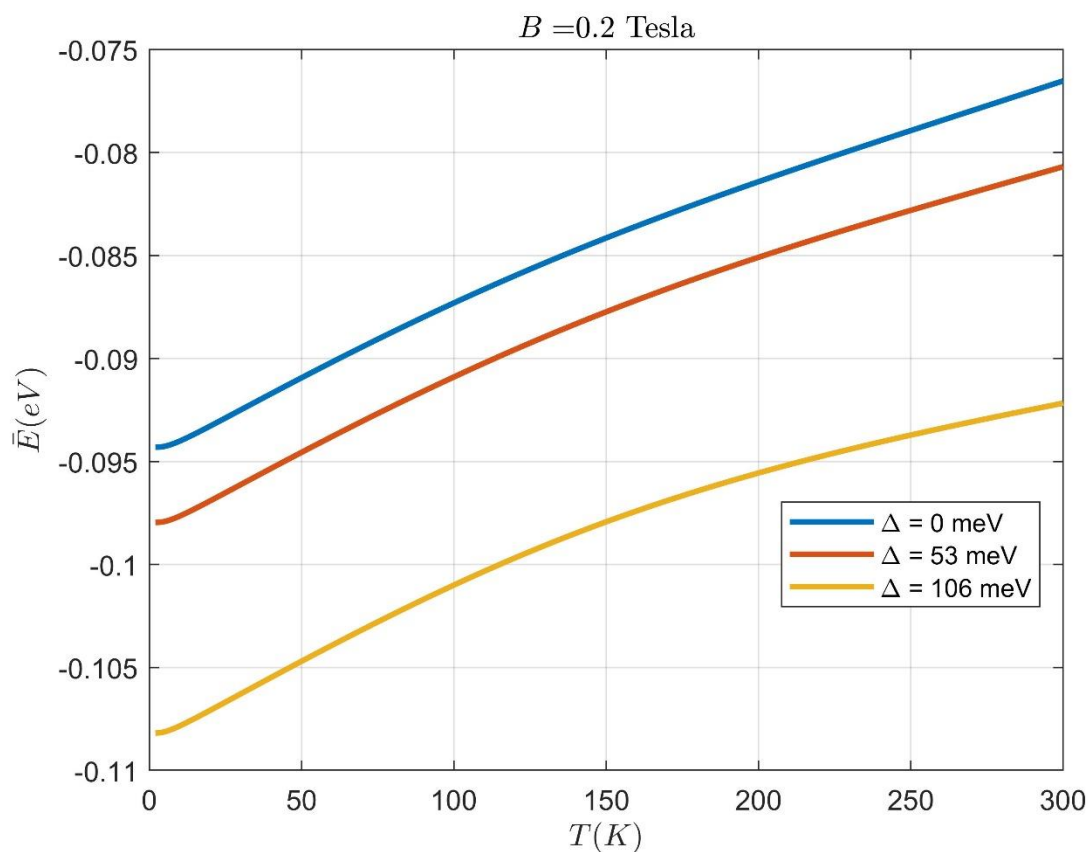


Figure 4.19 Statistical average energy of gapless and gapped graphene versus temperature at constant magnetic field of 0.2 T .

The previous behavior is also observed in Figure 4.20 where the field reaches higher value of $B = 1.5 \text{ T}$. As B increases, the rise in \bar{E} becomes more consistent, and the differences between the curves decreases, tending to be more constant.

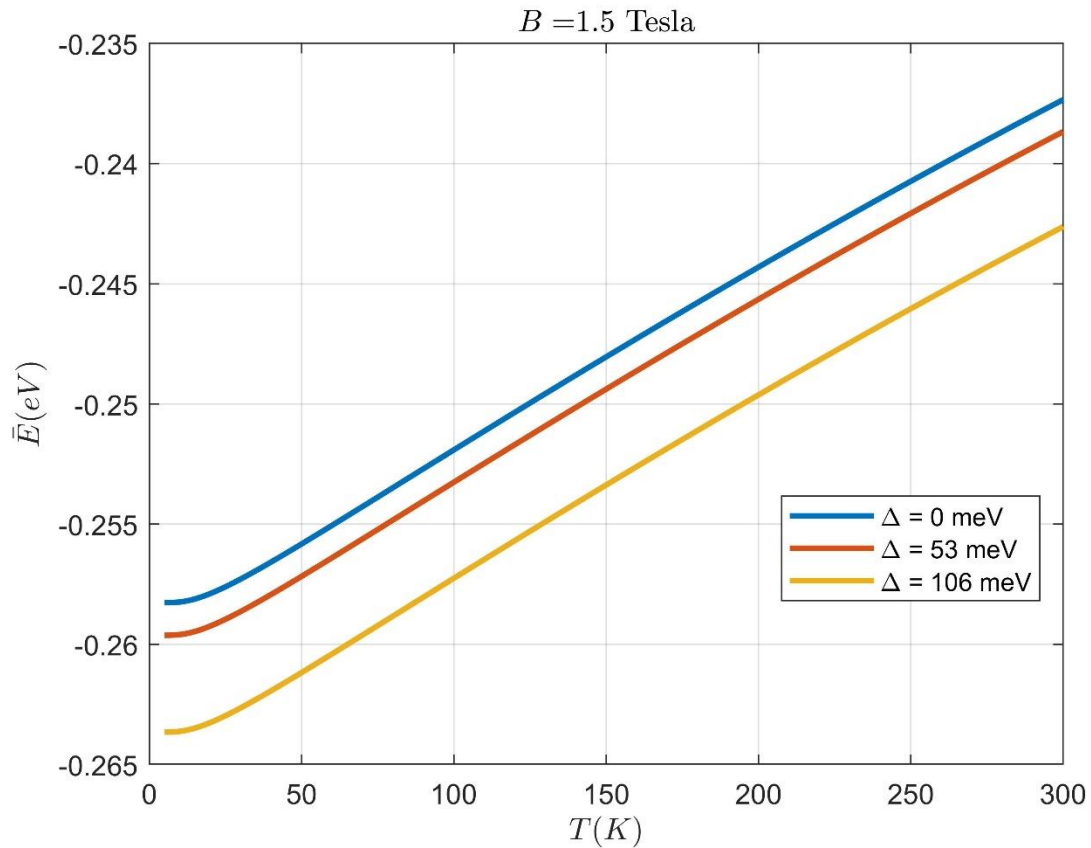


Figure 4.20 Statistical average energy of gapless and gapped graphene versus temperature at constant magnetic field of 1.5 T.

Across all Figures of \bar{E} versus T, there is a noticeable trend where the total average energy shifts to more negative values due to the introduction of the band gap. The larger the gap, the greater the shift. In addition, the larger the field, the less the average energy at any given temperature and band gap value.

The increase in average energy with temperature can be explained as follows: The increase in temperature is translated to extra thermal energy. Charge carrier gains this energy, enabling them to be excited to higher energy states which in turns rises its average energy.

Landau quantization is a possible interruption to the decrease in the average energy as the magnetic field strength increases to higher values. As indicated before, the spacing between Landau levels is proportional to B . Consequently, higher fields lead to more widely spaced levels, and thermal energy may not be sufficient to occupy the higher states in their new positions. Another point to take into consideration is the effect of magnetic field on DOS of non-gapped and gapped graphene. As discussed earlier, the density of states is inversely proportional to B . Thus, increase the magnetic field reduces the number of states including higher energy states. Therefore, Landau quantization and DOS lead to \bar{E} lowering.

There are several explanations to the reduction in the average energy when the band gap becomes larger. First, the separation between levels increases as the gap increases. Secondly, the presence of a band gap in graphene leads to a restriction on the carrier's movements through conduction and valence bands and leads to zero density of states up to energy equals to the gap value.

The total average energy is plotted as a function of the magnetic field strength at constant temperature $T=40$ K in Figure 4.21 This figure includes three curves, each corresponding to different band gap value : $\Delta= 0$ meV, $\Delta= 53$ meV and $\Delta= 106$ meV. The general behavior observed in all three curves is a decrease in total average energy as the magnetic field strength increases.

This decrease is attributed to the behavior of Landau Levels in graphene. As mentioned earlier in Section 4.1.1, as the magnetic field strength increases, the Landau levels become more widely spaced. This phenomenon results in a reduction of available states for electrons and holes at each level. Consequently, charge carriers tend to occupy lower energy levels more rapidly, resulting in a reduction of the total average energy.

In a more detailed analysis, the redistribution of density of states as the magnetic field increases, as discussed in section 4.1.2, implies also that electrons and holes tend to occupy lower energy states predominantly. Therefore, the total average energy of the system decreases because the average energy of the charge carriers is reduced.

This figure indicates that the introduction of a band gap leads to a decrease in the average energy under the same magnetic field conditions. For example, the average energy in the case of a 106 meV band gap, as shown in orange curve, is lower than that in the case of 53 meV band gap, as shown in red curve, and lower than in the gapless case, as shown in blue curve. The effect of band gap on the average energy was discussed in section 4.2.1.

In the absence of a magnetic field ($B = 0$), the total average energy of the system is observed to be 0 meV , -26.5 meV , and -53 meV for band gap values of 0 meV , 53 meV , and 106 meV , respectively. This indicates that each band gap imposes its own characteristic energy level on the system when no magnetic field is applied. This occurs because without a magnetic field, there are no additional energy effects like Landau quantization affecting the energy levels.

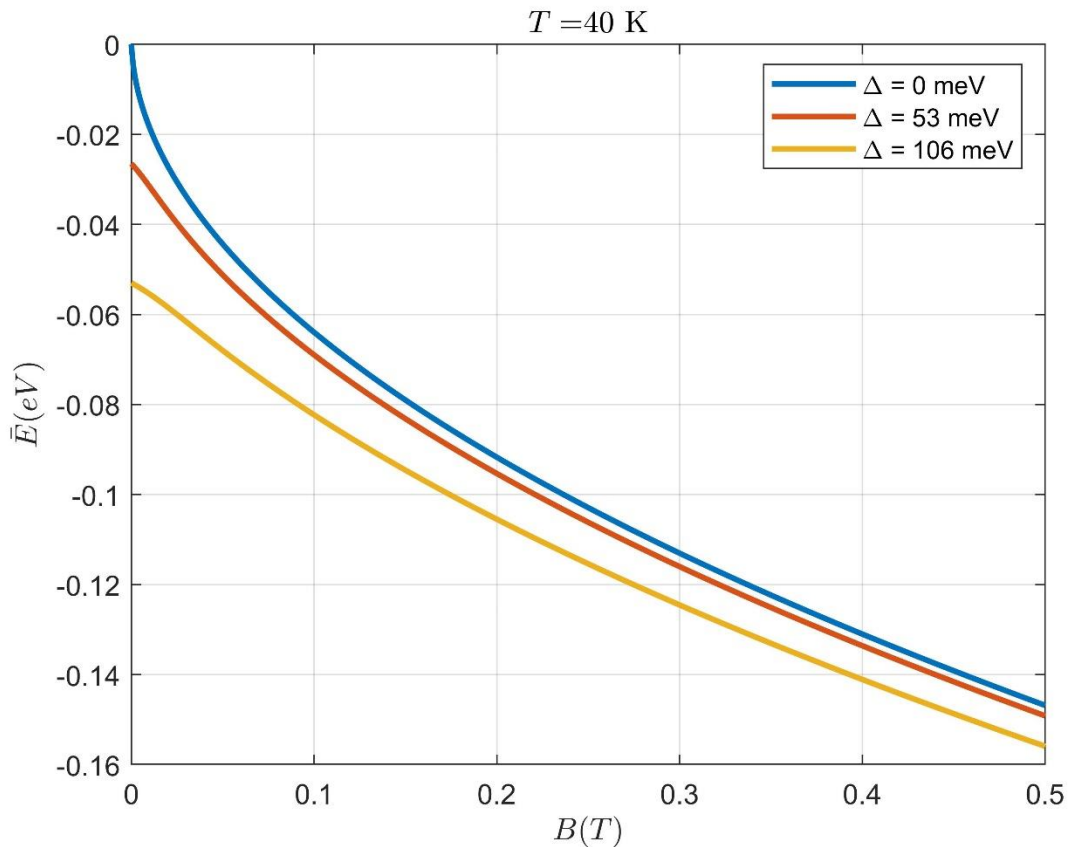


Figure 4.21 The statistical average energy versus magnetic field strength at constant temperature of 40 K for the three values of the band gap

4.2.2: Specific Heat Capacity

Specific heat capacity (C_v) is calculated and plotted in Figure 4.22 as a function of temperature at constant magnetic field strength for both non-gapped and gapped graphene. The curve's legend indicates the following: blue curves correspond to $\Delta = 0$ meV, red curves correspond to $\Delta = 53$ meV and orange curves correspond to $\Delta = 106$ meV. (C_v) is calculated at very low magnetic field of 0.02 T. There are observable differences in its behavior due to the introduction of band gap.

Regardless of the band gap value, the general trend observed in all curves is that the specific heat with temperature increases up to a certain point, after which it gradually decreases as the temperature continues to rise, forming a sharp peak.

Subsequently, the curves exhibit a second, broader increase in the specific heat at higher temperatures with a lower (C_v) value compared to the first peak. However, the shape and the position of the peak depend on the band gap values. This peak is called Schottky anomaly (Hoi, Phuong et al. 2019). For instant, the introduction of band gaps shifted the center of that peak toward higher specific heat capacity values and lower temperatures. The higher the gap value, the greater the shift. In addition, increasing the band gap value makes the first peak sharper.

In particular, gapless graphene, $\Delta = 0$ meV, peaks at $T = 10$ K with $C_v = 0.913 k_B$. In addition, the specific heat capacity of gapped graphene with $\Delta = 53$ meV reaches a maximum value of $0.941 k_B$ at $T = 9$ K. Furthermore, gapped graphene, $\Delta = 106$ meV, forms a peak at $T = 7$ K with a higher value of the specific heat capacity, $C_v = 0.965 k_B$.

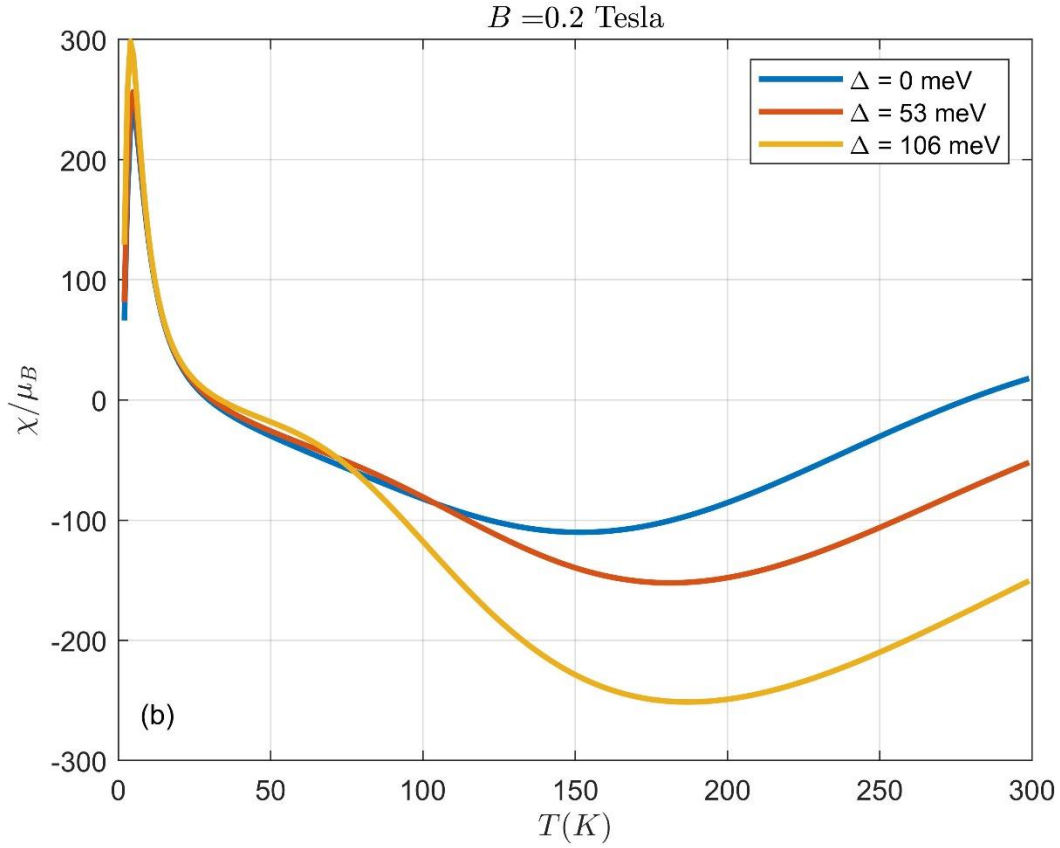


Figure 4.22 Specific heat capacity versus temperature of gapped and non-gapped graphene at a constant value of magnetic field , $B = 0.02\text{T}$.

The effects of increasing the magnetic field strength to 0.2 T are displayed in Figure 4.23. A higher field affected the specific heat capacity in a different manner. The three curves that correspond to different band gap values peak approximately at the same temperature, $T = 30 \text{ K}$. However, the maximum value of the specific heat capacity is nearly the same for blue and red curves, $C_v = 0.917 k_B$. Orange curve reaches a higher value of C_v at that temperature, $C_v = 0.928 k_B$. In general, at this value of the magnetic field, there is a slight change in the values of the specific heat capacity due to the presence of different band gap values. Similar to Figure 4.22, the Schottky anomaly peak is presented in the three curves.

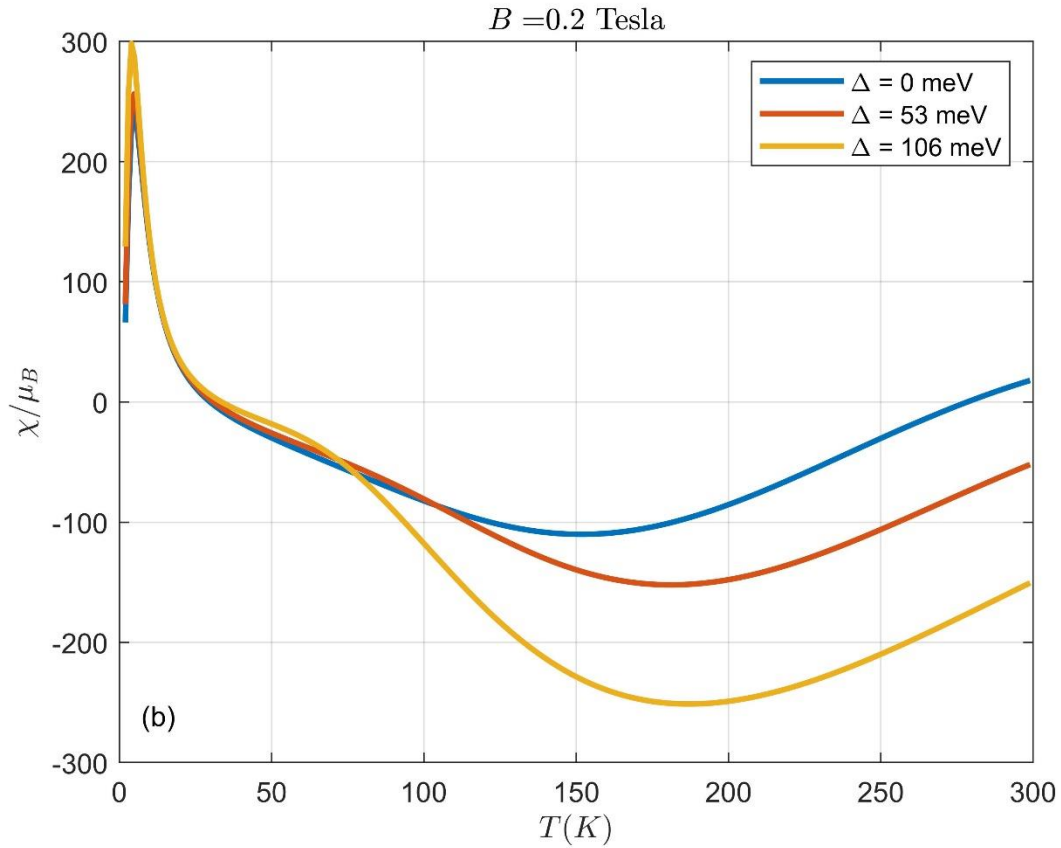


Figure 4.23 Specific heat capacity versus temperature of gapped and non-gapped graphene at a constant value of magnetic field , $B = 0.3\text{T}$.

Further increase in the magnetic field strength to 1.5 T effects on the C_v is presented in Figure 4.24. The non-gapped and gapped graphene have identical C_v values and behavior. All curves reaches maximum value of $0.908 k_B$ at $T = 60\text{ K}$.

As a result, increasing the magnetic field at which the specific heat capacity is calculated leads to a shift in the peak toward higher temperatures. Regardless of the magnetic field value, the increase in the specific heat as temperature increases is because charge carriers can cross the energy gap with greater thermal energy induced by higher temperature values.

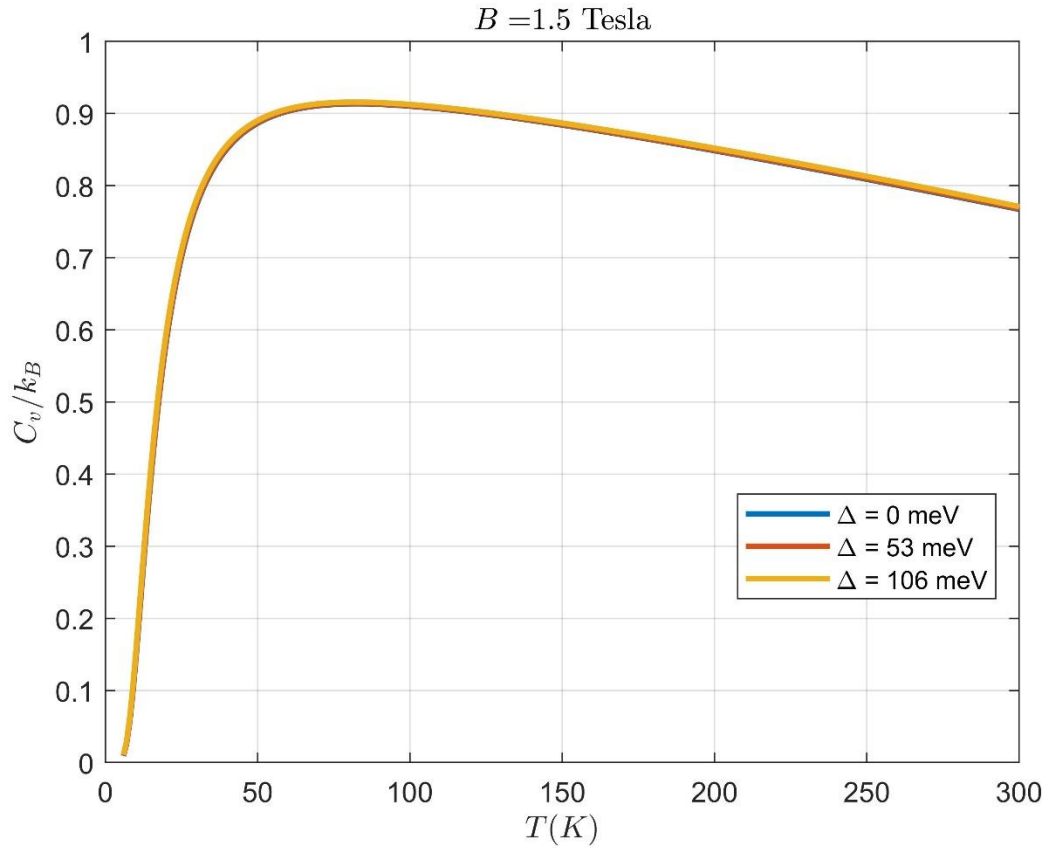


Figure 4.24 Specific heat capacity versus temperature of gapped and non-gapped graphene at a constant value of magnetic field, $B = 1.5$ T.

The specific heat capacity peak appeared in the specific heat versus temperature curves at the previous three values of the magnetic field was also observed in other studies on gapless graphene at different magnetic field values of $B = 2.5, 5$ and 10 T. However, these peaks was appeared at lower temperature regime $T < 14$ K. In addition, the shift of the peak toward higher temperature values as the magnetic field is increased was also presented (Lin, Ho et al. 2012).

Specific heat capacity versus magnetic field strength at constant temperature is also an excited topic to study. Figure 4.25 shows the relation of C_v versus B for gapless and gapped graphene at $T = 3$ K. Regardless of the band gap value, specific heat exhibit increase with B

at lower range. After that, C_v tends to decrease with B . Due to this changes in the behavior, a peak is formed. Again, this peak is called Schottky anomaly. However, peak's position alters from one curve to another. As the band gap changes from zero to higher values, the C_v curve is shifted upward toward higher specific heat values. Specifically, the peaks occur at $B = 0.01$ T and $C_v = 0.780 k_B$, $C_v = 0.902 k_B$ and $C_v = 0.961 k_B$ for $\Delta = 53$ and 106 meV, respectively.

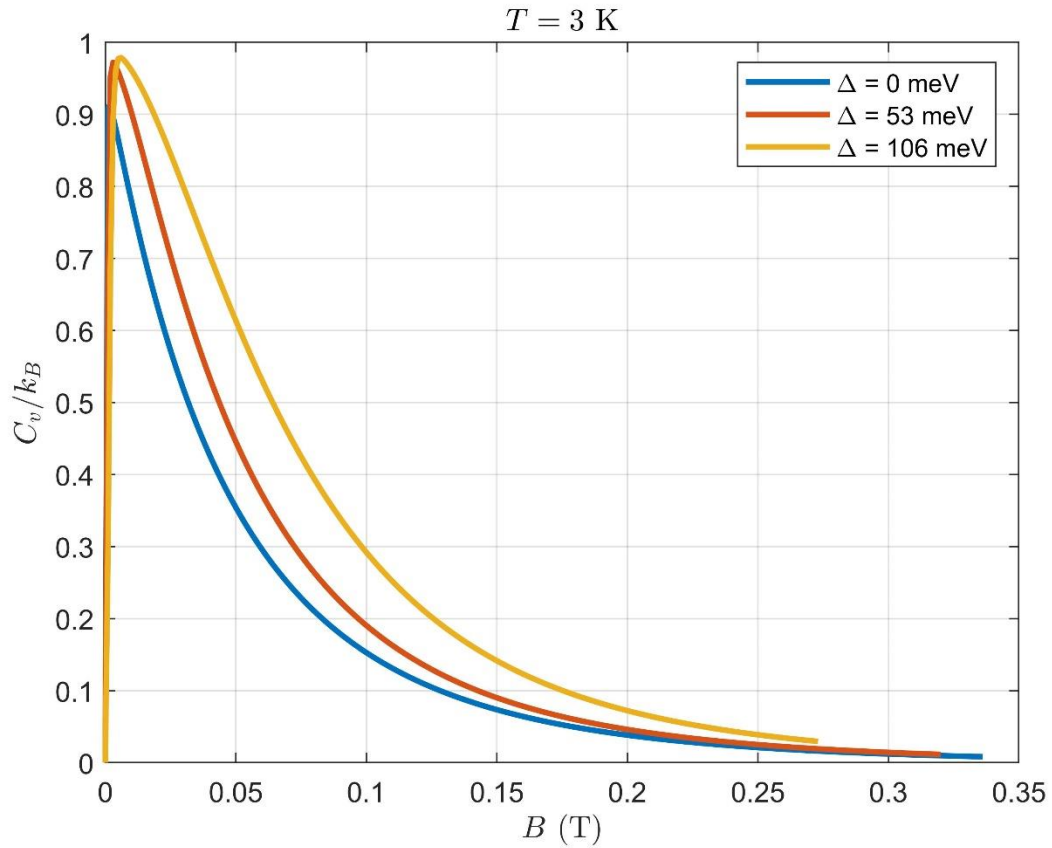


Figure 4.25 Specific heat capacity versus magnetic field strength of gapped and non-gapped graphene at a constant value of Temperature, $T = 3$ K.

The manner at which C_v behaves with magnetic field at $T = 5$ K is also plotted in Figure 4.26. The trend is similar to that resulted in lower temperature but with a more shift due to the presence of the band gap. However, the three curves peak at higher specific heat

value, compared to that in Figure 4.25. Gapless, 53 meV and 106 meV gap graphene approximately peak at $(0.01, 0.897k_B)$, $(0.01, 0.950k_B)$ and $(0.01, 0.974k_B)$, respectively. Differences in the case of 106 meV is more clear.

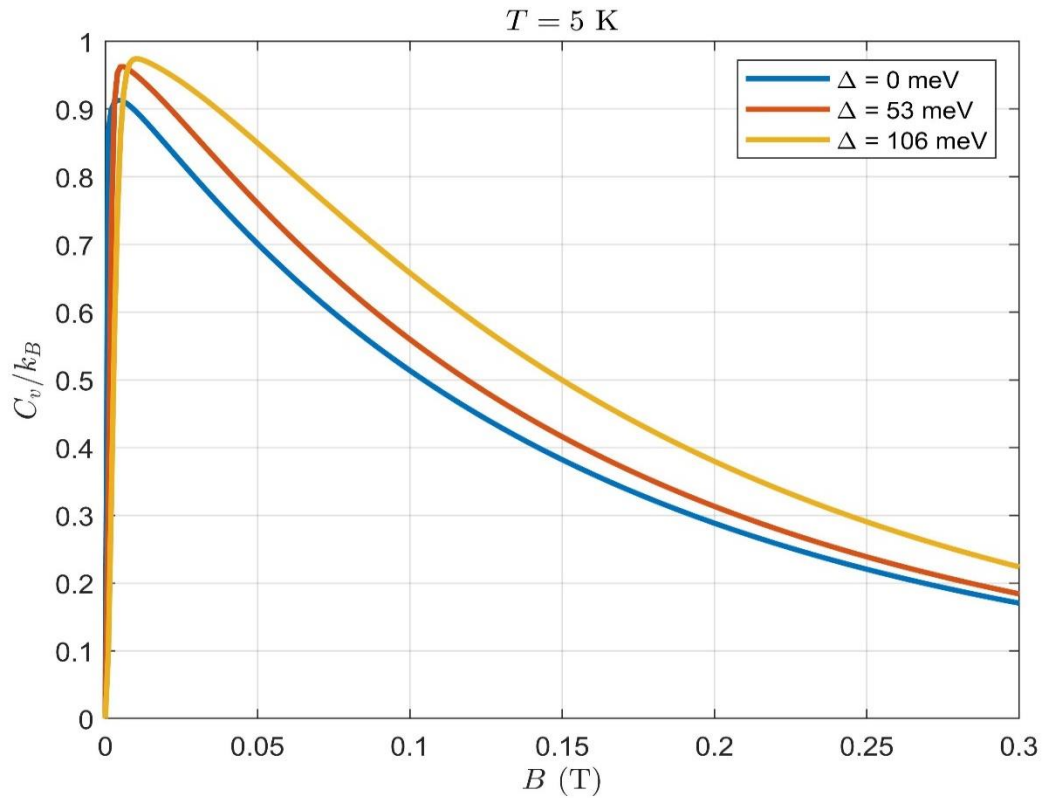


Figure 4.26 Specific heat capacity versus magnetic field strength of gapped and non-gapped graphene at a constant value of Temperature, $T = 5$ K.

The relation between specific heat capacity and magnetic field is also studied at $T = 10$ K and plotted in Figure 4.27. The behaviour of specific heat with B at this temperature is similar to that of lower temperatures in Figure 4.26 and Figure 4.25. Band gap introduction shift the C_v curve of gapless graphene upward and forward. Gapless, 53 meV and 106 meV gap graphene approximately peak at $(0.02, 0.913k_B)$, $(0.02, 0.941k_B)$ and $(0.03, 0.960k_B)$, respectively.

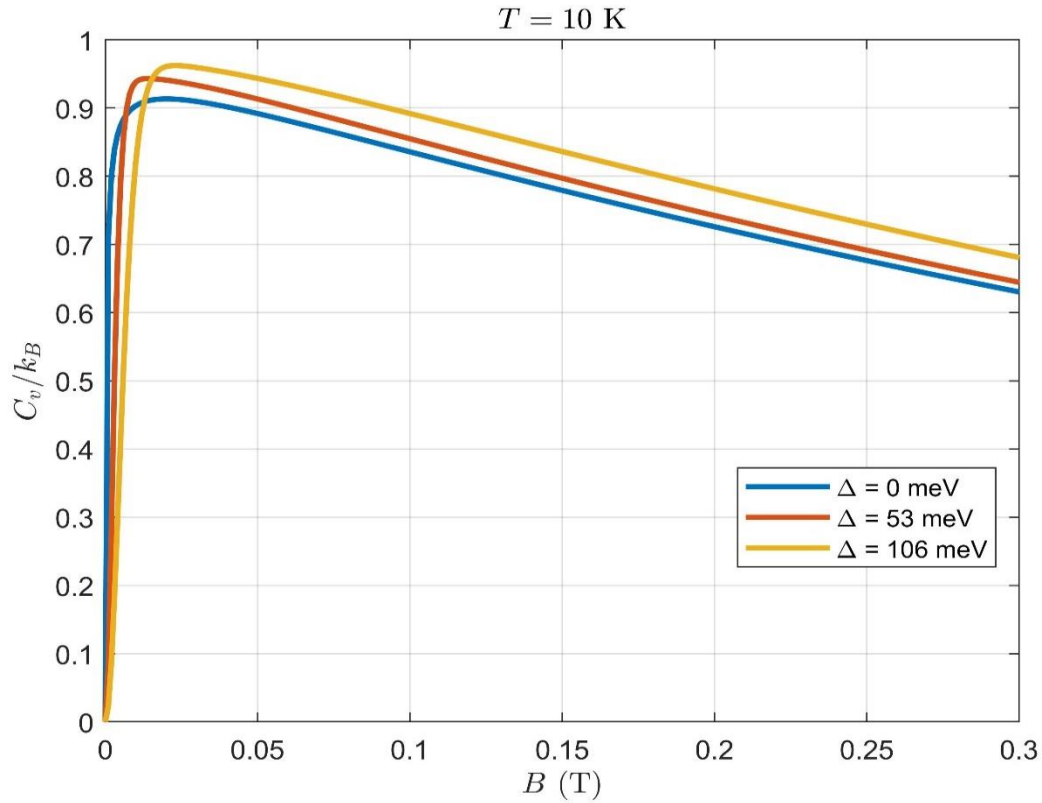


Figure 4.27 Specific heat capacity versus magnetic field strength of gapped and non-gapped graphene at a constant value of Temperature, $T = 10$ K.

These peaks were observed in studies on gapless graphene specific heat capacity as a function of the magnetic field strength at constant temperatures of 1, 2, 3 and 4 K but in a different range of the magnetic field strength. No peaks appear within the range $B \leq 0.5$ T (Lin, Ho et al. 2012).

4.2.3: Entropy Calculations

The general behavior of the entropy (S) is illustrated in Figure 4.28 as a function of temperature for both non-gapped and gapped graphene under magnetic field strength of 0.02 T. Three differently colored curves corresponding to each band gap value are presented.

There is a general trend of increasing entropy with rising temperature regardless of the gap. Notably, at lower temperatures, the rate of increase in entropy is more pronounced compared to higher temperature ranges. Furthermore, the change in entropy at higher temperatures is smaller in the case of bigger band gap.

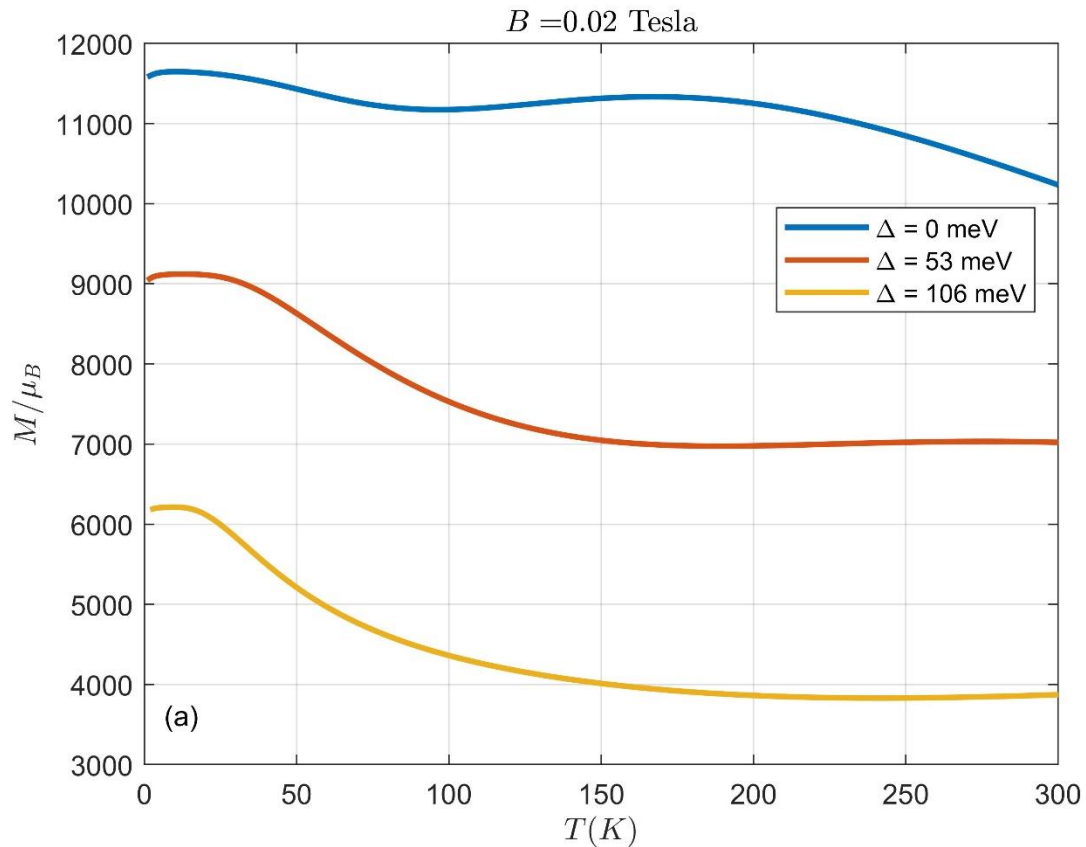


Figure 4.28 Entropy versus temperature of gapless and gapped graphene at constant magnetic field strength of $B = 0.02T$.

Figure 4.29 highlights a consistent trend where entropy of graphene at $B = 0.2 T$ generally increases with rising temperature. Band gap introduction displaces the curve of entropy upward toward higher S values. For example, entropy reaches maxima of $1.56 k_B$, $1.52 k_B$ and $1.49 k_B$ for $\Delta = 0 meV$, $\Delta = 53 meV$ and $\Delta = 106 meV$, respectively.

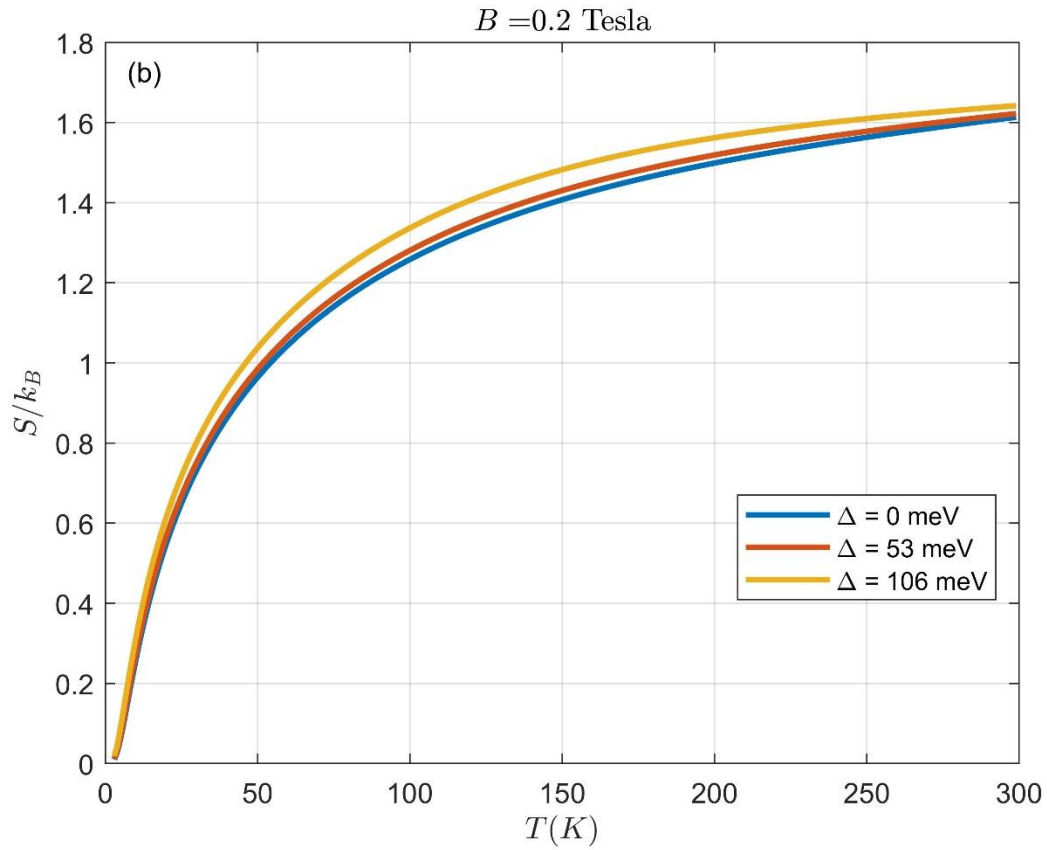


Figure 4.29 Entropy versus temperature of gapless and gapped graphene at constant magnetic field strength of $B = 0.2T$.

Raising the magnetic field strength to $1.5 T$, leads to an identical entropy curves regardless of the band gap value. This behavior is illustrated at Figure 4.30. The effects of band gap introduction diminishes at that value of B . All curves reach their common maxima of $1.14 k_B$. As one can notice from the three figures, 4.28-4.30, the entropy dependence on temperature is similar despite the strength of the magnetic field.

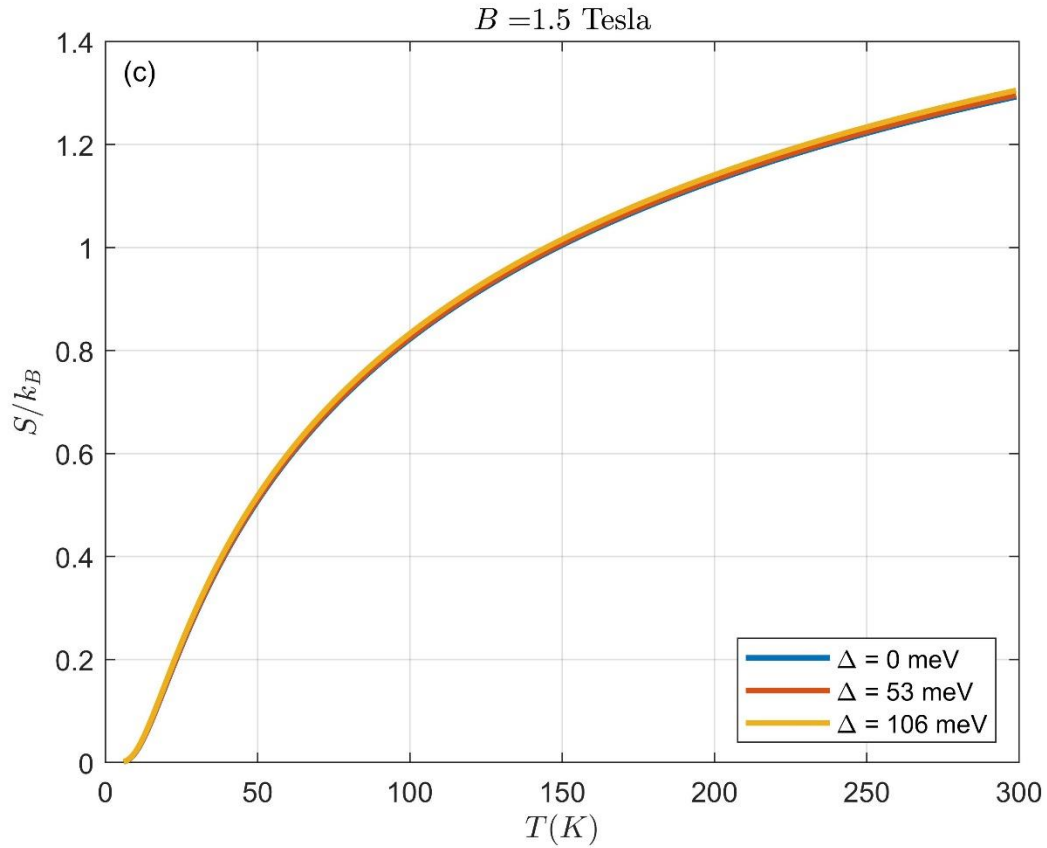


Figure 4.30 Entropy versus temperature of gapless and gapped graphene at constant magnetic field strength of $B = 1.5 \text{ T}$.

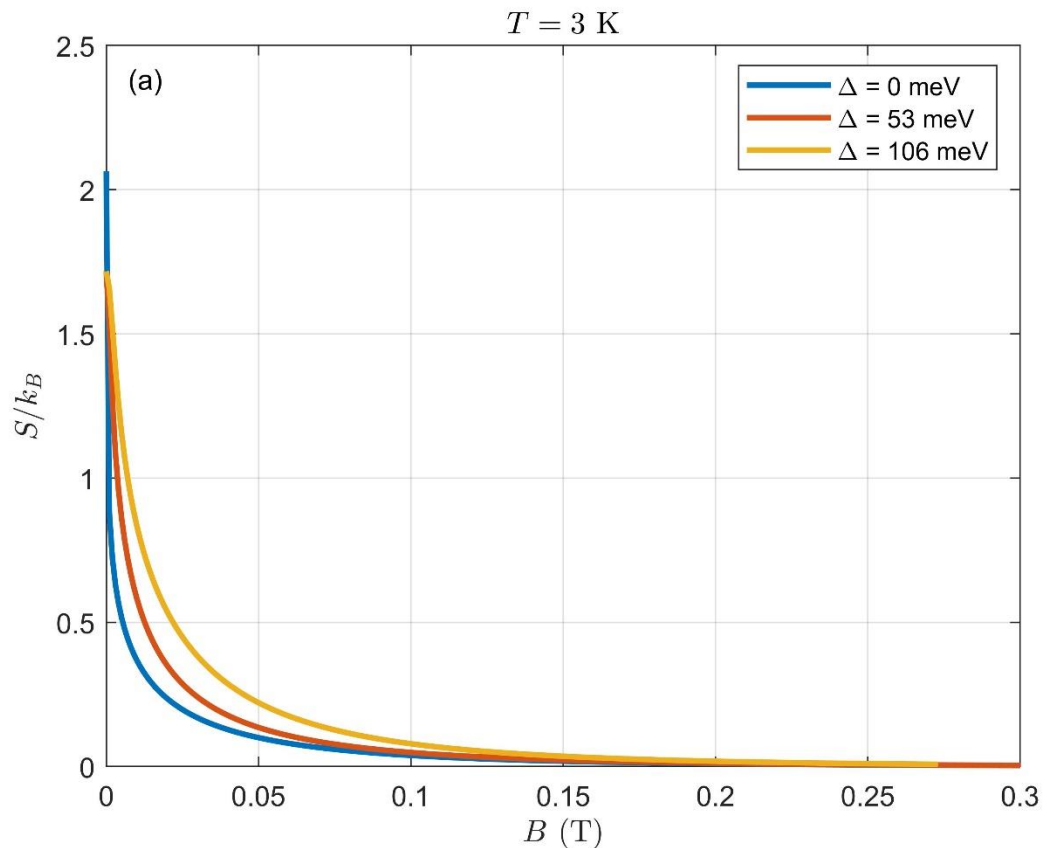
Statistical mechanics and thermodynamics can be used to understand the increase in entropy with temperature. The disorder, as well as the entropy, tends to increase as the temperature rises due to the thermal activity of graphene. Atoms and electrons gain more energy due to higher temperatures. This energy allows them to move and vibrate more, leading to an increase in the number of microstates that the electron can access, which in turn increases the entropy (Tolman 1979).

Raising temperature in gapped graphene gives electrons enough excitation energy to cross the band gap. Also, it increases the entropy as a result of increase in the number of

accessible states. As the band gap becomes larger, the energy needed for the excitation also becomes higher.

One possible interpretation of the increase in the entropy values of gapped graphene compared to the non-gapped is that the density of states becomes denser around the bandgap in gapped graphene, as appear in Figure 4.8. This leads to more possible microstates and higher entropy values.

Entropy versus magnetic field of gapped and non-gapped graphene at constant temperature is also plotted in Figure 4.31. Three subplots corresponding to three temperatures: (a) $T = 3\text{ K}$, (b) $T = 5\text{ K}$ and (c) $T = 10\text{ K}$. In all subplots and regardless of the band gap value, entropy decreases with B . until S reaches zero. Band gap presence lead to a relatively small shift of the non-gapped graphene curve toward higher entropy values. In addition, at 3 K , entropy reaches zero value in the plotted range. While at higher temperatures, as in subplot b and c, entropy does not reach zero in the plotted range.



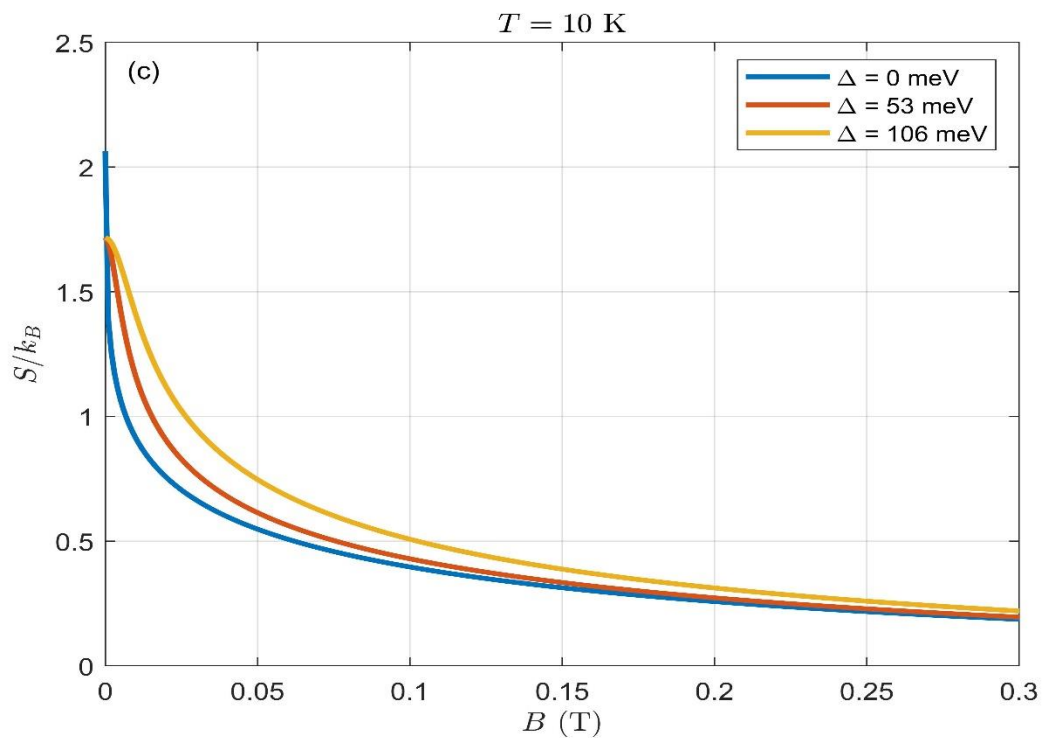
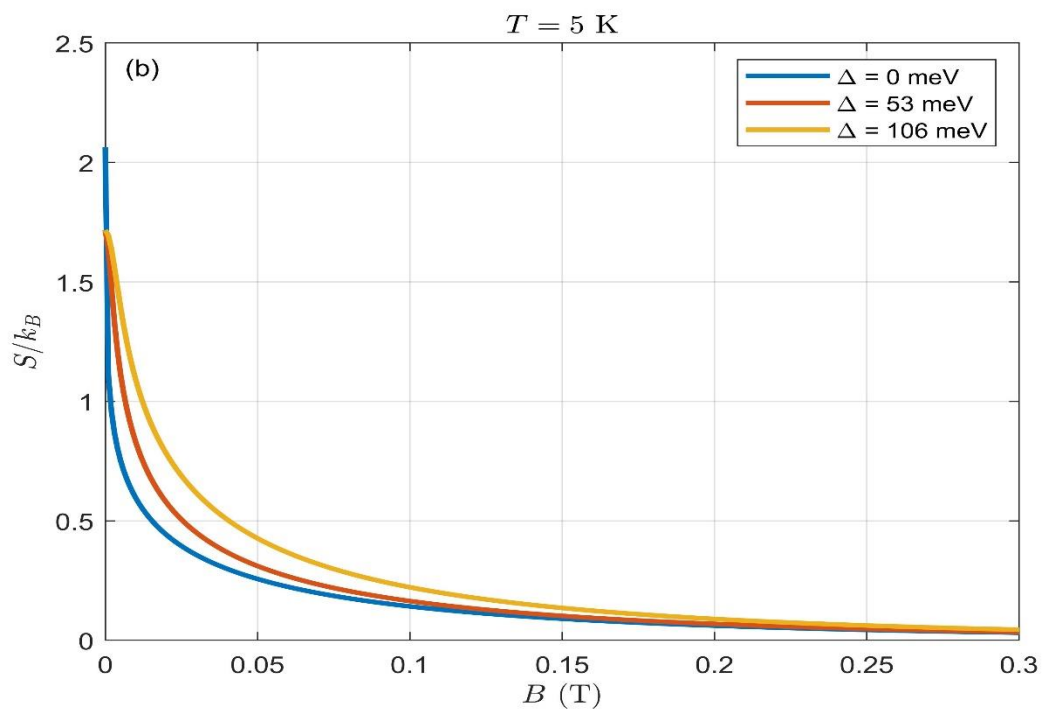
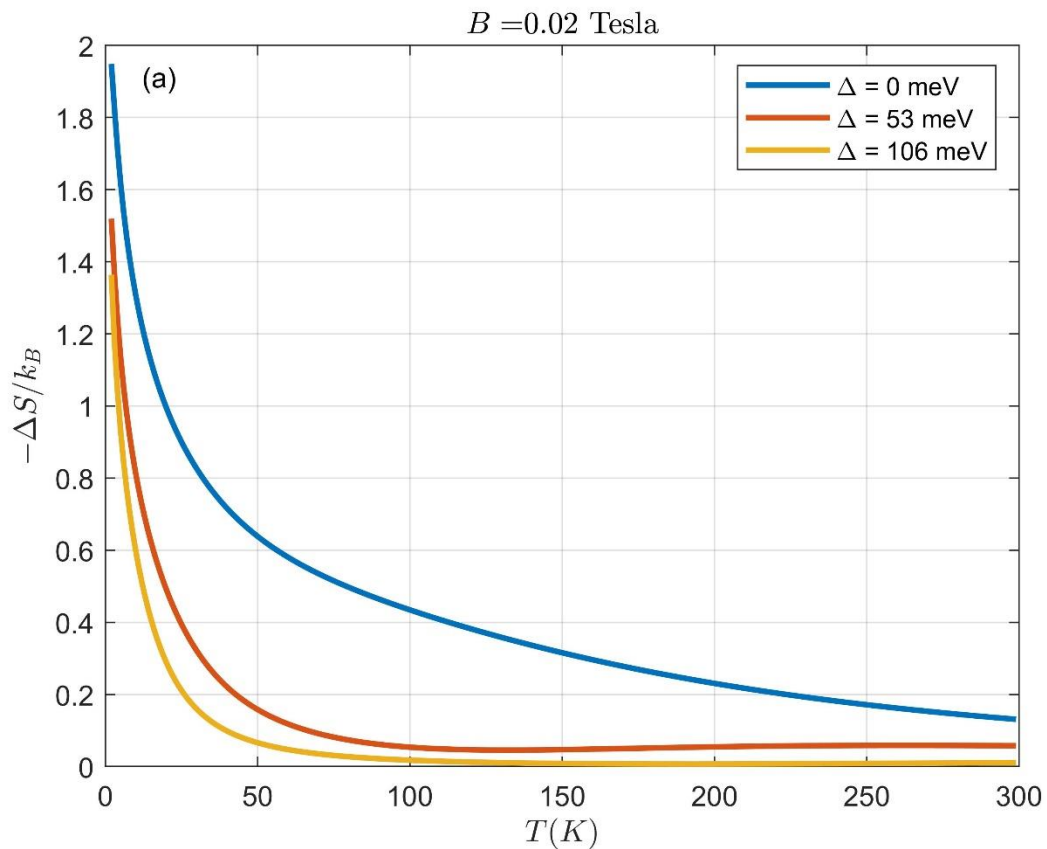


Figure 4.31 Entropy versus magnetic field of gapless and gapped graphene at different temperatures: (a) $T = 3 \text{ K}$, (b) $T = 5 \text{ K}$ and (c) $T = 10 \text{ K}$

Change in entropy ($-\Delta S$) is associated with switching the magnetic field on or off and it is important for studying the Magneto Caloric Effect in materials. Change in entropy ($-\Delta S$) is plotted in Figure 4.32 as a function of temperature at (a) $B = 0.02 T$, (b) $B = 0.2 T$ and (c) $B = 1.5 T$ for both gapped and non-gapped graphene. As appear from the figure, ($-\Delta S$) decreases as temperature becomes higher until reaches a fixed constant value. This behavior is valid for all values of Δ . However, band gap introduction shifts the blue curve of non-gapped graphene toward smaller values of ($-\Delta S$).



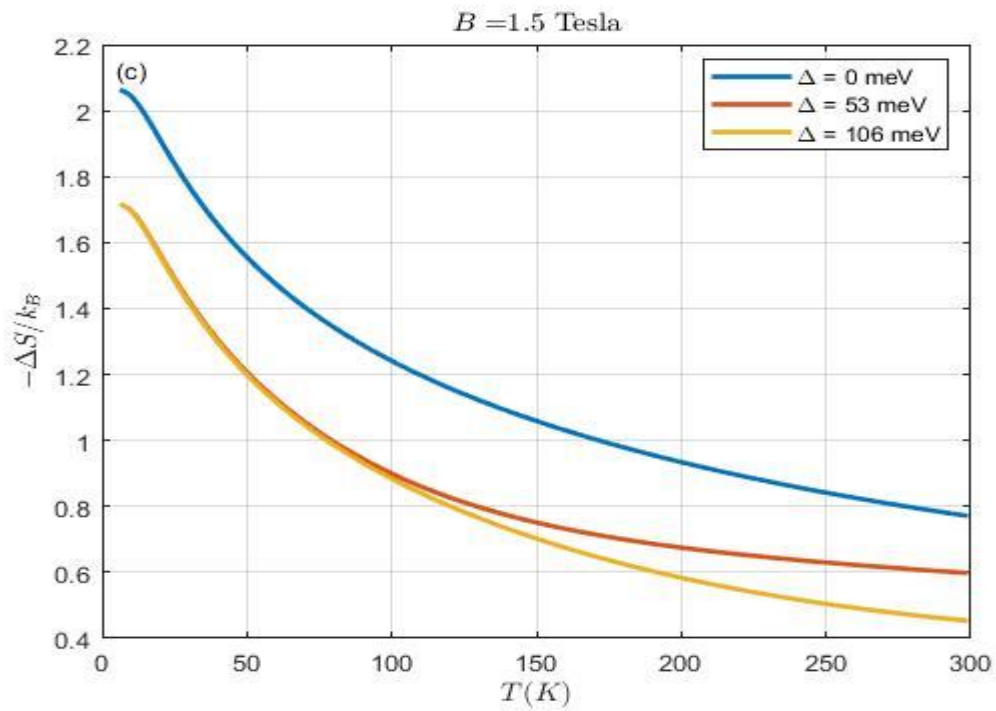
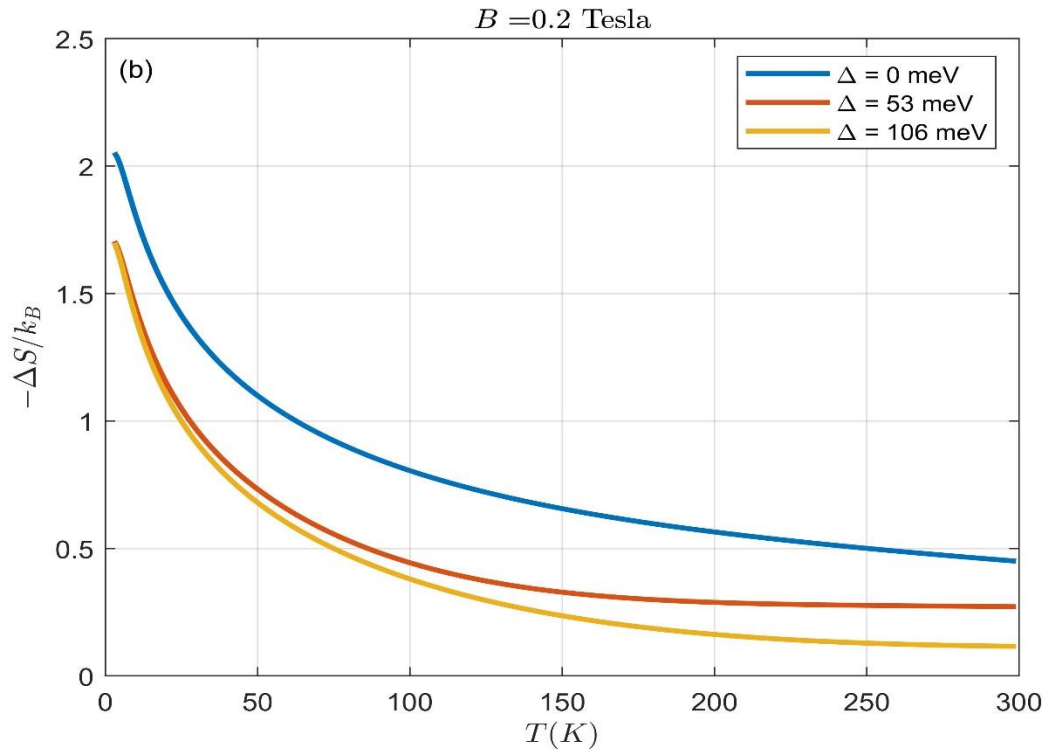
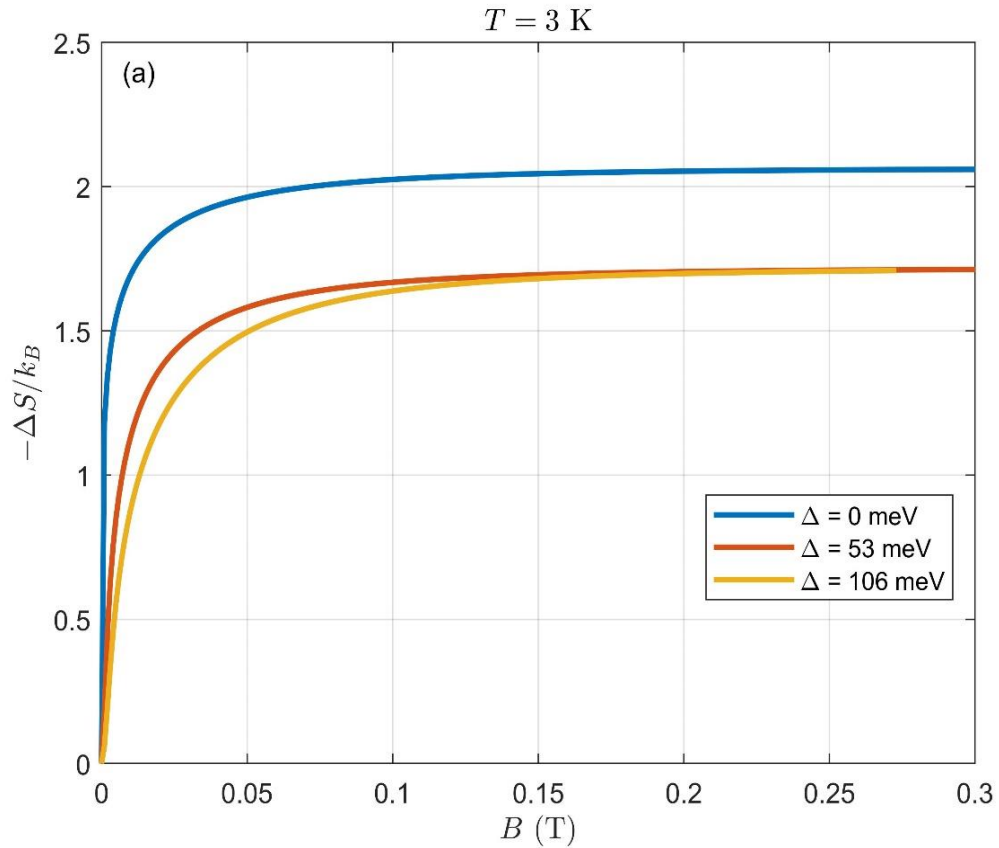


Figure 4.32 Change in entropy of graphene versus temperature at three values of the band gap at (a) $B = 0.02T$, (b) $B = 0.2T$ and (c) $B = 1.5 T$

Comparing the curves for a given band gap value in graphene reveals that higher magnetic fields increase the magnitude of the negative of the entropy change ($-\Delta S$) at each temperature, which in turns enhancing the Magneto Caloric Effect (Tishin and Spichkin 2014).

In addition, the relation between ($-\Delta S$) and magnetic field at constant temperature is investigated through Figure 4.33. Three subplots corresponding to different temperature values: (a) $T = 3K$, (b) $T = 5 K$ and (c) $T = 10 K$. For all curves represented in three subplots, ($-\Delta S$) increases with magnetic field. At very low range of B , the rate of increase in ($-\Delta S$) is large. However, after a certain B the curves tend to reach constant value. Band gap affect the values but not the behavior of ($-\Delta S$). The introduction of $\Delta = 53 meV$ and $\Delta = 106 meV$ has the same effect with a little bit differences in a small range of magnetic field.



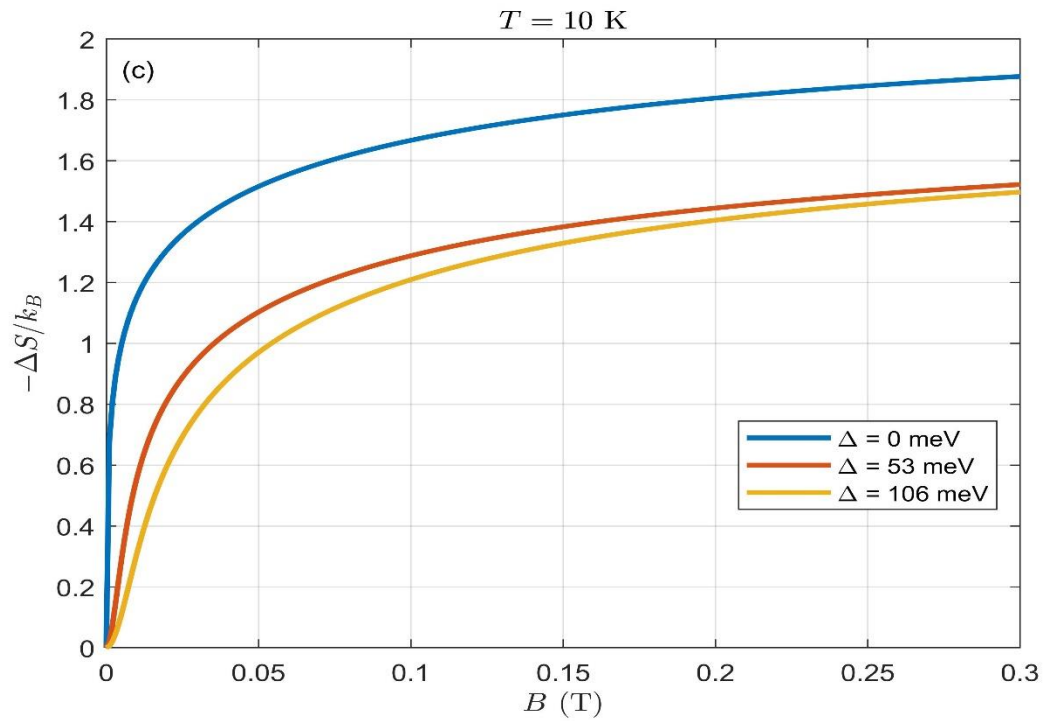
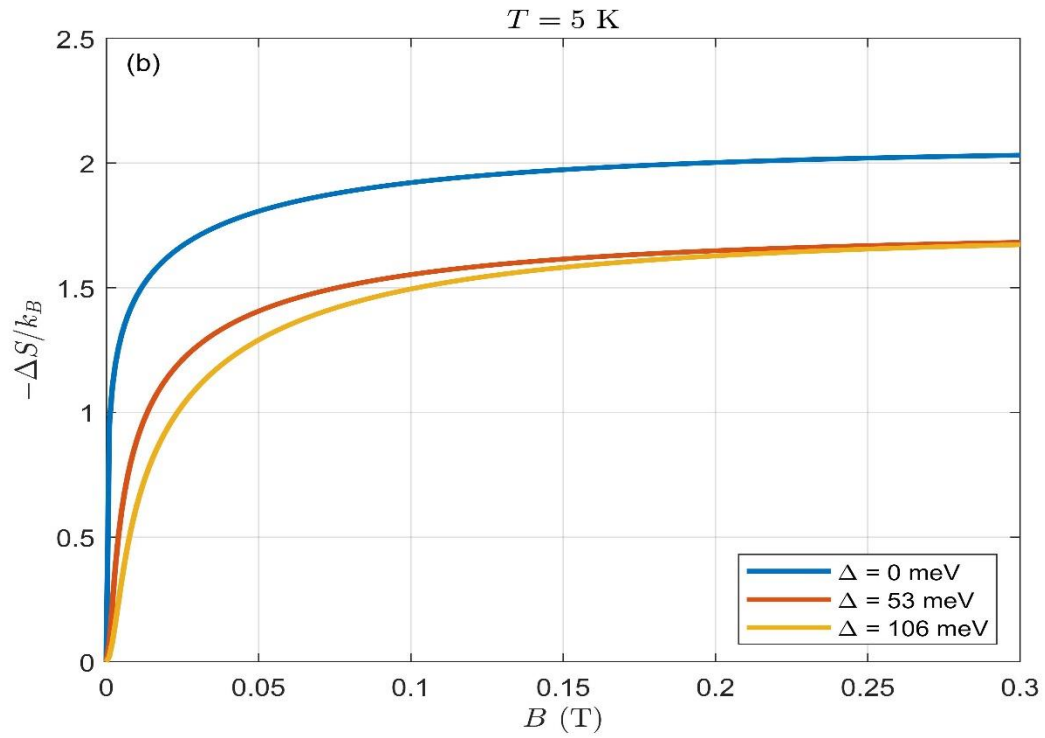


Figure 4.33 Change in entropy as a function of magnetic field strength at a constant value of temperature: (a) $T = 3 \text{ K}$, (b) $T = 5 \text{ K}$ and (c) $T = 10 \text{ K}$.

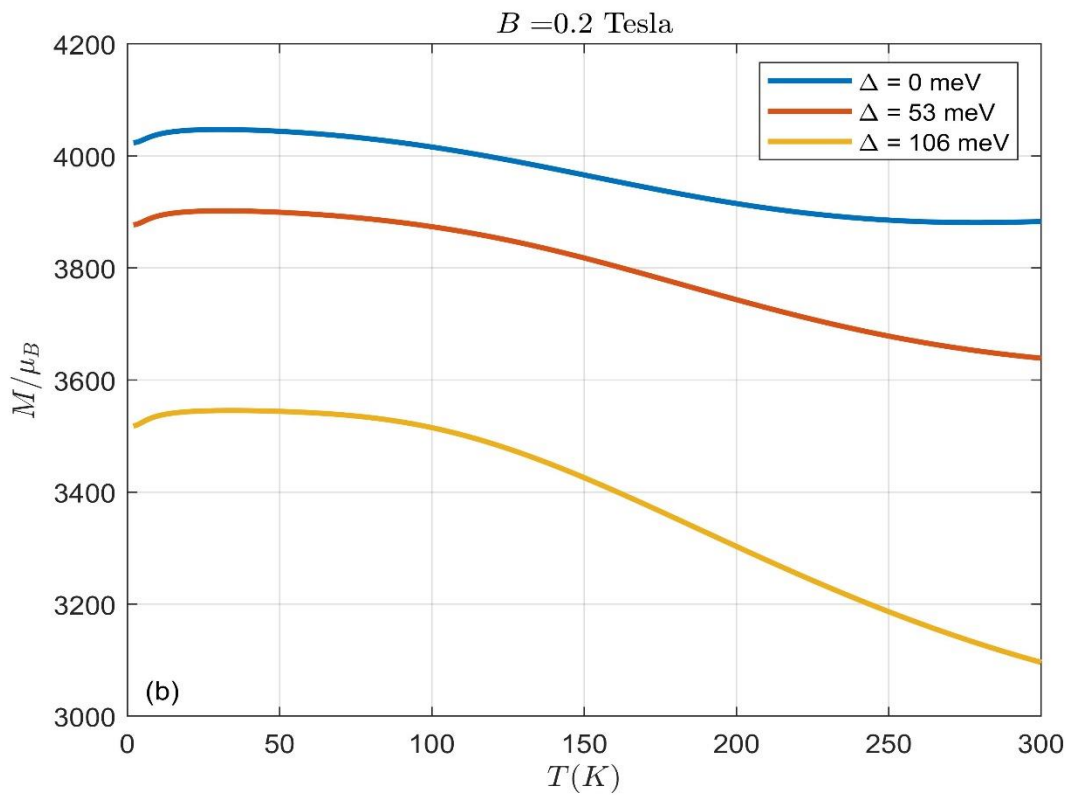
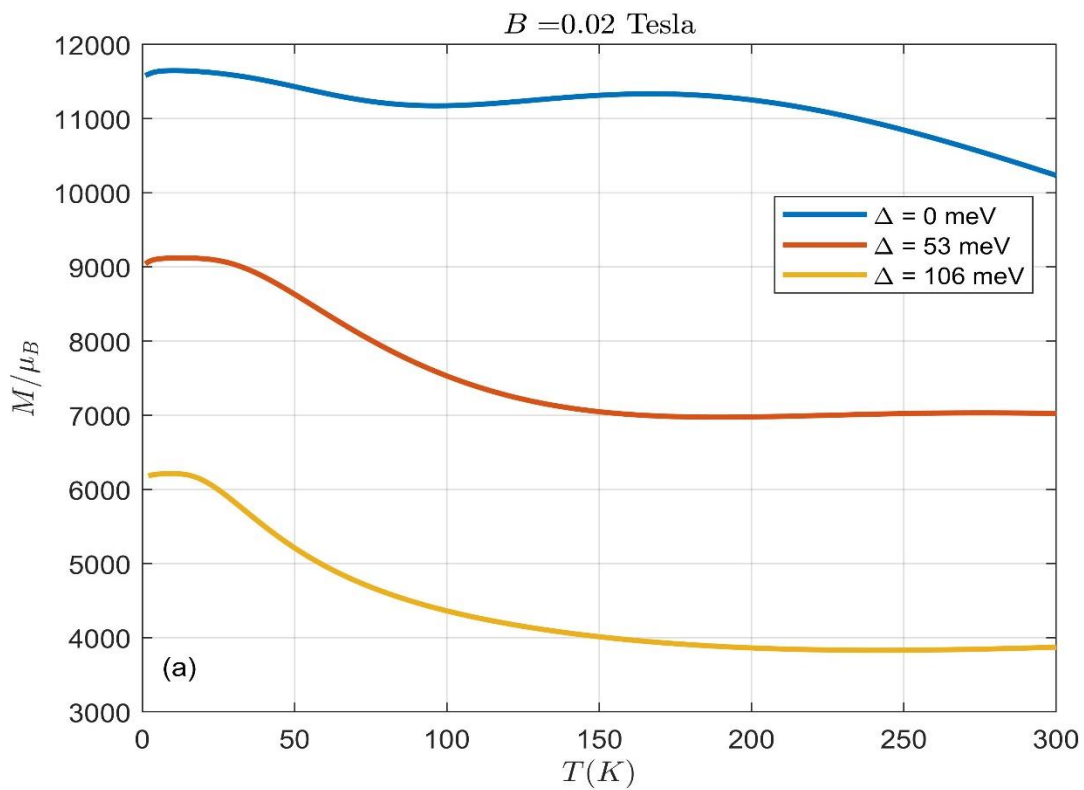
4.3: Magnetic Properties of Graphene Monolayer

4.3.1: Magnetization

The response of graphene to an applied magnetic field can be understood through the study of its magnetization (M). For this analysis, the calculated magnetization of non-gapped and gapped graphene versus temperature at four different magnetic field strengths is plotted in Figure 4.34. As observed from subplot (a) in the figure, magnetization of non-gapped at lower magnetic field strength of 0.02 T exhibits two maxima in the plotted temperature regime. However, gapped graphene curves exhibit one maxima. After this maxima, magnetization is highly decreased. In addition, the value of (M) is reduced to lower values as the band gap is increased.

The consistency of the magnetization behavior increases with magnetic field strength as visible from (b), (c) and (d) subplot. Moreover, as the field reaches 0.2 T and more, the two maxima observed in gapless graphene is reduced to one in the range of plotted temperature. Increasing the field strength to $B = 0.3 T$, (c) subplot, makes the behavior of the magnetization over the three values of the band gap approximately consistent with a vertical displacement proportional to the Δ value. Furthermore, the reduction in the magnetization due to the introduction of the band gap is reduced as the magnetic field strength increases.

Because levels are discrete in the presence of magnetic field, there will be rapid fluctuations in the population of these Landau levels as the thermal energy ($k_B T$) approaches the energy difference between Landau levels, which will result in maxima in the magnetization.



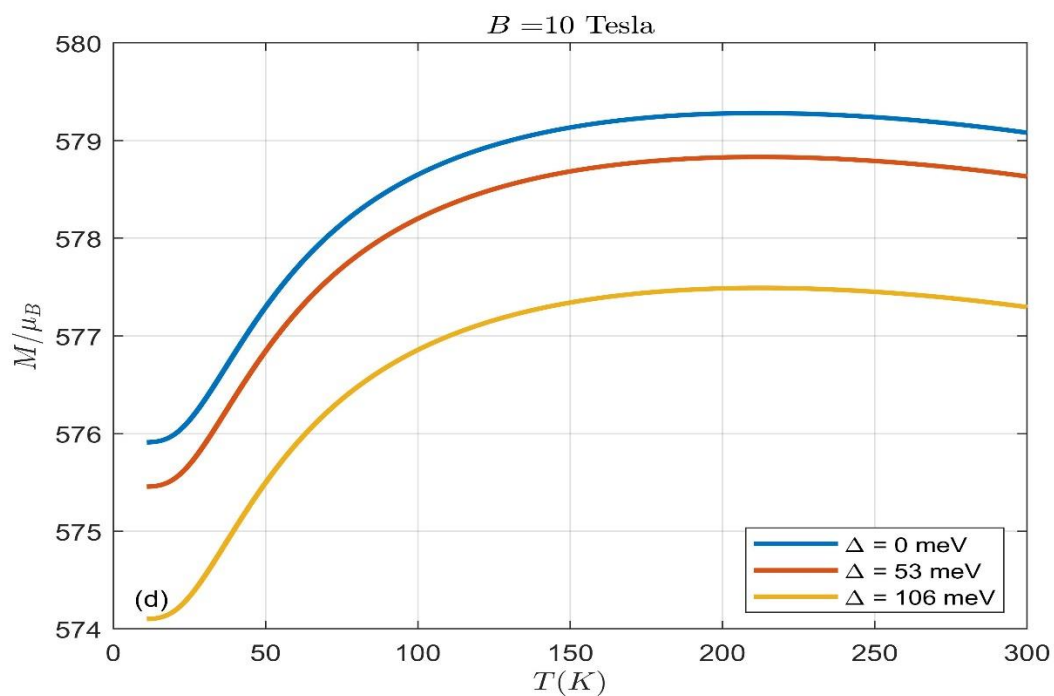
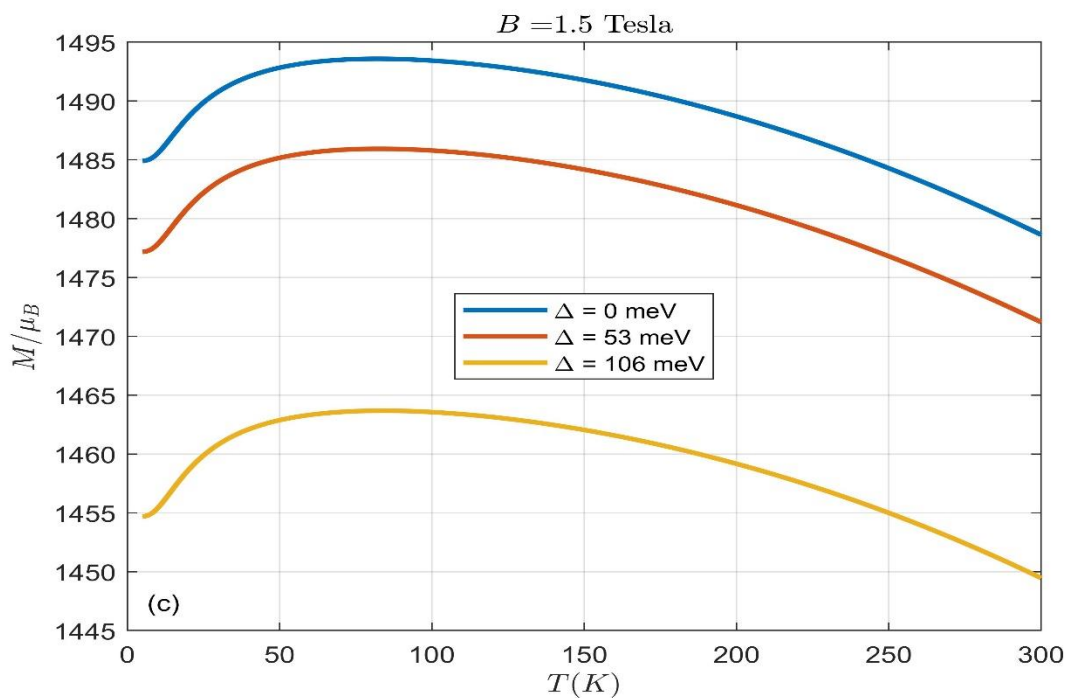


Figure 4.34 Magnetization versus temperature for three values of the band gap , $\Delta = 0$ meV, $\Delta = 53$ meV and $\Delta = 106$ meV at four magnetic field strengths of, (a) $B = 0.02$ T (b) $B = 0.3$ T, (c) $B = 1.5$ T (d) $B = 10$ T.

The maxima observed in the curves of magnetization at lower temperatures is associated with the coexistence of different types of magnetic states (Jiang, Yang et al. 2015). This behavior in magnetization is also observed in nano-graphene bilayer (Jiang, Yang et al. 2015).

Another significant issue to study is the behaviour of magnetization versus magnetic field at constant value of temperature. Figure 4.35 represents the magnetization versus magnetic field strength at $T = 40\text{ K}$ for three values of Δ . At this temperature, magnetization of gapless graphene, subplot (a), decreases with magnetic field strength. The introduction of Δ , leads to less M values with respect to M for non-gapped graphene at any magnetic field value. However, as displayed in (b) and (c) subplots, magnetization exhibits an increase at tiny values of the field strength. After that increase, it continues to decrease.

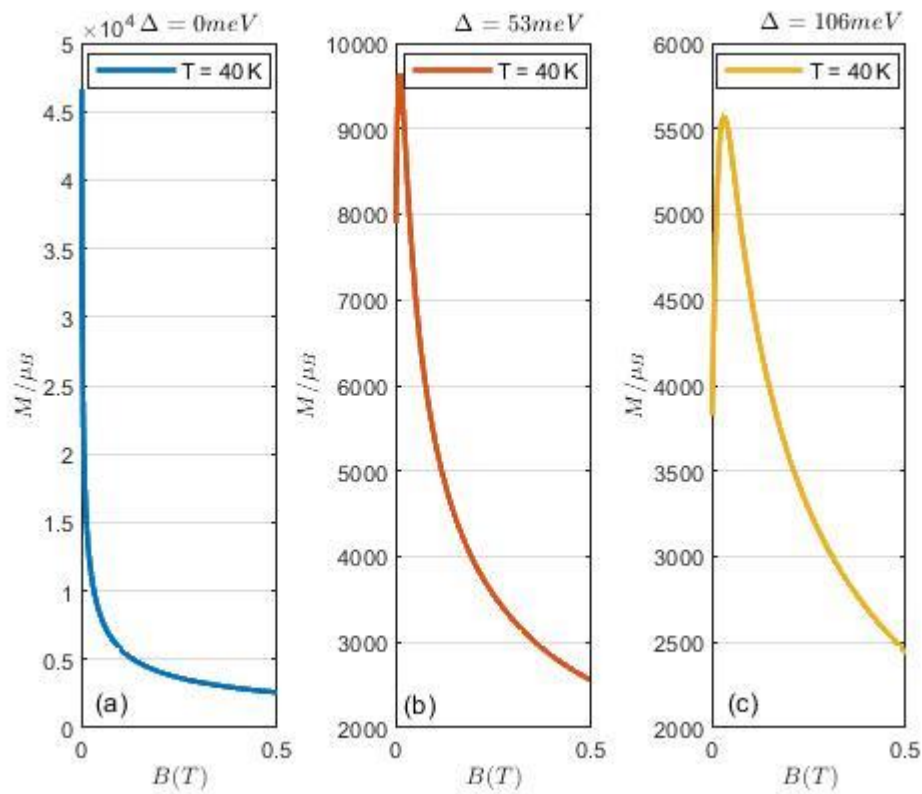


Figure 4.35 Magnetization versus magnetic field strength for three values of the band gap , (a) $\Delta = 0\text{ meV}$, (b) $\Delta = 53\text{ meV}$ and (c) $\Delta = 106\text{ meV}$ at $T = 40\text{ K}$.

The magnetization versus magnetic field strength is also plotted at $T = 80\text{ K}$ in Figure 4.36. M of gapless graphene decreases as the magnetic field increases in the plotted range as observed in (a) subplot. However, the magnetization in the case of gapped graphene exhibits an increase followed by a decrease. This is presented in (b) and (c) subplots. This behaviour in gapless and gapped graphene is in consistency with that observed in the case of lower temperature, $T = 40\text{ K}$.

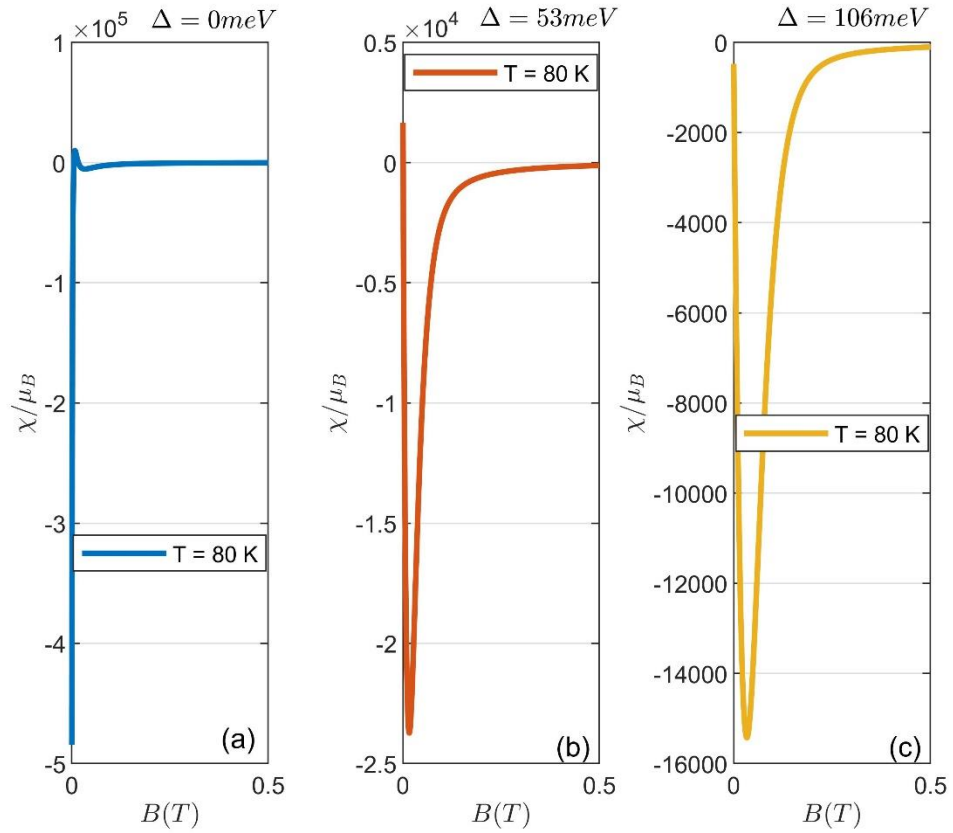


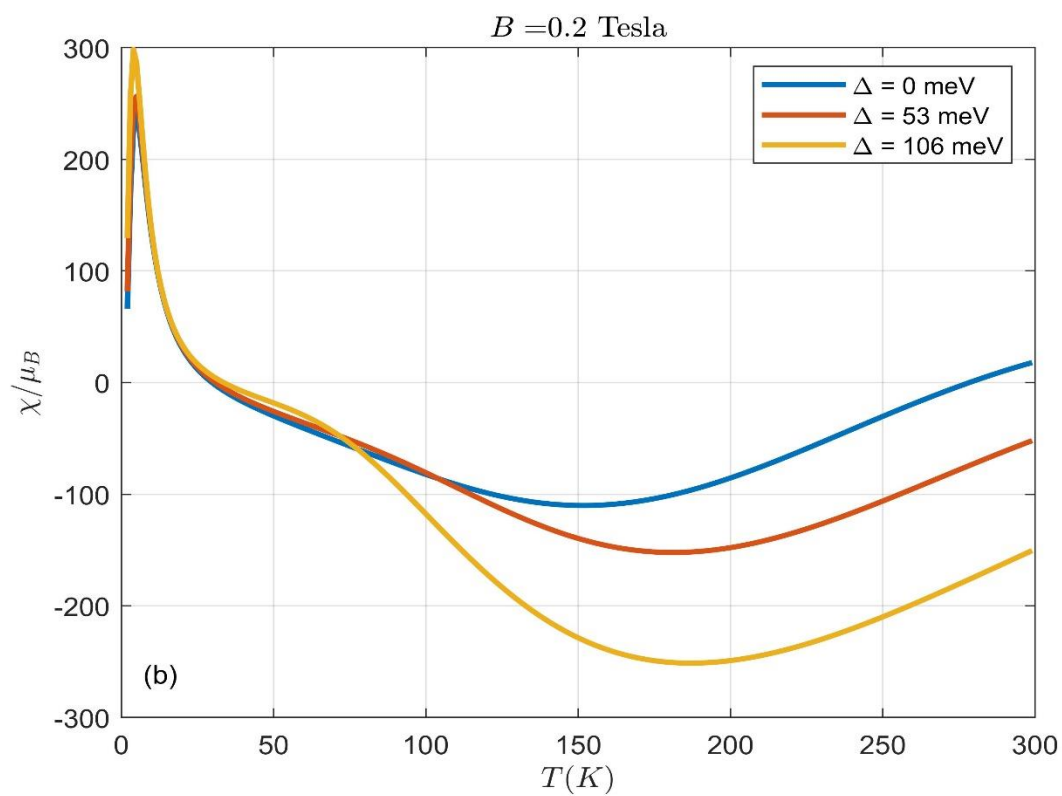
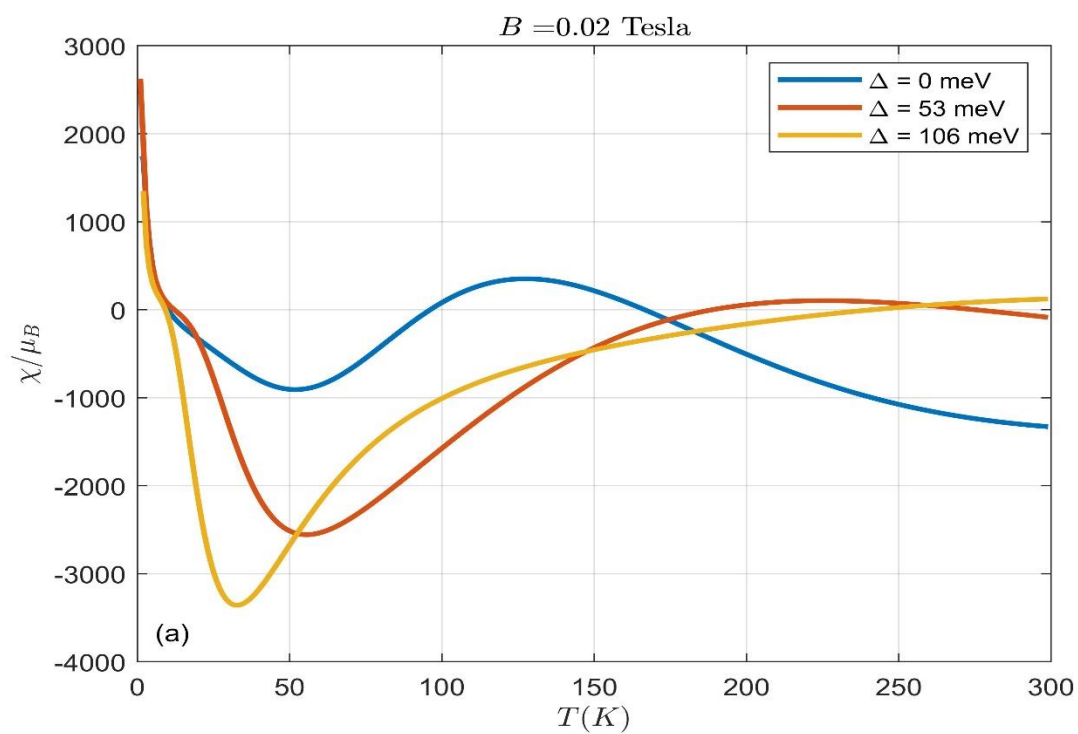
Figure 4.36 Magnetization versus magnetic field strength for three values of the band gap , (a) $\Delta = 0\text{ meV}$, (b) $\Delta = 53\text{ meV}$ and (c) $\Delta = 106\text{ meV}$ at $T = 80\text{ K}$.

4.3.2: Magnetic Susceptibility

Another important quantity to understand the magnetic properties of graphene is the magnetic susceptibility (χ). Magnetic susceptibility is plotted as a function of temperature at different magnetic field values for gapped and non-gapped graphene, as shown in Figure 4.37. Subplot (a) displays (χ) versus T at $B = 0.02 T$. For all curves, the magnetic susceptibility takes positive values at very small temperatures. As T increases, (χ) decreases and reaches negative values, After that , it increases but still negative. As the temperature goes to higher values, it reaches zero. In the regions, where magnetic susceptibility become less negative. Negative magnetic susceptibility reflect that graphene creates an opposite magnetic field to the applied one. This behavior is related to diamagnetic materials. The increase in negative susceptibility is due to the reduced diamagnetic effect at higher temperatures.

The three curves are representing different band gap values. As appear from the subplot, band gap introduction leads to changes in the susceptibility curve. Blue, red and orange curves, correspond to $\Delta = 0, 53$ and $106 meV$, reveal differences in the range of increasing and decreasing and also in the susceptibility values.

Studying magnetic susceptibility at large magnetic field of $0.2 T$, subplot (b), indicates that the effects of band gap introduction is less compared to the previous subplot. In particular, the effect of band gap introduction is clear approximately after $T = 100 K$. Rising the magnetic field up to $1.5 T$, leads to less noticeable effect due to band gap introduction as shown in (c) subplot. In addition, this unnoticeable effect is also observed in (d) subplot which corresponds to $B = 10 T$.



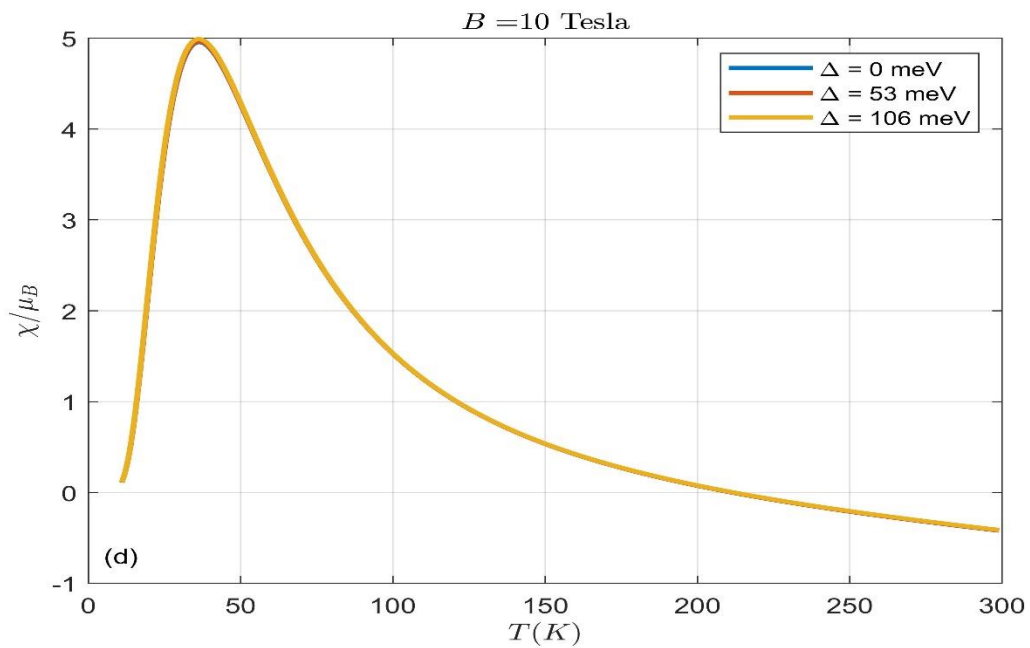
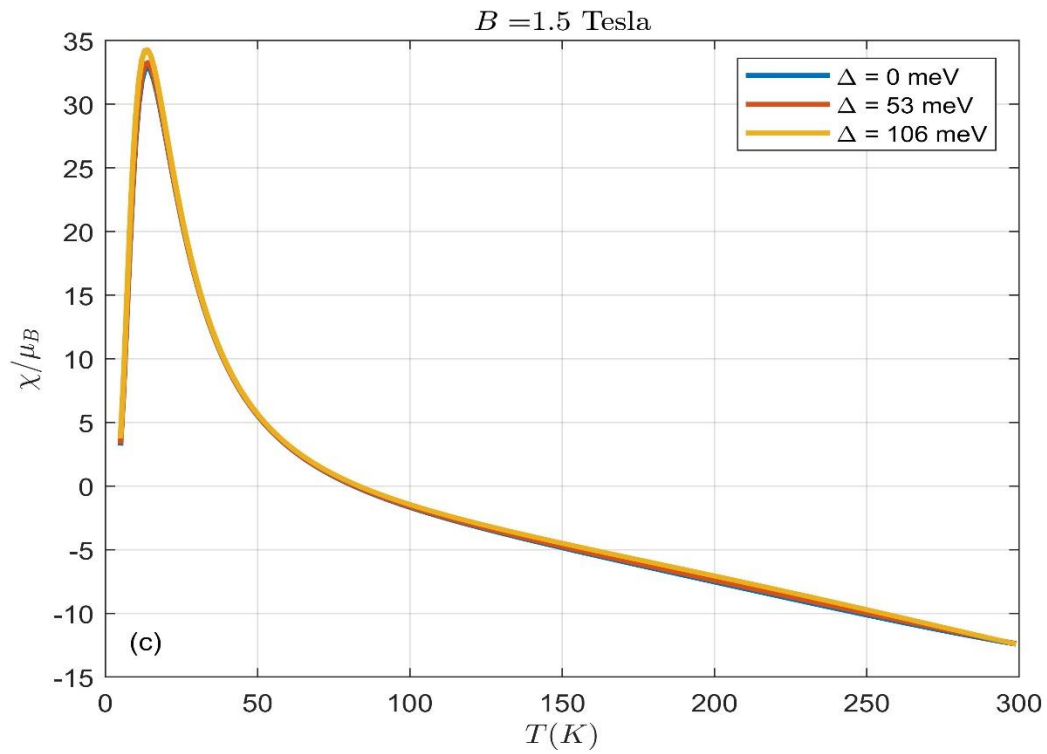


Figure 4.37 Magnetic susceptibility versus temperature for three values of the band gap, $\Delta = 0 \text{ meV}$, $\Delta = 53 \text{ meV}$ and $\Delta = 106 \text{ meV}$ at four magnetic field strengths of, (a) $B = 0.02 \text{ T}$ (b) $B = 0.2 \text{ T}$, (c) $B = 1.5 \text{ T}$ (d) $B = 10 \text{ T}$.

Another significant topic to study is the relation between magnetic susceptibility with magnetic field at constant temperature. Figure 4.38 is a plot of χ versus B at $T = 40\text{ K}$ for non-gapped and gapped graphene. Magnetic susceptibility is negative in the plotted range and at $T = 40\text{ K}$. As the three subplots display, χ starts from a large negative value. As magnetic field increases, it tends to be less negative until approaching zero. Introducing a band gap of $\Delta = 53\text{ meV}$, subplot (b), magnetic susceptibility become less negative compared to $\Delta = 0\text{ meV}$, subplot (a). However, a relatively large band gap of $\Delta = 106\text{ meV}$ exhibits a decrease in magnetic susceptibility followed by an increase as pictured in (c) subplot. One important note about gapless graphene is that magnetic susceptibility reaches positive values in certain range of the magnetic field strength.

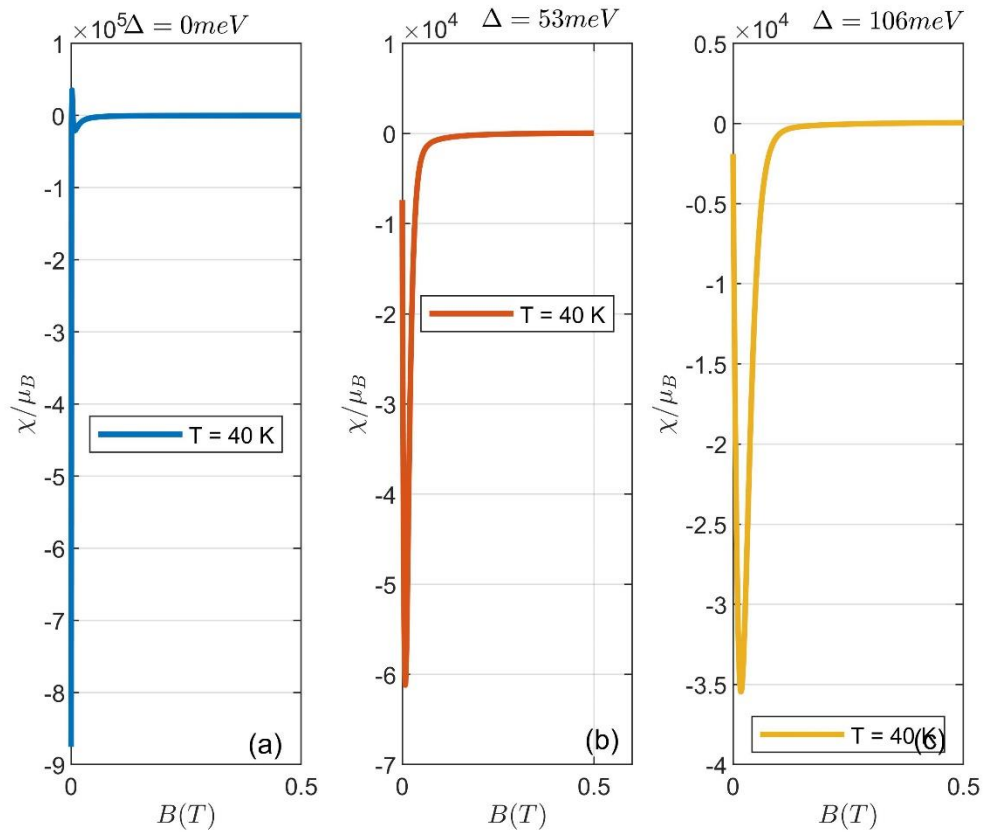


Figure 3.38 Magnetic susceptibility versus magnetic field strength for three values of the band gap, (a) $\Delta = 0\text{ meV}$, (b) $\Delta = 53\text{ meV}$ and (c) $\Delta = 106\text{ meV}$ at $T = 40\text{ K}$.

Also the relation between magnetic susceptibility of gapless and gapped graphene with magnetic field at constant temperature is studied at $T = 80\text{ K}$ as shown in Figure 4.39. For $\Delta = 0\text{ meV}$, which represented in (a) subplot, magnetic susceptibility is tend to be less negative as the field strength become higher reaching positive values. More increase in B , causes χ to decrease again toward negative values and then increases again until reaching zero susceptibility. In (b) subplot, magnetic susceptibility starts from positive value and as the magnetic field increases it decreases to negative values. After that, it increases to less negative values until reaching zero. In (c) subplot, χ goes to less negative values as the B increases. After that, it converges to zero.

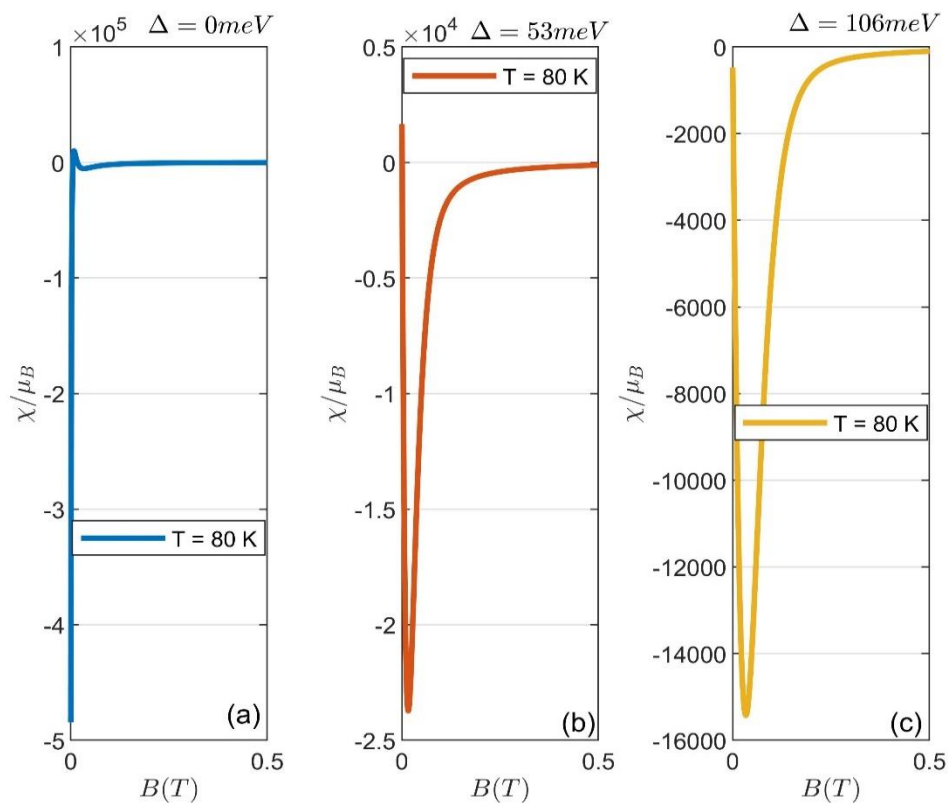


Figure 4.39 Magnetic susceptibility versus magnetic field strength for three values of the band gap , (a) $\Delta = 0\text{ meV}$, (b) $\Delta = 53\text{ meV}$ and (c) $\Delta = 106\text{ meV}$ at $T = 80\text{ K}$.

Negative magnetic susceptibility indicates the diamagnetic behavior of graphene. In which graphene is magnetized opposite to the direction of the applied magnetic field. This is related

to Landau diamagnetism associated with the formation of Landau levels in gapless and gapped graphene in the presence of external magnetic field (Bustamante 2023). Other studies on graphene emphasized the diamagnetic behavior of gapless and gapped graphene with 1 eV gap value (Gutiérrez-Rubio, Stauber et al. 2016). However, positive magnetic susceptibility indicates the paramagnetic behavior of graphene at certain range of the magnetic field strength (Chuang, Roy et al. 2016). The change in Magnetic susceptibility from negative to positive is associated with the magnetic transition from diamagnetic to paramagnetic behavior and vice versa. This magnetic transition from diamagnetic to paramagnetic is also valid in graphene quantum dots (Chuang, Roy et al. 2016).

Chapter Five: Discussion

In this thesis, graphene behavior under different conditions was investigated. The Landau levels of gapless graphene (with no band gap) and gapped graphene (with band gaps of $\Delta = 53 \text{ meV}$ and $\Delta = 106 \text{ meV}$) under an applied magnetic field was plotted using MATLAB, offering a detailed analysis of their electronic characteristics. Analyzing graphene's energy spectra and density of states (DOS) provided valuable insights into how introducing a band gap affects its electronic structure. The investigation into the oscillatory patterns of the Fermi energy in response to magnetic fields highlights distinct Landau level formations, emphasizing the influence of electron concentration and bandgap on these patterns.

In addition, essential thermodynamic properties such as specific heat capacity, entropy, magnetization, and magnetic susceptibility across a range of magnetic field strengths and temperatures for both gapped and gapless graphene were computed in this thesis. Differences in these properties emerged due to the presence of a band gap, demonstrating graphene's distinctive thermal and magnetic behaviors under varying conditions. The schottky anomaly observed in the specific heat capacity curves plotted at constant magnetic field value is shifted toward higher C_v values and lower temperature at higher band gap values. In addition, band gap introduction increases the entropy of graphene as a function of magnetic field.

These findings contribute significant insights into the potential applications of graphene in electronic and thermoelectric devices, paving the way for future advancements in materials science and technology. A maxima was observed in the magnetization curves of gapless and gapped graphene. This peak is associated with a transition in the magnetic status of graphene monolayer. Moreover, these results have potential applications in magnetic memory storage and magnetic switching.

While this thesis focuses on the electronic, thermal and magnetic properties of gapless and gapped graphene, future work should explore the optical properties via the calculation of dipole matrix element and optical absorption coefficient.

References

Adewuyi, A. and W. J. Lau (2021). Nanomaterial development and its applications for emerging pollutant removal in water. Handbook of nanotechnology applications, Elsevier: 67-97.

Amthong, A. (2015). "A magnetic quantum dot in a diluted magnetic semiconductor/semiconductor heterostructure." Superlattices and Microstructures 80: 72-79.

Arora, S., et al. (2023). "Impact of Impurity on the Mean Energy, Heat Capacity, Free Energy, Entropy and Magnetocaloric Effect of Ga $1-\chi$ Al χ As Quantum Wire." Journal of Low Temperature Physics 212(1): 54-68.

Baig, N., et al. (2021). "Nanomaterials: A review of synthesis methods, properties, recent progress, and challenges." Materials advances 2(6): 1821-1871.

Balandin, A. A., et al. (2008). "Superior thermal conductivity of single-layer graphene." Nano letters 8(3): 902-907.

Bhattacharjee, N. (2012). Multi-colour transient spectroscopy on single wall carbon nanotubes, Itä-Suomen yliopisto.

Bolotin, K. I., et al. (2008). "Ultrahigh electron mobility in suspended graphene." Solid state communications 146(9-10): 351-355.

Bustamante, J. V. (2023). Singular orbital diamagnetism and paramagnetism in graphene, Université Paris-Saclay.

Chamon, C. (2000). "Solitons in carbon nanotubes." Physical Review B 62(4): 2806.

Chen, G. (2022). "Correlated and topological physics in ABC-trilayer graphene moiré superlattices." Quantum Frontiers 1(1): 8.

Chen, L., et al. (2020). "Porous carbon nanofoam derived from pitch as solar receiver for efficient solar steam generation." Global Challenges 4(5): 1900098.

Chen, Z.-G., et al. (2014). "Observation of an intrinsic bandgap and Landau level renormalization in graphene/boron-nitride heterostructures." Nature communications 5(1): 4461.

Choi, W., et al. (2010). "Synthesis of graphene and its applications: a review." Critical reviews in solid state and materials sciences 35(1): 52-71.

Chuang, C., et al. (2016). "Intrinsic magnetic properties of plant leaf-derived graphene quantum dots." Materials Letters 170: 110-113.

Cooper, D. R., et al. (2012). "Experimental review of graphene." International Scholarly Research Notices 2012(1): 501686.

De Martino, A. and R. Egger (2010). "On the spectrum of a magnetic quantum dot in graphene." Semiconductor Science and Technology 25(3): 034006.

Dutta, R., et al. (2021). "Electrical tuning of optical properties of quantum dot-graphene hybrid devices: Interplay of charge and energy transfer." The Journal of Physical Chemistry C 125(15): 8314-8322.

Elsaid, M. K., et al. (2020). "Impurity effects on the magnetization and magnetic susceptibility of an electron confined in a quantum ring under the presence of an external magnetic field." Chinese Journal of Physics 64: 9-17

Fukuyama, H. and R. Kubo (1969). "Interband effect on magnetic susceptibility. I. A simple two-band model." Journal of the Physical Society of Japan 27(3): 604-614.

Gammag, R. and C. Villagonzalo (2012). "Persistent spin splitting of a two-dimensional electron gas in tilted magnetic fields." The European Physical Journal B 85: 1-6.

Geim, A. K. (2009). "Graphene: status and prospects." science 324(5934): 1530-15.34

Geim, A. K. and K. S. Novoselov (2007). "The rise of graphene." Nature materials 6(3): 183-191.

Geoffrion, L. D. and G. Guisbiers (2020). "Quantum confinement: size on the grill!" Journal of Physics and Chemistry of Solids 140: 109320.

Ghosh, S., et al. (2008). "Extremely high thermal conductivity of graphene: Prospects for thermal management applications in nanoelectronic circuits." Applied Physics Letters 92(15).

Gu, N. (2011). Relativistic dynamics and Dirac particles in graphene, Massachusetts Institute of Technology.

Gutiérrez-Rubio, A., et al. (2016). "Orbital magnetic susceptibility of graphene and MoS₂." Physical Review B 93(8): 085133.

Ho, J., et al. (2008). "Landau levels in graphene." Physica E: Low-dimensional Systems and Nanostructures 40(5): 1722-1725.

Ho, J.-H., et al. (2007). "Modulation effects on Landau levels in a monolayer graphene." Nanotechnology 19(3): 035712.

Hoi, B. D., et al. (2019). "Schottky anomaly and Néel temperature treatment of possible perturbed hydrogenated AA-stacked graphene, SiC, and h-BN bilayers." RSC advances 9(71): 41569-41580.

Hou, C.-Y., et al. (2007). "Electron fractionalization in two-dimensional graphenelike structures." Physical review letters 98(18): 186809.

Iijima, S., et al. (1992). "Growth model for carbon nanotubes." Physical review letters 69(21): 3100.

Jiang, W., et al. (2015). "Study on magnetic properties of a nano-graphene bilayer." Carbon 95: 190-198.

Kharisov, B. I. and O. V. Kharissova (2019). Carbon allotropes: metal-complex chemistry, properties and applications, Springer.

Khordad, R. and H. R. Sedehi (2018). "Thermodynamic properties of a double ring-shaped quantum dot at low and high temperatures." Journal of Low Temperature Physics 190: 200-212.

Khordad, R., et al. (2022). "Susceptibility, entropy and specific heat of quantum rings in monolayer graphene: comparison between different entropy formalisms." Journal of Computational Electronics 21(2): 422-430.

Kim, N., et al. (2001). "Modified magnetic quantum dot with electric confining potentials." Physical Review B 63(23): 235317.

Kim, S., et al. (2012). "Direct measurement of the Fermi energy in graphene using a double-layer heterostructure." Physical review letters 108(11): 116404

Koshino, M. and T. Ando (2007). "Orbital diamagnetism in multilayer graphenes: Systematic study with the effective mass approximation." Physical Review B—Condensed Matter and Materials Physics 76(8): 085425.

Koshino, M., et al. (2009). "Magnetic field screening and mirroring in graphene." Physical review letters 102(17): 177203.

Krishnan, S. K., et al. (2019). "A review on graphene-based nanocomposites for electrochemical and fluorescent biosensors." RSC advances 9(16): 8778-8881.

Kroto, H. (1987). "JR heath, sc o'brien, rf curl, and re smalley." Astrophys J 314: 352-356.

Kumar, S. B., et al. (2010). "Magnetoresistive effect in graphene nanoribbon due to magnetic field induced band gap modulation." Journal of Applied Physics 108(3).

Kumar, Y. R., et al. (2020). "Graphene quantum dot based materials for sensing, bio-imaging and energy storage applications: a review." RSC advances 10(40): 23861-23898.

Lee, Y., et al. (2013). Band gap and correlated phenomena in bilayer and trilayer graphene. Micro-and Nanotechnology Sensors, Systems, and Applications V, SPIE.

Li, L., et al. (2008). "Large magnetocaloric effect in $\text{La}_{2/3}\text{Ca}_{1/3}\text{Mn}_{1-x}\text{Si}_x\text{O}_3$ ($x = 0.05-0.20$) manganites." Journal of Physics D: Applied Physics 41(17): 175002.

Lin, S.-Y., et al. (2012). "Magneto-electronic specific heat of graphene." Journal of the Physical Society of Japan 81(8): 084602.

Liu, X., et al. (2020). "Superior catalytic performance of atomically dispersed palladium on graphene in CO oxidation." ACS Catalysis 10(5): 3084-3093.

- Li, Z., et al. (2015). "Field and temperature dependence of intrinsic diamagnetism in graphene: Theory and experiment." Physical Review B 91(9): 094429.
- Masrouf, R. and A. Jabar (2018). "Size and diluted magnetic properties of diamond shaped graphene quantum dots: Monte Carlo study." Physica A: Statistical Mechanics and its Applications 497: 211-217.
- Mauter, M. S. and M. Elimelech (2008). "Environmental applications of carbon-based nanomaterials." Environmental science & technology 42(16): 5843-5859.
- McClure, J. (1956). "Diamagnetism of graphite." Physical Review 104(3): 666.
- Mucha-Kruczyński, M., et al. (2011). "Landau levels in deformed bilayer graphene at low magnetic fields." Solid state communications 151(16): 1088-1093.
- Myoung, N., et al" (2019) .Splitting of conductance resonance through a magnetic quantum dot in graphene." Physical Review B 100(4): 045427.
- Nasir, R., et al. (2009). "Thermodynamic properties of a weakly modulated graphene monolayer in a magnetic field." Journal of Physics: Condensed Matter 22(2): 025503.
- Nguyen, N. T. and F. Peeters (2008). "Magnetic field dependence of the many-electron states in a magnetic quantum dot: The ferromagnetic-antiferromagnetic transition." Physical Review B—Condensed Matter and Materials Physics 78(4): 045321.
- Novoselov, K. (2007). "Mind the gap." Nature materials 6(10): 720-721.
- Novoselov, K. S., et al. (2004). "Electric field effect in atomically thin carbon films." science 306(5696): 666-669.
- Osman, W., et al. (2021). "Electronic and magnetic properties of graphene quantum dots doped with alkali metals." Journal of Materials Research and Technology 11: 1517-1533.
- Pakdel, F. and M. A. Maleki (2024). "Confinement of Dirac fermions in gapped graphene." Scientific Reports 14(1): 14512.

Park, D., et al. (2021). "Energy spectrum of bilayer graphene with magnetic quantum structures studied using the Dirac equation." Semiconductor Science and Technology 36(11): 115015.

Peeters, F. and P. Vasilopoulos (1992). "Electrical and thermal properties of a two-dimensional electron gas in a one-dimensional periodic potential." Physical Review B 46(8): 4667.

Raoux, A., et al. (2014). "From dia-to paramagnetic orbital susceptibility of massless fermions." Physical review letters 112(2): 026402.

Roduner, E. (2006). "Size matters: why nanomaterials are different." Chemical society reviews .592-583 :(7)35

Rumyantsev, E., et al. (2021). "Zero energy states in graphene in Aharonov–Bohm magnetic dots via Wirtinger calculus." Physica E: Low-dimensional Systems and Nanostructures 134: 114851.

Ryan, C., et al. (2022). Characterization of coatings for straylight and photoluminescence suppression in the Raman Spectrometer for MMX (RAX). Advances in Optical and Mechanical Technologies for Telescopes and Instrumentation V, SPIE.

Sanchez, V. C., et al. (2012). "Biological interactions of graphene-family nanomaterials: an interdisciplinary review." Chemical research in toxicology 25(1): 15-34.

Sakurai, J. J. and J. Napolitano (2020). Modern quantum mechanics, Cambridge University Press.

Savage, N. (2009). "Graphene makes transistors tunable." Ieee Spectrum 46(9): 2

Schwabl, F. (2008). "Second Quantization." Advanced Quantum Mechanics: 3-32.

Sedehi, H. R. and R. Khordad (2021). "Magnetocaloric effect, magnetic susceptibility and specific heat of tuned quantum dot/ring systems." Physica E: Low-dimensional Systems and Nanostructures 134: 114886.

Semenoff, G. W., et al. (2008). "Domain walls in gapped graphene." Physical review letters 101(8): 087204.

Sheng, X.-L., et al. (2011). "T-carbon: a novel carbon allotrope." Physical review letters 106(15): 155703.

Shubha, B., et al. (2023). "Graphene-calculation of specific surface area." International Journal of Applied Engineering and Management Letters (IJAEML) 7(1): 91-97.

Simos, T. E. and G. Maroulis (2012). "OF COMPUTATIONAL METHODS IN SCIENCES AND ENGINEERING 2009."

Sun, L., et al. (2021). "Magnetic and thermodynamic behaviors of the graphene-like quantum dots: A Monte Carlo study." Journal of Magnetism and Magnetic Materials 528: 167820.

Sun, L., et al. (2021). "The magnetic behaviors and magnetocaloric effect of a nano-graphene bilayer: a Monte Carlo study." Superlattices and Microstructures 149: 106775.

Thaller, B. (2013). The dirac equation, Springer Science & Business Media.

Tishin, A. and Y. Spichkin (2014). "Recent progress in magnetocaloric effect: Mechanisms and potential applications." international journal of refrigeration 37: 223-229.

Tolman, R. C. (1979). The principles of statistical mechanics, Courier Corporation.

Tomar, R., et al. (2020). "Photocatalytic degradation of dyes by nanomaterials." Materials Today: Proceedings 29: 967-973.

Tu, L. T., et al. (2022). "Magneto-optical properties of gapped-graphene." Physica E: Low-dimensional Systems and Nanostructures 144: 115415.

Urade, A. R., et al. (2023). "Graphene properties, synthesis and applications: a review." Jom 75(3): 614-630.

Vaseghi, Z. and A. Nematollahzadeh (2020). "Nanomaterials: types, synthesis, and characterization." Green synthesis of nanomaterials for bioenergy applications: 23-82.

Wu, Q., et al. (2020). "Mechanical properties of nanomaterials: A review." Nanotechnology Reviews 9(1): 259-273.

Yampol'Skii, V., et al. (2008). "Voltage-driven quantum oscillations in graphene." New Journal of Physics .053024 :(5)10

Yang, C., et al. (2010). "Landau-level broadening due to electron-impurity interaction in graphene in strong magnetic fields." Physical Review B—Condensed Matter and Materials Physics 82(7): 075401.

Ye, X., et al. (2023). "Zero to three dimension structure evolution from carbon allotropes to phosphorus allotropes." Advanced Materials Interfaces 10(5): 2201941.

Zhang, M. K., et al. (2022). "Graphene/quantum dot heterostructure photodetectors: from material to performance." Advanced Optical Materials 10(24): 2201889.

Zhao, X., et al. (2014). "Lattice match and lattice mismatch models of graphene on hexagonal boron nitride from first principles." Journal of Physics: Condensed Matter 26(9): 095002.

Zhu, W., et al. (2020). "Fabrication of highly dispersed Pd nanoparticles supported on reduced graphene oxide for solid phase catalytic hydrogenation of 1, 4-bis (phenylethynyl) benzene." International Journal of Hydrogen Energy 45(15): 8385-8395.

الخواص المغناطيسية والإلكترونية والحرارية للجرافين أحادي الطبقة

أروى نزيه توفيق أبو غنام

د. مؤيد أبو صاع

د. عدلي صالح

أ.د. محمد السعيد

أ.د. حازم خنفر

أ.د. حسين شنك

أ.د. محمد أبو جعفر

ملخص

في هذه الأطروحة، تم استخدام برنامج الماتلاب لتحليل الخواص الإلكترونية والحرارية والمغناطيسية للجرافين عديم الفجوة وذو الفجوة تحت مجال مغناطيسي متعامد خارجي. تم رسم مستويات لانداو المرتبطة بوحود مجال مغناطيسي خارجي للجرافين عديم الفجوة وذو الفجوة. بالإضافة إلى ذلك، تمت دراسة تأثير الفجوة على كثافة مستويات الجرافين. إن تمال مستويات لانداو وكافة المستويات بين حزم التوصيل والتكافؤ صالحة لكل من الطبقة الأحادية من الجرافين ذو الفجوة وعديم الفجوة. عند درجة حرارة $0.3K$ تكون الذبذبات في طاقة فيرمي مع قوة المجال المغناطيسي أكثر وضوحاً من الموجودة على درجة حرارية أعلى ($4K$). يعتمد عدد الذبذبات عند درجة حرارة معينة على تركيز الإلكترونات وليس على قيمة فجوة الطاقة. تمت دراسة العديد من الكميات الديناميكية الحرارية والمغناطيسية كدالة لكل من شدة المجال المغناطيسي والحرارة. يؤدي ادخال فجوة الطاقة إلى ازاحة قمة شذوذ شوتكي نحو درجات حرارة منخفضة وقيم حرارة نوعية أعلى. عند درجة حرارة ثابتة، تزداد إنتروبيا الجرافين ذو الفجوة مقابل المجال المغناطيسي مع زيادة قيمة فجوة الطاقة. علاوة على ذلك، تم رسم وتحليل الأثر المغناطيسي الحراري في كل من الجرافين عديم الفجوة وذو الفجوة من خلال التغير في الإنتروبيا ($-\Delta S$). يتم التحقق من وجود أنواع مختلفة من الحالات المغناطيسية من خلال الحد الأقصى المرصود في مغنطة الجرافين. مما يجعلها مفيدة في تخزين الذاكرة المغناطيسية وتطبيقات التبادل المغناطيسي.

كلمات مفتاحية: الجرافين عديم الفجوة، الجرافين ذو الفجوة، الخواص الإلكترونية، الخواص الحرارية، الخواص المغناطيسية.